# Dispersive Properties of Dielectric Laser Mirrors and their Use in Femtosecond Pulse Lasers

dr. Róbert Szipőcs

Dissertation for PhD degree

SZTE TTK Szeged, Hungary
Department for Optics and Quantumelectronics
2000

# Contents

# Foreword

The work presented in this dissertation was carried out at the Optical Thin Film Laboratory and the Ultrafast Laser Technique Laboratory of the Research Institute of Solid State Physics and Optics of the Hungarian Academy of Sciences. The dissertation comprises the most important results I obtained in connection with understanding the "magic" phase properties of dielectric laser mirrors during the time period of 1992 to 1999. During my work I benefited from the help and support of many people and different research groups, whose contribution to my work I appreciate.

In the autumn of 1992, I visited the Laser Laboratory of International Center for Theoretical Physics (ICTP) in Trieste, Italy. During the visit I built a white-light interferometer with my colleauge Pál Apai, which was used to study the phase properties of my first dielectric mirror samples. This work resulted in the understanding of the connection between increased losses in dielectric mirrors and the rapid phase change on reflection as we were tuning the wavelength of our monochromator. During my second visit at ICTP in June, 1993, I worked out the computer code and the first chirped mirrors designs benefiting from the excellent atmosphere of the reseach facility and the people around. The support from ICTP and Prof. Denardo must be greatfully acknowledged here.

I am indebted to Kárpát Ferencz who was my supervisor at the Optical Coating Laboratory between 1987 and 1993, and helped my work with relevant references, usefull discussions on technological questions and at last, but not at least, performing dozens of coating runs to manufacture dispersive mirror samples for our study.

I wish to thank Prof. Zsolt Bor for his help in this work in every aspect, especially for bringing the brilliant idea of using spectrally decomposed white light interferometers for rapid phase dispersion measurements on laser mirrors. Without these interferometers, we could not have achieved such results as building a compact lasers system at the University of Groningen that generated the world's shortest laser pulses with 4.5 fs pulse duration in 1997.

In particular, I wish to thank Ambrus Kõházi-Kis for his valuable contribution to our common work on some of the theoretical aspects of gradient index dielectric mirrors.

I am also indebted to Ferenc Krausz, who directed my attention to femtosecond pulse laser systems and to the problems arising from the phase properties of dielectric mirrors used previously in broadband lasers. I also benefited from the technical knowledge and the illuminating scientific atmosphere of his research group at the Technical University of Vienna during my visits between 1993 and 1995. Ferenc shared his knowedge with me on femtosecond pulse lasers, especially on Ti:sapphire lasers, that helped me understand the limiting factors in state of the art laser systems. It resulted in fruitful discussions, improved dispersive mirror designs - and a common patent on mirror-dispersion-controlled laser oscillators.

I wish to thank for the privilage of working with other research groups from this scientific field on different application problems, such as on the problem of white-light continuum compression (with Andrius Baltuska, Maxim Pshenichnikov, Douwe Wirsma at the University of Groningen, the Netherlands), on the problem of ultrabroadband chirped mirrors for broadband feedback and dispersion control in broadly tunable femtosecond pulse lasers (with Elmar Mayer, Jasper Möbius, Arno Euteneuer, Martin Hofmann, Prof. Rühle at the Philipps Universitat of Marburg, Germany), on the problem of diode pumped femtosecond pulse systems (with Irina Sorokina, Evgenij Sorokin, Ernst Wintner), on infrared femtosecond pulse optical parametric oscillators (with János Hebling, Elmar Mayer, Prof. Kuhl at Max Planck Institut Stuttgart, Germany), and on white light interferometry used to measure the dispersion of laser mirrors (with Attila Kovács, Károly Osvay, Gábor Kurdi, János Hebling, Zsolt Bor at the JATE University of Szeged, Hungary.)

Finally, I wish to thank my loved parents for their constant moral support and for their financial contribution to my research during the initial 6-7 years of my work at the Insitute.

dr. Róbert Szipõcs

September 30, 2000

Chapter 1

# General introduction and related previous works

## 1.1 Femtosecond pulse solid state lasers

One of the main trends of laser physics today is ultrafast laser technology. Recent research on high power semiconductor laser diodes and broad fluorescence emission band solid-state laser materials had paved the way for compact, reliable, broadly tunable all-solid-state continuous wave (cw), picosecond (ps) and femtosecond (fs) pulse laser sources. One approach is based on Ti:Sapphire (Ti:S) [1], which can be efficiently pumped by the frequency doubled output of AlGaAs diode-pumped neodymium lasers. Alternatively, the direct diode pumping of colquiriite laser active materials such as $LiCaAlF_6:Cr^{3+}$ (Cr:LiCAF) [2], $LiSrAlF_6:Cr^{3+}$ (Cr:LiSAF) [3], and $LiSrGaF_6:Cr^{3+}$ (Cr:LiSGAF) [4] became feasible by the use of enhanced mode-matching schemes [5] or, by using "improved" beam quality AlGaInP semiconductor lasers operating near 670 nm [6]. The latter approach might offer greater simplicity, efficiency, compactness and cost effectiveness. The importance of these features for wide-ranging applications needs no explanation. These advances in laser technology offered the possibility of constructing laser oscillators generating optical pulses in the sub-20-fs regime using different mode-locking techniques such as self-mode-locking of the laser [7].

Because of the dominant role of soliton-like pulse shaping in ultrashort pulse solid-state lasers [8], femtosecond pulse generation relies on net negative, i.e. anomalous intracavity group-delay dispersion (GDD). Solid-state gain media always introduce a certain amount of frequency dependent positive (normal) dispersion in the cavity, which dispersion must also be balanced by anomalous dispersion. Brewster-angled prism pairs [9] built into the laser cavity were the only low loss sources of broadband negative GDD until I initiated a new solution, the use of negative dispersion (or phase correcting) dielectric laser mirrors, which will be the topic of this dissertation. In prism-pair controlled broadband lasers, a major

limitation to ultrashort pulse generation originates from the variation of the intracavity GDD with wavelength. The principal source of this higher order dispersion however, was found to be the prism pair [10, 11]. If the lasers are operated in the vicinity of zero GDD, the spectra of sub-20-fs pulses from prism-pair controlled oscillators are asymmetric with a broad shoulder [10] or double-peaked [8, 11], depending on whether the soliton-like pulses are, respectively, third- or fourth-order dispersion limited. This deviation from the ideal $sech^2$ pulse spectrum causes a weak but significant pedestal in the time domain, the length of which may substantially exceed the pulse duration defined as the full width at half maximum (FWHM) intensity. This degradation in pulse quality may be unacceptable in a number of spectroscopic applications requiring high temporal resolution. An additional problem in the time domain is the increased sensitivity of pulse width to cavity and prism alignment. Cavity mirror alignment changes the position of the resonator axis and thus the glasspath through the prisms. Hence any small cavity realignment calls for subsequent readjustment of the prism positions and orientation to restore the original pulse width and the corresponding spectrum. This makes "turn-key" operation and thus the integration of these devices in complex systems (e.g. chirped pulse amplification (CPA) systems) rather difficult. Furthermore, the minimum prism separation sets a constraint on the resonator length and, in turn, the size and repetition rate of femtosecond pulse solid state laser oscillators.

## 1.2 Optical thin film devices in femtosecond pulse lasers

Continuous wave, ps and fs lasers contain optical coatings as important functional elements, e.g. high reflectors (HR), output couplers (OC) and antireflection (AR) coatings. These optical elements are based on the interference phenomenon of light. Their theoretical analysis generally relies on the well-known scattering matrix formalism [12,13] derived from the Maxwell equations. Laser performance strongly depends on the quality of optical coatings: reflectances of high reflectors should approach the ideal 100% value at the operation wavelengths in order to minimize intracavity losses and output coupling has to be set to specific values to ensure optimal operation. In broadband mode-locked or broadly tunable laser systems, broadband intra- and extracavity mirrors covering possibly the whole fluorescence spectrum of the laser active medium are needed; the reflectivity of such mirrors is not determined solely at the operation wavelengths but at the pump wavelength(s) as well.

In the case of high reflectors, a combination of materials with the highest refractive index ratios ($n_H/n_L$) is usually favoured since the higher the ratio, the higher the theoretical reflectance and bandwidth of standard quarterwave stacks. Among its competitors, the $TiO_2/SiO_2$ pair has the highest ratio over the near infrared spectral range [14]. At the optical coating laboratory of the Research Institute for Solid State Physics in Budapest, Hungary, a BAK 550 box coater supplied with an ESQ 110 electron beam gun (products of Balzers AG) is used for depositing laser optical coatings. The unconventional coating deposition technology (termed reactive electron beam deposition under reduced oxygen pressure), results in relatively high density optical coatings of the $TiO_2/SiO_2$ and $Ta_2O_5/SiO_2$ material pairs with low absorption and scattering losses. For details on all of these, see Ref. [14]. For application problems requiring high density coating with even lower scattering and absorption losses, ion-based technologies were used in collaboration with our partner company MLD Technologies (USA) [15].

In the case of Ti:sapphire lasers, for instance, the useful bandwidth of our low dispersion quarterwave mirrors made of $TiO_2/SiO_2$ material pair is limited to approximately 180 nm around 800 nm [14]. Typical spectral transmittance and group delay of such high reflectors and output couplers forming the cavity of a prism-pair controlled Ti:sapphire laser oscillator are shown in Fig. 1.2.1 and Fig. 1.2.2.

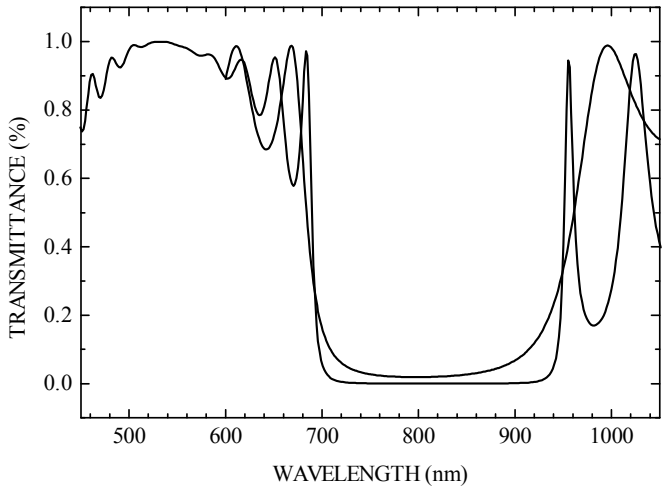


Fig. 1.2.1 Computed transmittance of a standard quarterwave high reflector (continuous line) and a quarterwave output coupler (dotted) used in a prism pair controlled Ti:sapphire laser [14]

*Besides the high-order dispersion existing in prism pair controlled fs laser systems, the bandwidth of low dispersion dielectric mirrors forming the laser cavity appeared to be the main limiting factor for obtaining optical pulses below 10 fs, directly from a laser oscillator.*

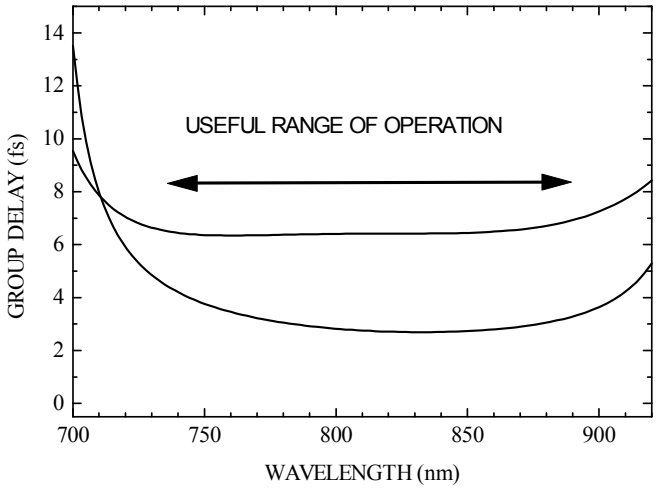


Fig. 1.2.2 Computed group delay on reflection of a standard quarterwave high reflector (continuous line) and a quarterwave output couper (dotted) designed for a Ti:sapphire laser [14]

The problem of designing broadband dielectric mirrors for sub-10-fs or broadly tunable femtosecond solid-state laser systems is twofold. First of all, the mirrors have to have *continuous high reflectivity over a broad spectral range* without any drop in reflectivity regardless of wavelength. Secondly, the mirrors have to exhibit a *smooth, possibly negative variation of the group delay vs. frequency function over the whole operation range* allowing femtosecond mode-locked operation of the laser. These two requirements can be fulfilled by properly designed metallic mirrors, although their reflectivity is considerably lower than that of a dielectric mirror and therefore they usually can not be used as intracavity broadband mirrors in femtosecond laser oscillators. Previously proposed solutions to extend the high reflectivity range of dielectric mirrors, such as (i) deposition of low- (high-) pass stacks as a single coating [16] and (ii) deposition of multilayer stacks with variation of thickness in arithmetic or geometric progression [17] do not meet the above listed requirements (for details see Refs. [14] and [18-20]. Briefly, all of the previously used broadband dielectric mirrors exhibited rapid change of the reflected phase at specific wavelengths in the high reflectivity zone of the broadband mirrors, causing resonant losses [18] and extremely strong high-order dispersions [19-20] around these wavelengths, thus preventing their use in broadly tunable femtosecond oscillators [14].

## 1.3 Topic of the dissertation

In 1992, I realized the importance of the phase properties of dielectric laser mirrors in (broadband) femtosecond pulse lasers. In previous studies in the field of optical interference coatings, however, the wavelength dependent phase change on reflection had not been considered in coating design due to the fact that it was not specified for these optical devices. Hence I started working on a topic with practically no preceedings, no references.

In this dissertation I summarize the most important results I obtained during my studies on this topic up to now. I clarified the main physical effects responsible the frequency dependent phase change on reflection from multilayer dielectric mirrors and, as a consequence, introduced a novel technology for ultrashort pulse generation in 1993 that became known as *dispersive dielectric mirrors, negative dispersion mirrors, phase correction mirrors* or *chirped mirrors* [21, 22].

After the general introduction, in Chapter 2, I introduce the two main physical effects responsible for phase dispersion of dielectric laser mirrors: the effect of the frequency dependent penetration depth and the effect of resonances.

In Chapter 3, I present a mathematical approach to explain the dispersive properties of gradient index (or rugate) dielectric mirrors based on Fourier analysis. I introduce the concept of chirped dielectric mirrors for broadband dispersion control, in which the Bragg wavelength is varied gradually along the optical distance measured from the substrate.

In Chapter 4, I discuss the design of discrete layer chirped mirrors. These special laser mirrors exhibite high reflectivity and negative GDD over broad frequency ranges. The design technique, deposition technology and quality control permit higher-order contributions to the mirror phase dispersion to be kept at low values or to be chosen such that high-order phase errors introduced by other system components (e.g., the gain medium, prism pairs) are cancelled. They can be utilized for broadband feedback, intra- and extracavity dispersion control in femtosecond pulse lasers. First I present a conversion routine developed for transforming gradient index chirped mirrors into discrete value step-index and, as a second step, into two-index equivalents. Then I introduce an alternative, more straightforward approach referred to as frequency domain synthesis of (two-index valued) chirped mirrors. Both approaches result in suitable initial designs for further optimization. Based on an initial design obtained by either of these means, we search for the best solution for a certain

application problem, bearing in mind the constraints on the parameters set by the technology. Finally, I take a specific design goal: the first application problem I solved. I investigate the effect of deposition errors on this specific design, and show measured dispersion functions taken after the coating deposition process. The measured dispersion data correspond to a mirror set that was used to build a commercial sub-10-fs mirror-dispersion controlled Ti:sapphire laser.

In Chapter 5, an alternative approach for realizing dispersive dielectric laser mirrors with pure negative quadratic phase shift on reflection is introduced. I refer to them as multi-cavity thin-film Gires-Tournois interferometers: their dispersive properties originate from coupled resonances in multiple λ/2 cavities embedded in the layer structure in contrast to chirped mirrors. These devices exhibit extremely low reflection losses over a bandwidth of standard quarterwave mirrors.

In Chapter 6, I take different application problems, and show how to define the target functions for the computer optimization of these different designs. I also present some of the designs I obtained along with their measured dispersion functions.

The replacement of the conventional thin film optics with these novel optical thin film devices made it feasible to build Kerr-lens mode-locked, mirror-dispersion-controlled solid-state lasers delivering nearly bandwidth-limited 7.5 fs pulses from Ti:Sapphire lasers [23-24] around 0.8 ###m, and sub-20-fs pulses from Cr:LiSAF and Cr:LiSGaF [25-26] lasers around 840 nm. This technology has been commercialized for femtosecond pulse lasers as well; negative dispersion mirrors were developed for mirror-dispersion-controlled, tunable, sub-100-fs Ti:S lasers such as the Coherent Vitesse XT laser. Similary, I developed ultrabroadband chirped mirrors for broadband feedback and dispersion control in broadly tunable cw, ps and fs solid state lasers (such as the Coherent MIRA 900 laser) [27]. All of these applications are addressed in detail later in this dissertation.

Further applications of dispersive dielectric mirrors that have already been accomplished include, for example, their use for broadband feedback and dispersion control in broadly tunable fs pulse parametric oscillators [28], broadband third- and fourth-order dispersion control in pulse compression schemes used in CPA systems [29-30] and in white light continuum compression experiments [31] supporting pulses below 5 fs [32].

# Chapter 2

# Phase properties of dielectric laser mirrors: physical effects responsible for dispersion

## 2.1 Definitions

The optical properties of optical interference coatings are fully described by their wavelength (or frequency) dependent complex amplitude reflectance $r(\lambda)$ and transmittance $t(\lambda)$ functions.

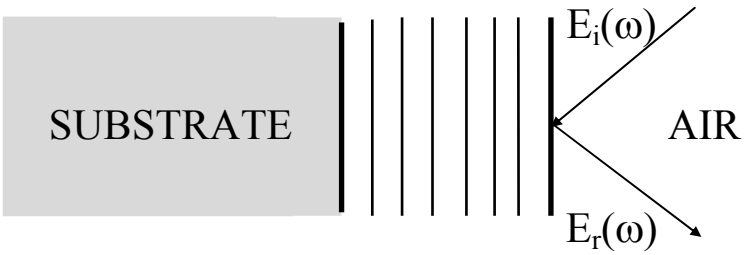


Fig. 2.1.1 Definition of the complex amplitude reflectance in case of dielectric multilayer coatings

The amplitude reflectance is defined as the complex ratio of the reflected and the incident electric field at the air/coating interface of the multilayer coating (see Fig. 2.1.1) :

$$\bar{r}(\omega) = \frac{E_r(\omega)}{E_i(\omega)} \tag{2.1.1}$$

Upon transmission through a spectral filter, optical pulses could become orders of magnitudes longer than the initial pulse due to spectral narrowing and/or dispersion, but in special cases such as optical tunelling [33], considerable spectral broadening and pulse shortening can be observed. The same effect can be easily observed, however, in ultrabroadband laser oscillators utilizing chirped mirrors for intracavity dispersion control [24], in which the bandwidth of the intracavity spectrum is comparable to that of the output coupler.

In the case of dielectric high reflectors, (intensity) reflectance, which is calculated as $R(\omega) = |r(\omega)|^2$, can be usually considered $R(\omega) \cong 1$, hence the frequency dependent phase shift on reflection $\varphi(\omega) = -\arg(\bar{r}(\omega))$ determines the shape of a femtosecond pulse after reflection on a dielectric multilayer mirror. Group delay, group-delay dispersion (GDD), third-order dispersion (TOD) and fourth-order dispersion (FOD) are calculated as the first, second, third and fourth derivative of phase shift $\varphi(\omega)$ respectively, by the angular frequency $\omega$. Recently, phase properties of dielectric multilayers were discussed by A. Tikhonravov et al. from the aspect of mathematical complex analysis [34]. Below I briefly summarize the main *physical effects responsible for* the frequency dependent group-delay on the reflection function, i.e. the *dispersion of multilayer dielectric mirrors*.

## 2.2 Dispersion of multilayer dielectric mirrors: the frequency dependent penetration depth

The first effect, the *frequency dependent penetration depth*, can be easily studied on the most widely used dielectric high reflector, the quarterwave ($\lambda/4$) stack, the operation of which is depicted in Fig. 2.2.1. A quarterwave stack consists of alternating high (H) and low (L) index layers of $\lambda/4$ optical thicknesses. As a result, a quarterwave mirror exhibits the highest reflectivity at the tuning (or reference) wavelength $\lambda$, at which wavelength the partial reflections on the high/low index interfaces meet exactly in phase, as shown in Fig. 2.2. The reflectivity of the $\lambda/4$ stack gradually decreases with increased detuning from the reference wavelength, in accordance with the increased phase difference between the partial reflections.

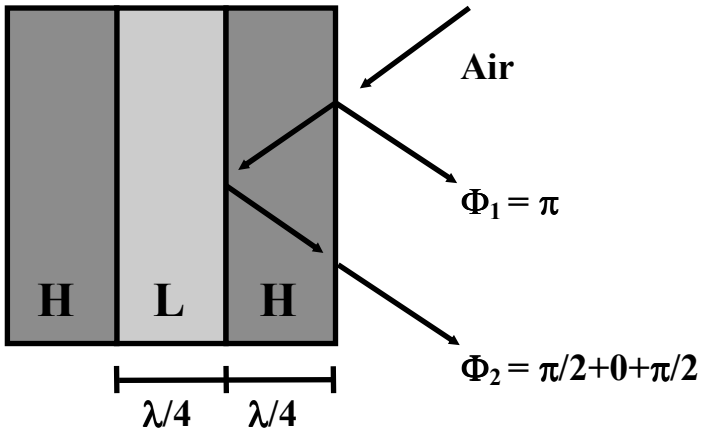


Fig. 2.2.1 Dispersion of dielectric high reflectors: operation of a quarterwave stack

The lower the reflectivity the higher the penetration depth [35] of the electric field into the coating (see Fig. 2.2.2.), which causes a frequency dependent group delay on reflection (see Fig. 2.2.3). The shape of the group delay vs. wavelength function exactly follows that of the standing wave electric field distribution in the multilayer stack [35], indicating that the group delay in this particular case is ultimately determined by the penetration depth [35]. I wish to point out that quarterwave stacks exhibit a positive TOD at the reference wavelength, that can be used for (usually partial) compensation of the negative TOD of prism pair controlled laser oscillators.

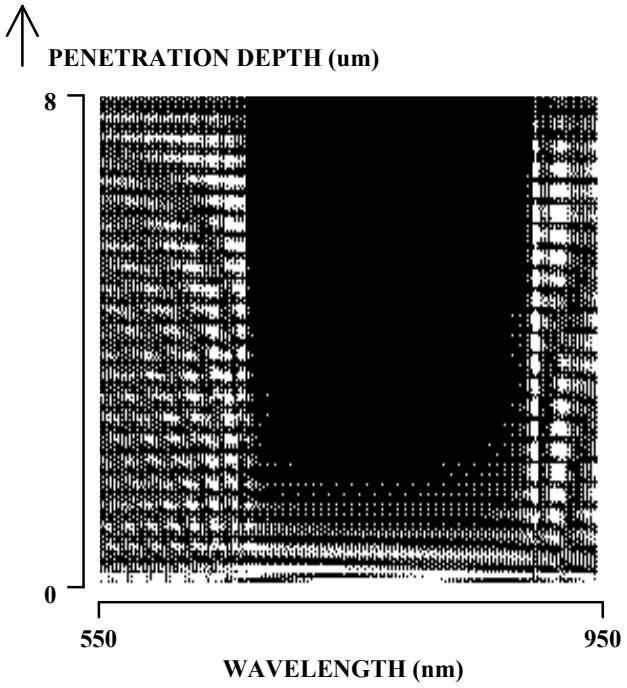


Fig. 2.2.2 Computed standing-wave electric field distribution in a quarterwave stack comprising $TiO_2/SiO_2$ layers with $\lambda/4$ optical thicknesses at 800 nm

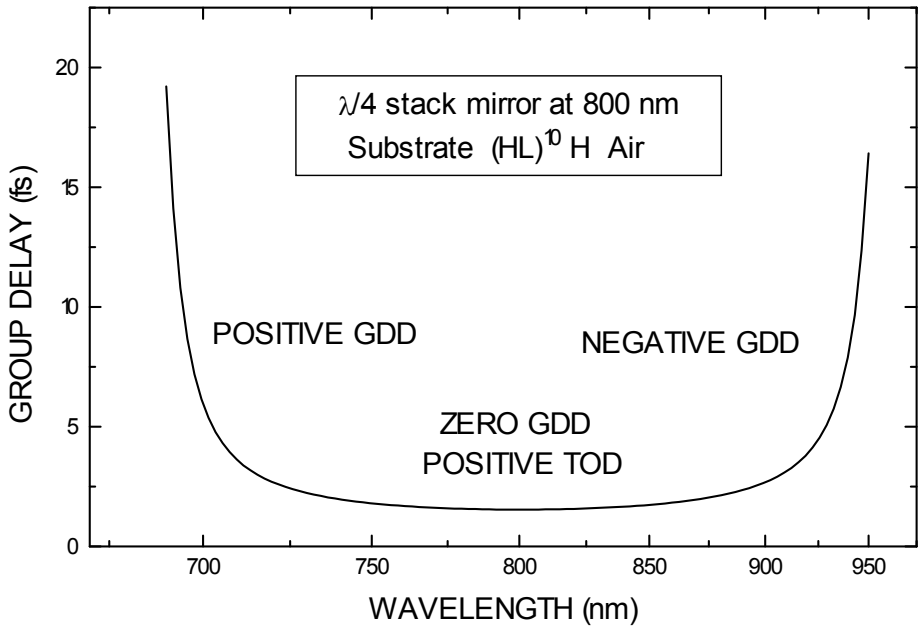


Fig. 2.2.3 Group delay vs. wavelength function of a quarterwave mirror corresponding to the standing-wave field distribution

## 2.3 Dispersion of multilayer dielectric mirrors: resonances

The second effect that I refer to as *resonance* can be studied in its simplest form in a thin film realization of a Gires-Tournois interferometer (GTI) [36]. The general structure of GTI is shown in Fig. 2.3.1. It consists of an (ideal) R = 100% high reflector, a resonant cavity, which is similar to that of a Fabry-Perot filter, and a top reflector, the reflectivity of which is set for the application problem.

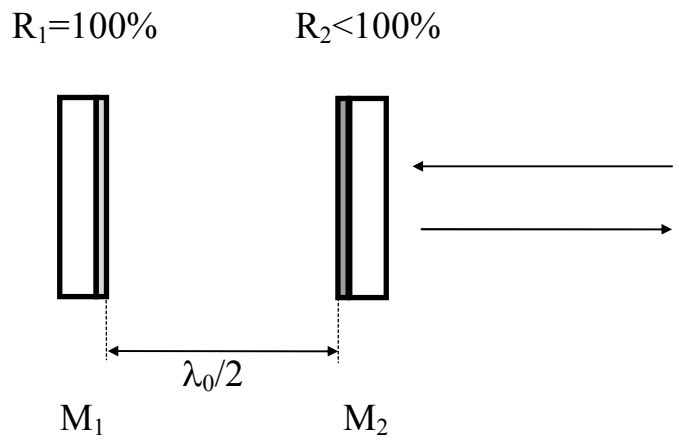


Fig. 2.3.1 Dispersion of dielectric high reflectors: a Gires-Tournios interferometer

A thin film realization of such a (highly dispersive) GTI may have the structure of *Substrate* | $(HL)^{10}$ *H 2L H* | *Air*, where *H* and *L* correspond to λ/4 layers of high (H) and low (L) index dielectric materials, and the layer denoted by *2L* plays the role of the resonant cavity. The computed group delay vs. wavelength function of this thin film GTI is plotted in Fig. 2.3.2. At resonance, a GTI introduces the highest group delay - when the electric field is localized in the resonant cavity. At shorter wavelengths, a GTI shows a negative (anomalous) dispersion, while at longer wavelengths its group delay vs. wavelength function exhibits an opposite slope, i.e. normal dispersion. Initially, thin film GTI-s were succesfully applied for dispersion control in mode-locked dye lasers [37].

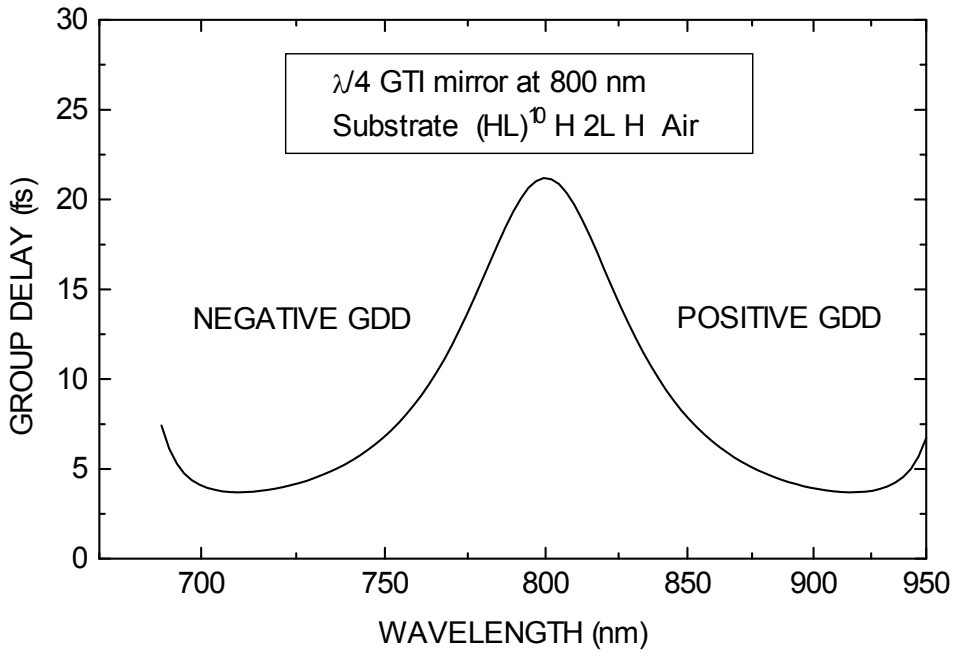


Fig. 2.3.2 Group delay vs. wavelength function of a Gires-Tournois interferometer

Later mirror-dispersion-controlled (MDC) fs pulse, mode-locked solid state lasers were built this way [25], however, the pulse duration of these lasers were limited at around 40-50 fs according to the limited negative dispersion bandwidth of thin film GTI-s [25].

# Chapter 3

# Phase properties of dielectric laser mirrors: a mathematical approach based on Fourier analysis

In this chapter, theoretical considerations on phase properties of dielectric laser mirrors are presented. As a starting point, an analogy between *graded index dielectric laser mirrors and one-dimensional (1D) phase volume holograms written by two counter-propagating laser pulses* [38] is established. Based on these results, formulae are presented that can be efficiently utilized to synthesize *graded index* chirped dielectric mirrors with prescribed dispersion properties.

## 3.1 Holography of wave packets in 3D medium

In the following I show that the interference pattern formed by two counter-propagating (Gaussian) pulses exhibiting different chirp parameters are capable of forming "chirped mirrors" in a holographic (or photorefractive) medium with the assumption that the local change of the refractive index is proportional to the exposure in the phase volume hologram [22]. If one of the pulses (reference) is chirp free (i.e., dispersion free: $\tau(\omega)$ is constant at any $x$ position), the interference pattern records the temporal structure (chirp) of the signal pulse in the spatial domain. After recording such an interference pattern in a volume holographic medium, the chirp of the signal pulse is almost perfectly compensated when reflected on the corresponding (spatially chirped) hologram, i.e., a nearly *ideal graded index chirped mirror* for dispersion compensation is constructed.

The following calculations are based on the paper of Mazurenko [38]. Our calculations are restricted, however, to investigating the one dimensional spatial structure of the recorded phase volume hologram in the particular case when the hologram is written by two counter-propagating laser pulses.

Let us consider two Gaussian light pulses, one of them being dispersion free and the other one linearly chirped, with dimensionless (linear) chirp parameters $a_1 = a \neq 0$ and $a_2 = 0$. The time dependent electric field of the pulses can be written as:

$$E_k(t) = E_{0,k} \exp\left(-\frac{t^2}{2\,T_k^{\,2}}\right) \cos\left(\omega_0 t + a_k \frac{t^2}{T_k^{\,2}}\right), \tag{3.1.1}$$

where $T_k$ is defined as the half width at 1/e maximum intensity time duration, $E_{0,k}$ is the electric field amplitude of the $k$-th light pulse ($k$=1,2) and $\omega_0$ is the (common) central frequency of the two pulses.

We investigate a practical situation when the two light pulses exhibit the same $\Delta\omega$ spectral bandwidth. Using $T_0$ for the transform limited pulse duration ($T_0 = 1/\Delta\omega$), the pulse duration $T_k$ and the group delay dispersion (GDD = $\partial^2\varphi/\partial\omega^2$) parameters, $D_k$ of the $k$-th light pulse can be expressed as:

$$T_k = T_0\sqrt{1+4\,a_k^{\,2}} = T_0\sqrt{1+\frac{D_k^{\,2}}{T_0^{\,4}}} \tag{3.1.2}$$

$$D_k = 2a_k T_0^2 = \frac{2a_k T_k^{\,2}}{1+4\,a_k^{\,2}} \tag{3.1.3}$$

We consider the particular case when the two pulses are propagating in an opposite direction along the $x$-axis (in one dimension). The temporal and spatial dependence of the electric field can be written as:

$$E_1(t,x) = E_1\left(t-\frac{x}{c}\right) \qquad \text{and} \qquad E_2(t,x) = E_2\left(t+\frac{x}{c}\right) \tag{3.1.4}$$

The time averaged intensity distribution along the $x$-axis, $P(x)$ can be calculated as

$$P(x) = \int_{-\infty}^{\infty}\left(E_1\left(t-\frac{x}{c}\right) + E_2\left(t+\frac{x}{c}\right)\right)^2 dt \tag{3.1.5}$$

After expansion we obtain

$$P(x) = \int_{-\infty}^{\infty}\left(E_1\left(t-\frac{x}{c}\right)^2 + E_2\left(t+\frac{x}{c}\right)^2 + 2E_1\left(t-\frac{x}{c}\right)\,E_2\left(t+\frac{x}{c}\right)\right)dt \tag{3.1.6}$$

By transforming the *t* variable inside the integral in the first two terms we get

$$P(x) = \int_{-\infty}^{\infty} (E_1(t)^2 + E_2(t)^2)dt + 2\int_{-\infty}^{\infty} E_1\left(t - \frac{x}{c}\right) E_2\left(t + \frac{x}{c}\right)dt \qquad (3.1.7)$$

We can transform the *t* variable also in the second integral of Eq. 3.1.7:

$$P(x) = \int_{-\infty}^{\infty} (E_1(t)^2 + E_2(t)^2)dt + 2\int_{-\infty}^{\infty} E_1(t)E_2\left(t + \frac{2x}{c}\right)dt \qquad (3.1.8)$$

The second integral in Eq. 3.1.8 is the convolution of the electric field functions defined in Eq. 3.1.1:

$$K(x) = \int_{-\infty}^{\infty} E_1(t)E_2\left(t + \frac{2x}{c}\right)dt = [E_1(t) * E_2(-t)]\,|_{-\frac{2x}{c}} \qquad (3.1.9)$$

In Eq. 3.1.9, * denotes convolution.

To calculate the convolution in Eq. 3.1.9, we take the Fourier transform of the $E_k$ electric field functions. Then we multiply the Fourier transforms and take the inverse Fourier transform of the product. This procedure is well-known from convolution-theory. The Fourier-spectra of the two pulses are composed of positive and negative frequency components. Taking the product of the two spectra, cross-products of the negative and positive components can be neglected in practical cases. Finally, we come to the following formula:

$$K(x) = \frac{1}{4}E_{0,1}E_{0,2}T_0\sqrt{\pi}\left(\frac{1+4a^2}{1+a^2}\right)^{\frac{1}{4}} \exp\left(-\frac{x^2}{c^2T_0^2(1+a^2)}\right)\cos\left(2k_0x - \frac{a\,x^2}{c^2T_0^2(1+a^2)} - \varphi\right) \qquad (3.1.10)$$

In Eq. 3.1.10, $k_0$ denotes the central wavenumber corresponding to central frequency $k_0 = \omega_0/c$ and φ is a constant phase-factor. The result shows that the length of the interference pattern is $L = c\,T_0\sqrt{(1+a^2)/2}$ and the modulation of the interference pattern is described by a Gaussian function. Periodicity of the fringes at position *x* can be described by the corresponding wavenumber $k_K(x)$, which wavenumber is calculated as the first derivative of the argument of the cosine function:

$$k_K(x) = 2\left(k_0 - \frac{a\,x}{c^2T_0^2(1+a^2)}\right) \qquad (3.1.11)$$

Equation 3.1.11 shows that the wavenumber of the interference pattern is a linear function of $x$. Here we recall that the Bragg condition for reflection is fulfilled at position $x$ when the wavenumber of the Bragg grating (i.e., the phase volume hologram written by the interference pattern) is $k_K(x) = 2|k_P| = 2\omega/c$, where ω denotes the angular frequency of the electric field. Calculating the wavenumber of the electric field as the function of $x$ corresponding to the chirped optical pulse at time $t = 0$ we obtain:

$$k_P(x) = k_0 - \frac{2ax}{c^2 T_0^2 (1+4a^2)} \tag{3.1.12}$$

Supposing that the pulse exhibits a relatively strong linear chirp (a >>1) we obtain:

$$k_K(x) = 2\left(k_0 - \frac{1}{a}\frac{x}{c^2 T_0^2}\right) \text{ and } k_P(x) = k_0 - \frac{1}{2a}\frac{x}{c^2 T_0^2} \tag{3.1.13}$$

Assuming that all the frequency components are reflected at the position where the Bragg condition is fulfilled, Eq. 3.1.13 shows the following: the phase volume hologram written by the interference pattern of the two counter-propagating pulses fully compensates the dispersion of the linearly chirped pulse when the chirped pulse is reflected on the corresponding phase volume hologram.

It is worth mentioning that the same result could have been obtained without any restriction on the chirp parameter $a$ if the Gaussian reference pulse had been replaced with an (ideal) Dirac delta pulse in Eq. 3.1.9.

Finally, let me summarize the results in Chapter 3.1. Theoretically, it is possible to record a 1D phase volume hologram compensating the linear (or higher-order) chirp of any broadband laser pulse if we are able to provide a dispersion-free reference pulse of high enough bandwidth for the recording. The structure of *the recorded phase volume hologram preserves the dispersive features of the chirped pulse converting its τ(ω) function to the spatial domain*. When a chirped pulse is reflected on the corresponding phase volume hologram, its dispersion is compensated and we obtain a practically dispersion free, i.e. transform limited, reflected pulse.

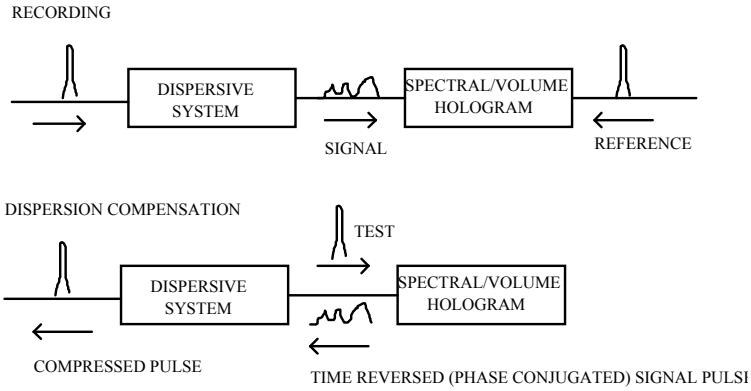


Fig. 3.1.1 Arrangement for dispersion compensation and time reversal of femtosecond pulses by means of femtosecond holography

In order to obtain a time reversed replica of the signal pulse, the signal pulse must be replaced by a dispersion free read-out pulse, as shown in Fig. 3.1.1. The arrangement might well be suited for dispersion compensation in CPA systems, in which the temporal spread of the stretched, then time reversed and finally amplified seed pulses can be easily compensated using the pulse stretching elements.

## 3.2 Femtosecond spectral holography

Spectral holography [38, 39] may be considered as a temporal analog of traditional spatial-domain Fourier transform holography. In traditional holography the spatially patterned signal beam is recorded as a set of fringes due to interference with a spatially uniform reference beam. When illuminating the hologram with a uniform read-out beam, we reconstruct either the real or the conjugate image of the original signal beam, depending on the geometry. In the time domain, the reference is (an ideal) short pulse with a broad, regular spectrum. The signal is a shaped pulse with a frequency dependent phase and amplitude, i.e., a complex amplitude function. During holographic recording in a "*2-f*" system, the complex amplitude of each spectral component of the signal pulse is recorded. When illuminating the spectral hologram, we recall either a real or a time-reversed (conjugate) copy of the signal pulse, also depending on the geometry. *One of the possible applications of spectral*

*holography is full dispersion compensation* since the time reversed (conjugated) signal pulse is transformed back to its original temporal (and spatial) shape when passing through the same apparatus which caused its temporal (and spatial) distortion (see Fig. 3.1.1). It is worth noting here that when we measure the dispersion of an optical element (e.g., the solid state gain medium) using the technique termed *spectrally resolved white-light interferometry* [40, 41] and design a chirped dielectric mirror for dispersion compensation, we practically do the same: we record the interference pattern of a signal and a reference beam in the frequency domain (using a white light source, not a mode-locked laser, see Chapter 4.6 for details), and then we retrieve the phase vs. frequency function corresponding to the medium by processing the spectrally resolved interference pattern recorded on a CCD camera. With this information, a coating design is made with the same dispersive properties that we measured over the intended wavelength range but with opposite sign (dispersion compensation), not forgetting about the technological limitations.

In spectral holography, one of the crucial questions is how to provide a chirp-free, short reference pulse with a broad, regular spectrum for the recording. In CPA systems, a properly shaped seed pulse might well be suited for such purposes. In pulse compression schemes developed for white light continuum compression, subsequent recording of spectral holograms with narrow band reference and signal pulses with adjustable time difference between the two pulses (and adjustable exposure time) might be the solution of the problem.

Because of certain technological limitations on realizable index profiles and the overall layer thickness existing in present optical thin film technology, I considered alternative holographic solutions for broadband dispersion control in femtosecond CPA systems and in experiments dealing with white light continuum compression. Furthermore, optical thin film devices such as chirped mirrors are not capable of following the dynamic spatial and/or temporal changes in the systems mentioned above and this calls for subsequent readjustment of these systems to restore the optimal dispersion and thus the pulse width of such systems. One of the possible solutions of the latter problem is using dynamic (spectral) holography, i.e., using photorefractive media instead of conventional holographic media for spectral holography. Recently, some promising experiments to this end were performed by Danailov et al. [42, 43].

### 3.3 Fourier-transform synthesis of mirrors with prescribed spectral phase

Concerning the analogy between phase volume reflection holograms and chirped mirrors discussed in Chapter 3.1, I present our results published in detail in Ref. [22].

Optical coating designers widely use the as Fourier-transform technique for designing gradient-index optical filters, often known as rugate filters, with prescribed spectral properties. These works are based on the papers of Sossi and Kard, who showed that [44-46]

$$\frac{1}{2}\int_{-\infty}^{\infty}\frac{d\ln[n(x)]}{dx}\exp(ikx)dx = Q(k)\exp[i\Phi(k)] \tag{3.3.1}$$

where $n(x)$ is the refractive index, $k = 2\pi/\lambda$ is the wavenumber in air, and $x$ is twice the optical distance from the center of the inhomogeneous layer to physical position $z$:

$$x = 2\int_{0}^{z} n(u)du \tag{3.3.2}$$

In Eq. 3.3.1, $Q(k)$ is an appropriate function of the desired reflectance or transmittance. Using partial integration and Fourier-transform one can derive:

$$\ln\left[\frac{n(x)}{n_0}\right] = \frac{i}{\pi}\int_{-\infty}^{\infty}\frac{Q(k)}{k}\exp\{i[\Phi(k)-kx]\}dk \tag{3.3.3}$$

when $n(\infty) = n(-\infty) = n_0$, and $Q(k)$ and $\Phi(k)$ are even and odd functions of $k$, respectively.

In general, optical coating design techniques based on Eq. (3.3.3) differ in the choice of $Q(k)$ and $\Phi(k)$ [44-53], which are usually termed Q-function and phase factor, respectively. A variety of techniques exists because of the fact that no simple, "universal" Q-function and phase factor have been found, although different approximate formulae have been successfully applied in the case of smooth refractive index dependence. *It has been revealed that distortions in the Fourier-transformation originate from neglecting the multiple internal reflections in Eq. (3.3.1)* (see Refs. [50, 51]) *the effect of which is striking in the case of dielectric structures consisting of discrete layers with high refractive index ratios ($n_H/n_L$).* In Chapter 3.1, the analogy between 1D volume reflection holograms and chirped mirrors was established. *In general, we can say that by controlling the amplitudes and phases of the gratings with various spatial frequencies forming the reflection hologram, one may control the amplitude and phase of each spectral component in a diffracted optical signal.*

In the field of optical interference coatings, however, the phase factor for optical coating design has not usually been considered by designers due to the fact that phase change on reflection is rarely specified for these optical devices. Later on, it was recognized that solutions of rugate filter synthesis problems depend greatly on the choice of the phase factor [47-49, 52, 53]. Since the phase shift on reflection was found not to be uniquely related to the amplitude reflectance modulus [52], it could be efficiently utilized to modify the refractive index profile without affecting the spectral performance.

In Ref. [22], our goal was to find a general formula to help us design dielectric high reflectors for dispersion control in femtosecond lasers, i.e. mirrors with prescribed dispersion properties. Taking into account the analogy between optical coatings and reflection holograms, we chose the Q-function and phase factor as the amplitude and phase of the complex amplitude reflectance, $r(k)$:

$$Q(k) = |r(k)| \tag{3.3.4a}$$

$$\Phi(k) = \varphi_r(k) \tag{3.3.4b}$$

where $\varphi_r(k) = \arg [r(k)]$.

In spite of its approximate nature, Eq. 3.3.3 supplemented with Eqs. 3.3.4a-b were the main results of Ref. [22]. It was demonstrated that the formulae were well suited for constructing chirped dielectric rugate mirrors with preset phase and amplitude characteristics.

In a number of papers [47, 51, 53], it was shown that if we introduce a linear phase

$$\Phi(k) = \Delta x\, k \tag{3.3.5}$$

in Eq. 3.3.3 it results in a displacement $\Delta x$ of the refractive index profile along the $x$ axis. By differentiating with respect to $k$, Eq. 3.3.5 can be rewritten in the form of

$$\Delta x = d\Phi\,(k) / dk \tag{3.3.6}$$

which is the *time-shifting theorem of Fourier analysis*. Previously, the theorem was successfully exploited to significantly reduce the optical thickness of synthesized rugate filters and to control the shape of the refractive index variation without affecting the spectral performance [47, 48, 53]. In Ref. [53], a general formula for the numerical calculation of the "optimal" phase function corresponding to the given design goal of reflectance versus

wavelength (or wavenumber) function is presented, which results in thinner rugate filters or lower index contrast than alternatives that arbitrarily constrain the phase.

I recall that the frequency dependent group delay (τ) upon reflection on a mirror is calculated in a similar manner:

$$\tau = d\varphi_r(\omega)/d\omega \qquad (3.3.7)$$

where $\varphi_r(\omega)$ is the frequency dependent phase change on reflection and $\omega = ck$ is the angular frequency of the incident electromagnetic wave. In order to relate Eq. 3.3.6 to Eq. 3.3.7, we calculated the increase in the group delay ($\tau_{DP}$) upon reflection corresponding to the displacement of the refractive index profile, e.g., a dielectric mirror, simply by dividing the increase in the optical path $x$ by $c$, the speed of light in vacuum:

$$\tau_{DP} = 2\,\Delta x / c \qquad (3.3.8)$$

Here I would like to comment on Eq. 3.3.3 in connection with gradient-index reflective structures, using some simple physical terms. First, *non zero reflectivity at wavenumber k (or at wavelength $\lambda = 2\pi/k$) calls for sinusoidal modulation in the logarithmic refractive index profile along the x axis with a periodicity $\lambda_{n(x)} = \lambda/2$, corresponding to $k_{n(x)} = 2k$*. Notice that the first term within the integral in Eq. 3.3.1, which can also be written in the form of $n'(x)/n(x)$, stands for the reflectance amplitude due to Fresnel reflection at position $x$ inside the inhomogeneous dielectric layer. The expression describes the change in the index divided by the average index, which can be derived from the classical Fresnel formula. For higher reflectances, higher amplitude modulations, i.e. higher Fresnel reflections are required, and *the modulation for a given value of the amplitude reflectance is inversely proportional to wavenumber k*. It also follows from Eq. 3.3.1 that *mirrors with broad reflectance bands and phase factors set to zero, i.e., dispersion-free mirrors require high refractive index modulations over very short optical distances, which leads to practically unrealizable solutions* [53]. It is worth mentioning here that this constraint on the refractive index modulation is analogous to the maximum intensity limit in pulsed laser amplifier systems for avoiding nonlinear effects such as self focusing. The former problem can be solved by spatially "chirping" the frequency components of the mirrors (chirped mirrors), while the latter one can be efficiently eliminated by temporally "chirping" the frequency components of the pulse (CPA, or chirped pulse amplification systems). Note, however, that using dielectric

mirrors at oblique angles of incidence for s-polarized light, the effective refractive index modulation and thus the reflectivity band of standard dielectric λ/4 or chirped mirrors can be increased.

In practice, the finite refractive index ratios set a limit to the bandwidth of the low dispersion reflective optics, such as high reflectors, dichroic mirrors and output couplers, which were developed for femtosecond laser oscillators containing prism pairs [8, 10, 11] and thus limit the ultimate bandwidth of these systems [8]. This constraint on the cavity bandwidth was overcome by the application of broadband (chirped) dielectric high reflectors. Additionally, they can provide a nearly constant negative GDD over most of the mirror bandwidth, which is needed for solitary pulse formation in the cavity of a femtosecond solid-state laser oscillator [8].

In the following, chirped dielectric rugate mirrors are introduced by generalising the concept of shifted structures. Dispersive and spectral properties of multiline rugate mirrors [51] and chirped broadband rugate mirrors, which have been synthesised by the use of Eq. 3.3.3, are calculated utilising the classic matrix multiplication technique [12, 13] and compared to their prescribed values.

### 3.3.1. Multiline, shifted rugate mirrors

To demonstrate the efficiency of the Fourier-transform technique in designing dielectric mirrors with prescribed dispersion properties, first we consider the following mirror specification. We require high reflectivities at three separate wavelengths: $\lambda_1$, $\lambda_2$ and $\lambda_3$ corresponding to wavenumbers $k_1$, $k_2$ and $k_3$, respectively. The high reflectivity zones centred at these wavelengths should have a Gaussian shape with the same mirror bandwidth in terms of wavenumber, which is determined by parameter $\sigma$. Furthermore, the group delay on reflection should be different at these separate wavelength regions in such a way, that a wavepacket of the lowest carrier frequency corresponding to wavenumber $k_1 = k_{01}/2$ should suffer the largest group delay upon reflection, while a wavepacket of the highest carrier frequency, which corresponds to wavenumber $k_3 = k_{03}/2$, should have the smallest value. Based on our considerations presented in Chapter 3.1, we expect that the specification described above should be fulfilled by a multiline rugate mirror design obtained from Eq.

3.3.3 by using the following Q-function and phase factor, which have been chosen as the amplitude and phase of the desired complex amplitude reflectance, $r(k)$:

$$Q(k)\exp[i\Phi(k)] = \sum_{i=1}^{3} \exp\left[-\frac{(k-k_{0i})^2}{2\sigma^2}\right] \exp[ia_i(k-k_{0i})] \qquad (3.3.9)$$

The refractive index profile shown in Fig. 3.3.1a has been generated by substituting $Q(k)$ and $\Phi(k)$ in Eq. 3.3.3 with the following parameters: $\sigma$ = 1.5 μm$^{-1}$, $k_{01}$= 2π / 0.4 μm$^{-1}$, $k_{02}$= 5/3 $k_{01}$, $k_{03}$= 7/3 $k_{01}$, $a_1$= 4 μm, $a_2$= 0 μm, $a_3$= -4 μm. The refractive index of the surrounding medium has been set equal to $n_0$ = 1.8. To achieve reflectances high enough, the modulation in the logarithmic refractive index profile has been increased by multiplying the right hand side of Eq. 3.3.3 by a factor of 35 in this specific case. Note, however, that it is unphysical with respect to Eq. 3.3.4a, but the problem originates from the approximate nature of Eq. 3.3.3. Similarly, $Q(k)$ may take values higher than 1 at some wavelengths in Eq. 3.3.9.

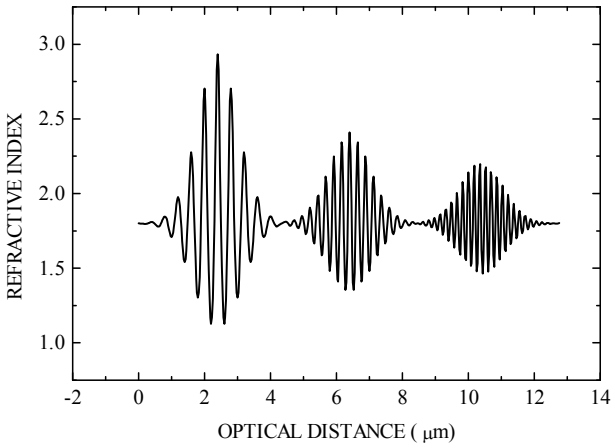


Fig. 3.3.1a Refractive index profile of a multiline, shifted rugate mirror design constructed by the use of Fourier transform

As one would expect, the multiline rugate mirror design consists of three well defined substructures corresponding to the three separate reflection bands corresponding to wavenumbers $k_{01}$, $k_{02}$ and $k_{03}$. The substructures are shifted relative to the geometrical centre of the inhomogeneous layer as defined by Eq. 3.3.6, the time shifting theorem of Fourier analysis. The corresponding shift parameters are $a_1$= 4 μm, $a_2$= 0 μm and $a_3$= -4 μm. It can also be clearly seen in the same figure, that *at lower frequencies a higher modulation in the*

*refractive index profile is needed to provide the same reflectance and mirror bandwidth than at higher frequencies*, as has been explained earlier.

By calculating the spectral performance of this multiline rugate mirror design, as shown in Fig 3.3.1b along with the specified reflectance values, we find that the structure exhibits high reflectances only at $k_1 = k_{01}/2 = 7.854\ \mu m^{-1}$, $k_2 = k_{02}/2 = 13.09\ \mu m^{-1}$ and $k_3 = k_{03}/2 = 18.176\ \mu m^{-1}$, as required. Distortions in the shape of the reflectance bands originate from multiple internal reflections within the substructures which is neglected during the application of Fourier transform, and from the multiplication factor we used in order to increase the refractive index modulation.

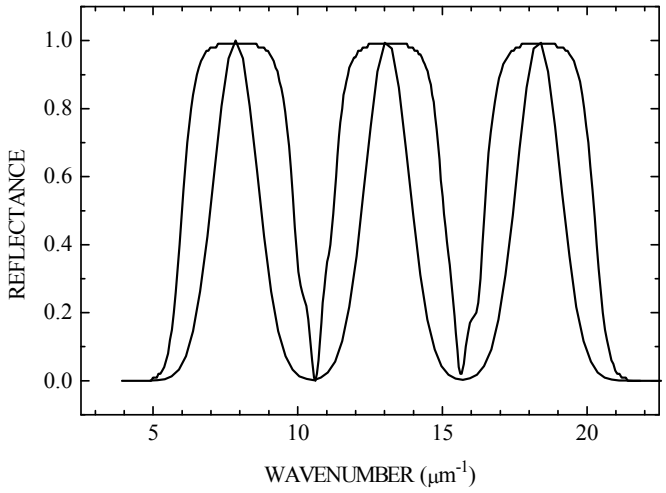


Fig. 3.3.1b Specified (dashed) and computed (continuous line) reflectance of a multiline, shifted rugate mirror design shown in Fig. 3.3.1a

With respect to the calculated group delay vs. wavenumber function, which is shown in Fig. 3.3.1c together with the specified values, we can conclude that the agreement between the specified and calculated values is fairly good. The group delay has been computed numerically by using the definition of Eq. 3.3.7. Note, that a constant group delay of $\tau_0 = 2 \times 6.388\ \mu m / (0.3 \times 10^{-9}\ m/s) = 42.583$ fs has been added to the calculated values. This group delay corresponds to the physical position mismatch between the centre of our inhomogeneous layer, which is our $x = 0$ position during the Fourier transform, and the top of the layer at the position of $x = 6.388\ \mu m$, where the phase shift on reflection is calculated. The slight parabolic change in the group delay functions around the mirror central frequencies is similar to the behaviour of quarterwave stacks consisting of discrete layers. It originates from

the increasing penetration depth of the electromagnetic field when the detuning from the mirror central frequency increases, as explained in detail in Chapter 1. This behaviour results in a positive third-order dispersion of the mirrors.

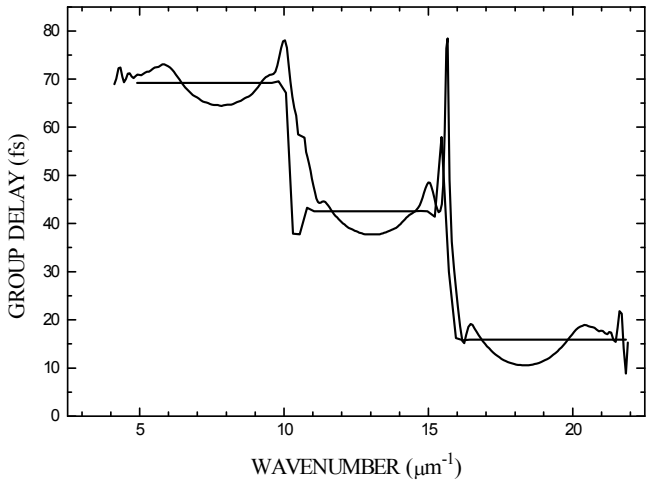


Fig. 3.3.1c Specified (dashed) and computed (continuous line) group delay of a multiline, shifted rugate mirror design shown in Fig. 3.3.1a

With respect to multiline, shifted rugate mirrors we can conclude, that a frequency dependent group delay function has been tailored by placing mirrors of different periodicities and finite bandwidths at different physical positions determined by Eqs. 3.3.5-3.3.8.

## 3.3.2. Chirped rugate mirrors

Generalizing this approach, now I introduce the concept of chirped dielectric rugate mirrors, in which the period of refractive index profile is linearly varied along the *x* axis in order to obtain high reflectivity and an approximately linearly decreasing group delay vs. frequency (or wavenumber) function over broad bandwidths. Its structure is derived from Eq. 3.3.3. as follows:

We define a second order phase factor $\Phi(k)$ as the function wavenumber, i.e. a second order phase shift on reflection (see Eq. 3.3.3b) written in the following form:

$$\Phi(k) = d_0 + d_1(k - k_0) + d_2(k - k_0)^2 \qquad (3.3.10a)$$

Then we define the Q-function $Q(k)$, i.e. the modulus of the complex amplitude reflectance (see Eq. 3.3.3a) as a Gaussian function:

$$Q(k) = \exp\left[-\frac{(k-k_0)^2}{2\sigma^2}\right] \tag{3.3.10b}$$

Calculating the frequency dependent displacement $\Delta x(k)$ of the refractive profile along the $x$ axis using Eq. 3.3.6 we obtain:

$$\Delta x(k) = d_1 + 2d_2(k-k_0) \tag{3.3.11}$$

or equivalently, using Eq. 3.3.8:

$$\tau_{DP}(k) = 2\frac{d_1 + 2d_2(k-k_0)}{c} \tag{3.3.12}$$

which is a linear function of the wavenumber, thus the angular frequency of the incident electromagnetic field.

Equation 3.3.11 shows that the different spatial frequency components are shifted linearly along the $x$ axis as functions of $k$, thus the second-order phase term in Eq. 3.3.9a results in a chirped dielectric rugate structure, as shown in Fig. 3.3.2a. The parameters that we used during the computations using Eq. 3.3.3 were: $k_0 = 2\pi$ / 0.4 $\mu m^{-1}$, which corresponds to our selected mirror central wavelength of 0.8 μm, $\sigma$ = 1.4 $\mu m^{-1}$, $d_1$ = 0 rad, $d_2$ = 0 μm, $d_3$ = -0.589 $\mu m^2$. The refractive index of the surrounding medium has been set $n_0$ = 1.8. In order to obtain reflectances high enough, we multiplied the right hand side of Eq. 3.3.3 by a factor of 8. *Using the method published by Southwell* [54-56], *the refractive index profile shown in 3.3.1 can be converted to a two-index solution by taking into account the dispersion of the coating materials as well. The two-value refractive index profile obtained after the conversion can be used as an initial design for further refinement, which will be discussed later in detail.*

In Fig. 3.3.2b, the computed reflectance of the chirped structure is presented along with the prescribed reflectance values. It is worth noting that the structure exhibits practically 100% reflectance from wavenumbers of 6.35 $\mu m^{-1}$ to 9.35 $\mu m^{-1}$, which correspond to wavelengths of 0.989 μm to 0.671 μm, respectively.

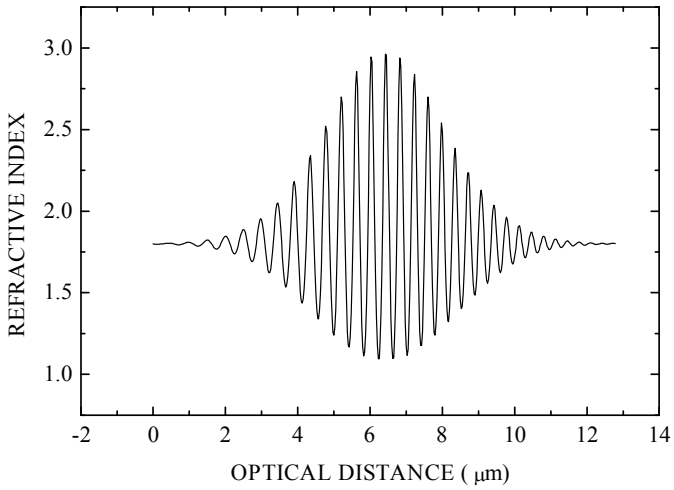


Fig. 3.3.2a Refractive index profile of a chirped gradient-index dielectric mirror design constructed by the use of Fourier transform

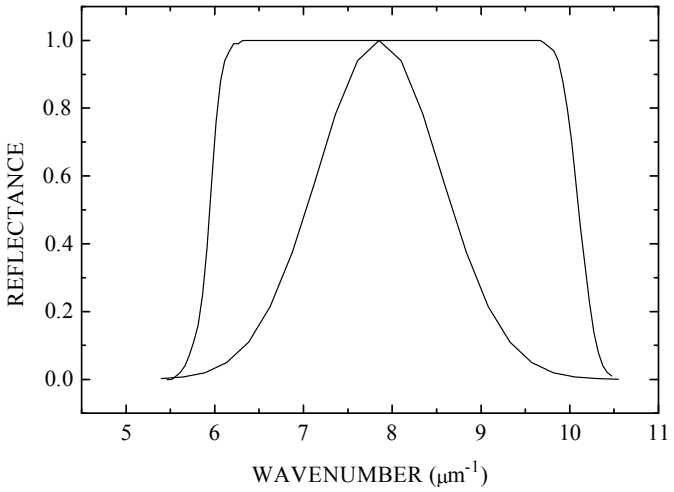


Fig. 3.3.2b Specified (dashed) and computed (continuous line) reflectance of chirped gradient-index mirror shown in Fig. 3.3.2a

Calculating the group delay introduced by the chirped mirror by using Eq. 3.3.7, the result of which is shown in Fig. 3.3.2c, we found that the group delay decreased monotonously with the function frequency (or wavenumber) over most of the high reflectivity band of the mirror. The mirror exhibits nearly constant GDD over the 6.5..9 $\mu m^{-1}$ wavenumber range corresponding to the wavelength range 1.0 to 0.7 μm. I note that a constant group delay of $\tau_0$ = 2 x 6.388 μm / (0.3 x $10^{-9}$ m/s) = 42.583 fs has been added to the prescribed group delay values. Although the calculated group delay vs. wavenumber function of the chirped structure slightly differs from the specified linear function, the design can be used as a starting design for further refinement after using the conversion method mentioned above.

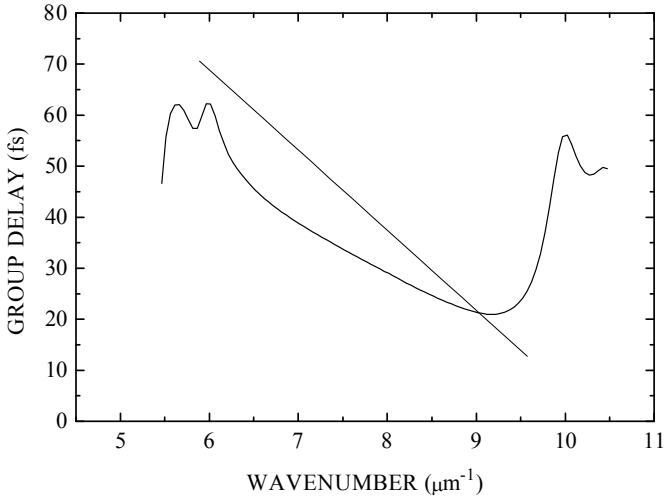


Fig. 3.3.2c Specified (dashed) and computed (continuous line) group delay of of chirped gradient-index mirror shown in Fig. 3.3.2a

# Chapter 4

# Design of discrete layer chirped mirrors

In this Chapter first I will investigate how to obtain an initial design consisting of discrete layers. First I present a conversion routine developed for transforming gradient index chirped mirrors into discrete value step-index and, as a second step, into two-index equivalents. I will derive the design from the formulae presented in Chapter 3.3 by applying the conversion methods presented in Refs. [55, 56]. This work is presented in Chapter 4.1.

In Chapter 4.2, I introduce an alternative, more straightforward approach referred to as *frequency domain synthesis of (two-index value) chirped mirrors*. Both approaches mentioned above result in suitable initial designs for further optimization.

In Chapter 4.3, I assume that I have an initial design obtained by either of these means. The aim is to find the best solution for a certain application problem bearing in mind the constraints on the parameters set by the technology (e.g., the refractive indices of available coating materials, the upper and lower limits of the individual layer thicknesses, the maximum overall thickness of optical coating), all of them depending on the technology utilized for coating deposition. Without disregarding generality, we restrict our treatment to the simplest practical case when the (chirped) laser mirrors are built of alternate discrete layers of high index ($TiO_2$) and low index ($SiO_2$) materials.

In the later chapters, I take a specific design goal: the first application problem I solved. I investigate the effect of deposition errors on this specific design, I show measured dispersion functions taken after the coating deposition process. The measured dispersion data correspond to a mirror set that was used to build a sub-10-fs mirror-dispersion controlled Ti:sapphire laser oscillator at the Advanced Photon Research Center of the Japan Atomic Energy Research Institute (Ibaraki, Japan).

By computing the electric-field distribution inside the two-index value chirped dielectric mirrors as a function of wavelength, I derive their dispersive properties purely from the wavelength dependence of the penetration depth of the incident optical field in accordance with our present physical (Chapter 2) and theoretical (Chapter 3) considerations.

## 4.1 Conversion of gradient index chirped mirror structures to discrete layer realizations

I thought that it might be interesting to present the chronological development of chirped mirrors before I ended up with the first designs consisting of nearly quarterwave layers of $TiO_2$ and $SiO_2$ [21, 57]. First, I investigated the dispersive properties of dielectric structures derived from the formulae in Chapter 3.3, and described by the following equation:

$$n(x) = \sqrt{n_H n_L}\,\exp\left( \ln\left(\sqrt{\frac{n_H}{n_L}}\right) * \exp\left(-\frac{x^2}{2\sigma^2}\right) * \sin[x * (k_0 + c_1 k_0 x)] \right) \qquad (4.1.1)$$

In Eq. 4.1.1, $n_H$ and $n_L$ denote the maximum and minimum values of the refractive index profile function where $n(x)_{MAX} = n_H = 2.3$ and $n(x)_{MIN} = n_L = 1.45$, according to the actual upper and lower limits of the refractive indices available; $x$ is defined as the optical distance similar to Eq. 3.3.2 (without the multiplication factor 2); $\sigma$ denotes the width of the Gaussian envelope function; $k_0$ denotes the wavenumber corresponding to the selected central wavelength ($\lambda_0$) fulfilling the Bragg condition $k_0 = 2k$, where $k = 2\pi/\lambda$, and $c_1$ is a linear (spatial) chirp parameter. With the parameters $\sigma = 2^{1/2}$ and $c_1 = \pm\ 0.02$, I obtained increasing or decreasing group delay functions with the frequency depending on the sign of the spatial chirp parameter $c_1$ as shown in Fig. 4.1.1.

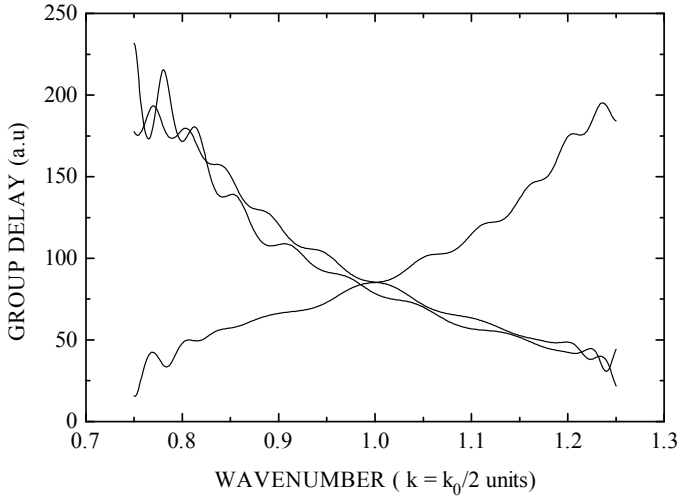


Fig. 4.1.1 Computed group delay vs. wavelength functions of positively (dashed) and negatively (continuous line) chirped gradient index profiles that are described in the text. The dotted curve corresponds to the discrete valued index profile shown in Fig. 4.1.2

I assumed the refractive indices on both sides of the dielectric structure be equal to $n_{ave}=(n_H n_L)^{1/2}$. The group delay functions were calculated by using the scattering matrix method [12, 13] after dividing the structure into 2048 sub-layers, which were assumed to have uniform refractive indices. As it can be seen in the figure, the group delay functions exhibit a positive or negative slope vs. the wavenumber (frequency) depending on the sign of the spatial chirp, *with some superimposed oscillatory behaviour*. I found that the amplitude of this *oscillatory behaviour is connected with parameters such as the shape and width ($\sigma$) of the envelope function*, the chirp parameter ($c_1$) and the amplitude of the refractive index modulation ($n_m$). It is worth mentioning here that a similar effect was observed by Southwell [56] in the case of (not dispersive) rugate filters, which oscillation was considerably reduced by the *proper choice of the apodization function*. It fits well with my previous theoretical calculations: using super-Gaussian or rectangular apodization functions, the oscillatory behavior was found to be even stronger. It will be shown later that the same behavior of the dispersive properties was observed in the case of chirped dielectric mirrors consisting of discrete layers.

Next I investigated similar structures consisting of nearly quarterwave thick layers with appropriately chosen refractive indices similar to that shown in Fig. 4.1.2, i.e., *sin(x)* function in Eq. 4.1.1 was replaced by a *sign[sin(x)]* function and the refractive index modulation was kept constant within a nearly quarterwave layer. The corresponding group delay vs. wavenumber function is plotted in Fig. 4.1.1 with dots. This gives practically the same curve that I obtained for the continuously varying refractive index profile determined by Eq. 4.1.1 with similar construction parameters. The group delay is computed for beam propagation to the direction of negative optical distances.

It must be pointed out that *by reversing the order of the deposition of the layer sequence* (or the direction of the incoming beam), *we reverse the slope of the group delay vs. wavenumber (frequency) function* of the chirped dielectric mirror structure, we get:

$$\tau_R(k_0 - \Delta k) \approx \tau(k_0 + \Delta k) \qquad (4.1.2)$$

where $\tau_R$ denotes the group delay vs. wavenumber function of the *spatially mirrored structure*.

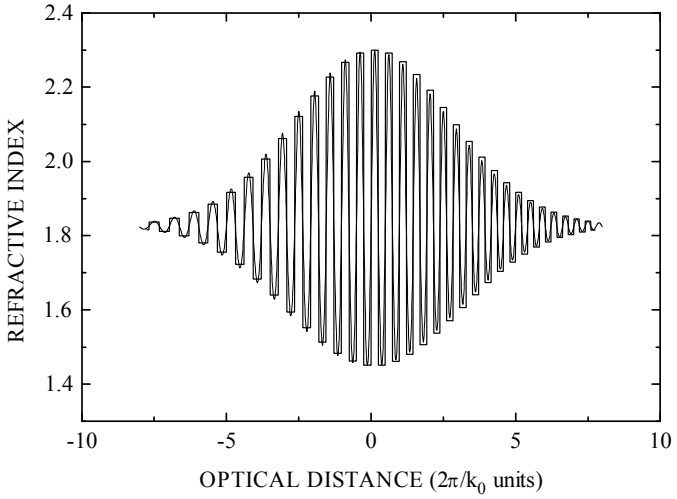


Fig. 4.1.2 Refractive index profile of a discrete value chirped dielectric mirror obtained by replacing the sin(*kx*) function with a sign[sin(*kx*)] function in Eq. 2.1.1

In practice, it means that *an initial chirped mirror design exhibiting a negative GDD can be easily converted to another design exhibiting a positive GDD of the same absolute value by revising the layer sequence, even in the case of chirped mirrors exhibiting a two-value refractive index profile*. For example, theoretically it would be possible to stretch and compress a bandwidth limited laser pulse to its original shape by properly designed chirped mirrors when the pulse first hits the structure from the right hand side (for stretching) and then from the left hand side (for compression). This feature directly follows from Eqs. 3.3.3 and 3.3.6 previously presented in Ref. [22]. Subsequently, similar "bulk chirped Bragg reflectors" for light pulse compression and expansion were proposed by Tournois and Hartemann [58].

Let me mention here that assuminging that there is no a lower limit to the layer thickness, the refractive index profile shown in Fig. 4.1.2 can be directly converted to a structure consisting of alternate layers of high and low index coating materials (such as $TiO_2$ and $SiO_2$) exclusively with the use of the conversion formula presented below. The formula shows that by mixing two layer materials with optical thicknesses that are small enough (e.g., 0.1 in $\lambda/4$ units) relative to the operation wavelength ($\lambda$), the composite layer exhibits an effective refractive index between the refractive indices of the two pure layer materials depending on their physical thickness ratio. In Eq. 4.1.3, $n_i$ is the refractive index of the *i*-th (nearly quarterwave) layer and $d_H$ and $d_L$ denote the physical layer thicknesses of elementary sublayers [54]:

$$n_i^2 = \frac{n_H^2 d_H + n_L^2 d_L}{d_H + d_L} \tag{4.1.3}$$

Practical realization of such structures depends on the thickness measurement accuracy of the coating deposition technology applied.

In general, we prefer optical coating designs consisting of nearly quarterwave layers because of technological purposes (e.g., minimizing stress in the coating, thickness control accuracy). Using the results published in Refs. [54, 55], it is possible to convert structures consisting of $N$ layers of different refractive indices (as shown in Fig. 4.1.2) into a two index solution consisting of $2N$ layers: we must convert each layer into $HL$ (or $LH$) equivalents using the following equations for the physical layer thicknesses $d_{i,H}$ and $d_{i,L}$

$$d_{i,H} = \frac{n_i^2 - n_L^2}{n_H^2 - n_L^2} d_i \tag{4.1.4a}$$

$$d_{i,L} = d_i - d_{i,H} \tag{4.1.4b}$$

Alternative methods of constructing two-index realization may be based on the recent work of Tournois [58] as well. It is worth pointing out that in Ref. [58], two basic solutions are proposed: (i) chirped Bragg reflectors consisting of half-wave stacks (i.e., half-wave chirped mirrors) and (ii) chirped Bragg reflectors consisting of quarter-wave stacks (i.e., quarter-wave chirped mirrors). In the former case, thin layers of $t_i << \lambda$ thicknesses are immersed in a medium of a different refractive index. The thickness $t_i$ of the $i$-th layer permits one to adjust the modulus of the elementary reflection coefficient $r_i$ in accordance with the formula presented in Ref. [58]. The stack is called half-wave because the optical distance between two adjacent thin layers is $\lambda/2$. However, when thin-film deposition technology is concerned, the half-wave stack solution causes serious technological problems as mentioned before: the relatively small thicknesses of the low refractive index layers compared to the high index components considerably increases the *internal stress* of the coating and this easily destroys a coating consisting of a large number of layers. Besides the standard (nearly quarterwave-stack) chirped dielectric mirrors with which we usually work, a combination of quarterwave layers and the thin layers mentioned above are proposed in Ref. [58].

In order to show the advantage and the weakness of the Fourier-transform technique and the conversion routine described above, below I present a chirped mirror design developed for full dispersion compensation in a white-light continuum compression experiment described in

Ref. [32]. Briefly, the estimated group delay dispersion of the white light continuum is ≅ 380 $fs^2$ at 600 nm and decreases to ≅ 220 $fs^2$ at 1 μm [32]. In order to compensate the nonlinear chirp of the continuum, chirped dielectric mirrors exhibiting high reflectivity and negative GDD with superimposed negative TOD from 600 nm to 1200 nm were developed using the design method described above. I introduced a quadratic spatial chirp parameter $c_2$ in Eq. 4.1.1 and modified the envelope function in order to obtain the index modulation best fitting the conversion routine parameters:

$$n(x) = \sqrt{n_H n_L}\,\exp\left( a * \frac{k_0}{k} \ln\left(\sqrt{\frac{n_H}{n_L}}\right) * \exp\left(-\frac{x^4}{2\sigma^4}\right) * \sin[x * (k_0 + c_1 k_0 x + c_2 k_0 x^2)] \right) \qquad (4.1.5)$$

where $n(x)_{MAX} = n_H = 2.315$ and $n(x)_{MIN} = n_L = 1.45$, $k_0 = 2*2\pi/0.8$ $\mu m^{-1}$ corresponding to our selected central wavelength of 800 nm, $\sigma = 5.49$ μm, $c_1 = 0.05$ and $c_2 = -0.002$ are dimensionless linear and quadratic spatial chirp parameters, $a = 1.35$ is dimensionless amplitude modulation factor. In Fig. 4.1.3, the refractive index profile obtained from Eq. 4.1.5 is shown.

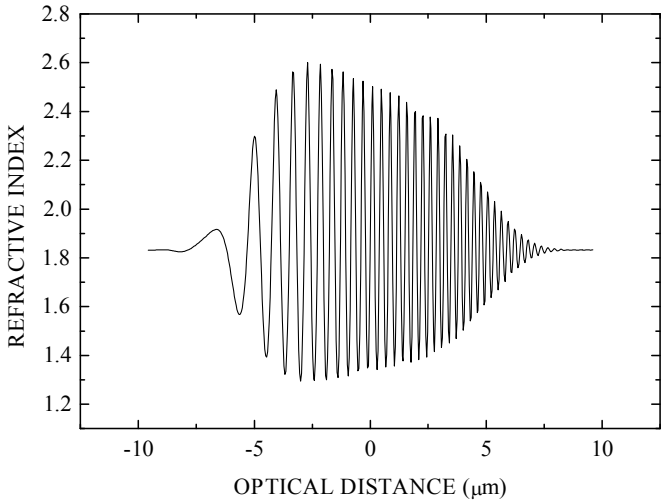


Fig. 4.1.3 Refractive index profile of an ultra-broadband gradient chirped dielectric mirror corresponding to Eq. 4.1.5. The mirror was developed for full dispersion compensation in the white-light continuum compression experiment described in Ref. [32].

First, the gradient index structure was converted to a step-index equivalent whose refractive index profile is shown in Fig. 4.1.4. Second, the step-index profile was converted to a two-index equivalent using Eqs. 4.1.4a-b that is shown in Fig. 4.1.5. It is worth mentioning here that the conversion routine results in a very interesting structure: the highest index modulations in the step-like index profile are converted basically to a λ/4 stack of high and

low index materials, while the lowest modulations are converted to λ/8 stacks exhibiting practically zero reflectivity at wavelength λ, as shown in Fig. 4.1.5. Between these two extremes, optical thickness values of the alternating high and low index layers gradually change resulting in a smoothly varying coupling coefficient over the layer structure. Note that partial reflectances at layer interfaces of a λ/4 stack meet in phase resulting in a high overall reflectivity while in a λ/8 stack they meet in anti-phase resulting in a low overall reflectivity.

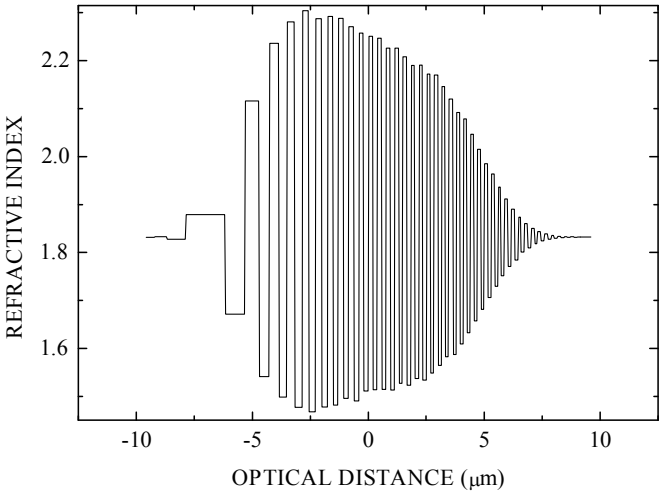


Fig. 4.1.4 Refractive index profile of the step-index equivalent of the gradient index profile shown in Fig. 4.1.3

Computed group delay functions and reflectance vs. wavelength functions of the gradient index structure, the step-index structure and the two-index equivalent are plotted in Fig. 4.1.6 and Fig. 4.1.7. As one would expect, the gradient index structure exhibit nearly ideal reflectance and group delay functions and the step-index equivalent still show very similar spectral response, in spite of the high partial reflectances at the layer interfaces. The two-index equivalent, however, is far from being an ideal solution of our application problem due to some resonant features occurring in both the reflectance and the group delay spectrum. Additionally, the structure still requires impedance matching layers at the substrate/coating and air/coating interfaces.

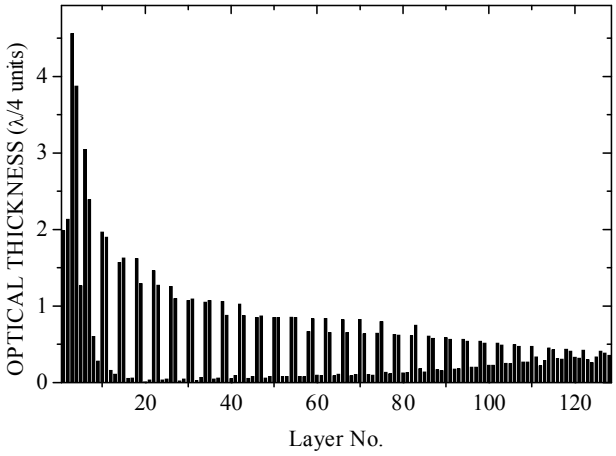


Fig. 4.1.5 Optical thickness coefficients of the two-index HL equivalent layers corresponding to the step-index profile shown in Fig. 4.1.4. Note that the highest amplitude index modulations are converted basically to λ/4 stacks while the lowest index modulations correspond to λ/8 stacks.

After a computer optimization process described in Chapter 4.3, it was possible to elliminate the resonant structures in both the reflectance and group delay functions (see Figs. 4.1.8 and 4.1.9). In our practice, oscillations in the group delay function are efficiently reduced by depositing two similar chirped mirror designs with slightly shifted central wavelengths and using them in pairs (see Fig. 4.1.9). As a preliminary experimental result, 6 fs pulses were obtained in the experiment described in Ref. [32] with the exclusive use of 4 pieces of dispersive mirrors.

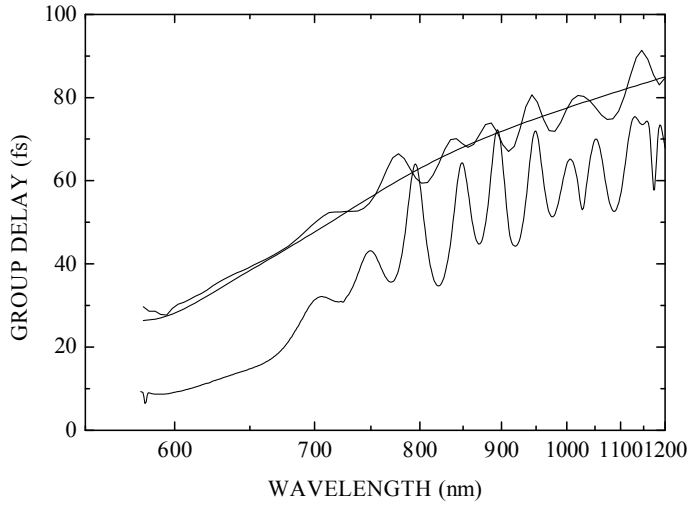


Fig. 4.1.6 Computed group delay vs. wavelength functions of the index profiles shown in Fig. 4.1.3 (continuous line), Fig. 4.1.4 (dashed line) and Fig. 4.1.5 (dotted line)

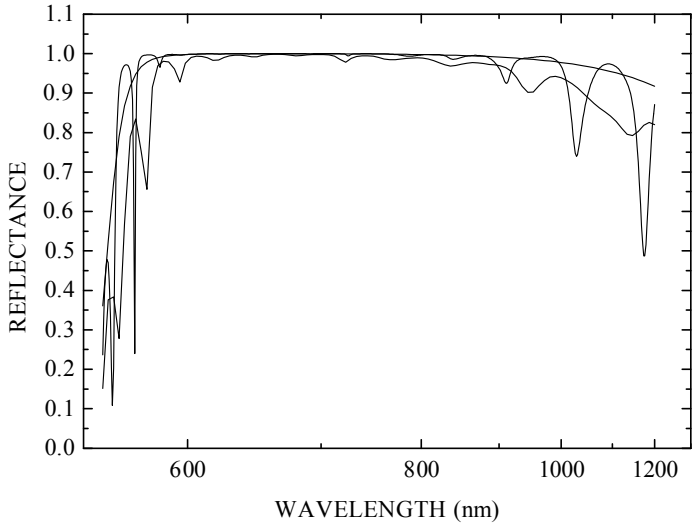


Fig. 4.1.7 Computed reflectance vs. wavelength functions of the index profiles shown in Fig. 4.1.3 (continuous line), Fig. 4.1.4 (dashed line) and Fig. 4.1.5 (dotted line)

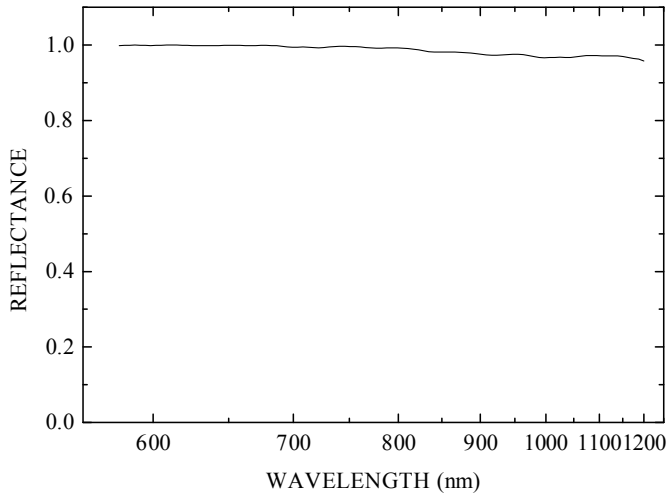


Fig. 4.1.8 Computed reflectance vs. wavelength function of the two-index equivalent after adding impedance mathing layers at the substrate/coating and coating/air interfaces and after computer optimization

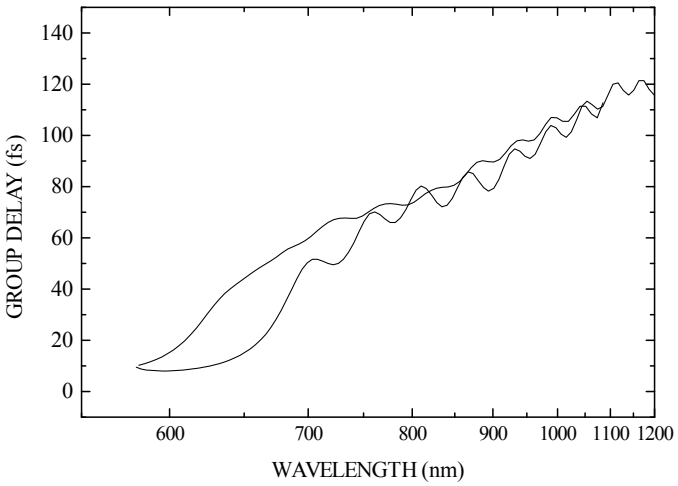


Fig. 4.1.9 Computed group delay vs. wavelength function (continuous line) of the two-index equivalent after adding impedance matching layers at the substrate/coating and coating/air interfaces and after computer refinement. Combination of two such chirped mirrors with slightly shifted central wavelengths results in lower oscillation in the overall group delay function (see dashed line). (The group delay is computed for two reflections in both cases.)

## 4.2 Frequency domain synthesis of chirped mirrors [59, 60]

In Chapter 4.1 I discussed a possibile approach for obtaining initial designs for ultrabroadband chirped mirrors (UBCM) with prescribed phase properties: using the Fourier-transform technique, UBCM-s with negative second-order and superimposed negative third-order dispersion were developed for the white-light continuum compression experiment reported in [32]. These mirrors exhibited high reflectivity (HR) from 580 to 1200 nm, i.e. over 267 THz. By the exclusive use of 4 pieces of such mirrors, 6 fs pulses were obtained in the same experiment. In spite of the fact that the spectrum supported sub-4-fs pulses [32], fluctuation in the group delay vs. frequency function did not allow us to reach this theoretical value.

In this Chapter I present an alternative, more efficient design approach [59, 60] to obtain an initial design for UBCM-s with broad reflection bands and basically linear group delay vs. frequency functions. The dielectric layer structure is described in the spatial frequency domain rather than by the individual layer refractive indices and optical thicknesses, thus the optimization (see Chapter 4.3) need to be performed only for a few (6-8) parameters instead of 40-60 parameters corresponding to the plurality of layers typically comprised in a chirped mirror design. This spatial frequency domain description can be understood on the basis of our theoretical work presented in Chapter 3.3.

We learned that the logarithmic refractive index modulation corresponding to different Bragg frequencies must be set inversely proportional to the frequency in order to obtain a uniform reflectivity over the HR range of the mirrors (see e.g., Eq. 3.3.3). In practice, however, it is rather difficult to fabricate such a design due to problems with the available optical materials and thickness control inaccuracies. However, the same behavior can be achieved in quarterwave stacks by detuning the relative optical thicknesses of the low (L) and high (H) refractive index layers, while keeping the Bragg period constant [58, 61]: $OT_L + OT_H = \Lambda/2$, where $OT_L$ and $OT_H$ stand for the optical thickness values of the low and high index layers and $\Lambda$ is the Bragg wavelength.

In connection with chirped mirrors, the term 'chirping' means that we change the Bragg wavelength along the plurality of layers, hence the different frequency components are reflected at different effective depths called penetration depth (see Chapter 2.2). Simple linear spatial chirping of the Bragg wavelength and a linear spatial detuning often referred to as 'double chirping' [61] do not automatically result in a linear group delay vs. frequency

function, let us just mention the problem of the frequency dependent refractive indices (dispersion) of the different layer materials. Usually, we have more general requirements regarding the dispersive properties of chirped mirrors including prescribed values for second-, third- and fourth-order dispersion as well.

I came to the conclusion that the most straightforward way to obtain an (initial) design is to describe the chirped mirror structure in the spatial frequency domain expecting that change of the local Bragg-wavelength ($\Lambda_i$) and local detuning ($\alpha_i$) of the *i*-th layer is a smooth function of *i*, hence it can be well approached by Taylor-series coefficients up to the third-order:

$$\Lambda_i = c_0 + c_1 \beta_i + c_2 (\beta_i)^2 + c_3 (\beta_i)^3 \qquad (4.2.1)$$

$$\alpha_i = d_0 + d_1 \beta_i + d_2 (\beta_i)^2 + d_3 (\beta_i)^3 \qquad (4.2.2)$$

In Eq. 4.2.1, $\beta_i = (i - n/2)/n$, where *n* stands for the number of unit periods ($i = 1..\ n$), and the *i*-th period is described as:

$$0.25\alpha_i \Lambda_i \ L \quad 0.5(1-\alpha_i) \Lambda_i \ H \quad 0.25\alpha_i \Lambda_i \ L \qquad (4.2.3)$$

Given the specification on the second-, third- and fourth-order dispersion for our chirped mirrors, we can perform our optimization process for the *c* and *d* coefficients only (6-8 parameters) - that results in an optimal solution within 1-2 minutes on a 266 MHz Pentium computer. Since the initial design is very close to the optimal solution, the final refinement process, when we perform the optimization for the individual layer thicknesses, usually also takes only 1 to 5 minutes.

Recently I used the above described algorithm for constructing chirped mirrors for the pulse-front-matched optical parametric amplifier described in Ref. [63]. The requirements for second- and third-order dispersion were $D_2 = -173\ fs^2$, and $D_3 = -110\ fs^3$, over the wavelength range of 550 to 750 nm. In order to get a physically feasible solution, these values were divided by 5 (5 overall reflections on chirped mirrors) for our specification. I chose our reference wavelength $\lambda = 640$ nm that corresponded to coefficient $c_0$, and obtained the design shown in Fig. 4.2.1.

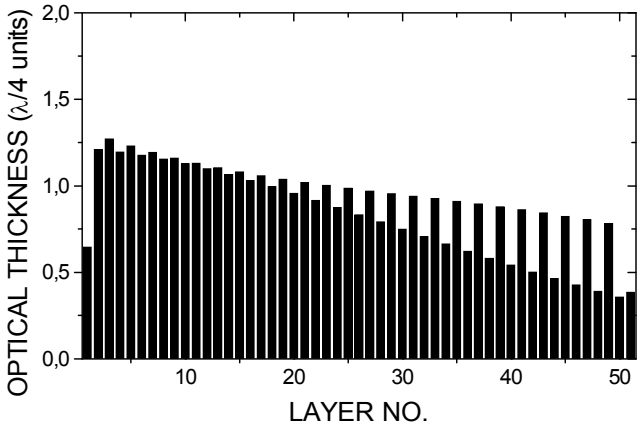


Fig. 4.2.1. Optical layer thickness coefficients of an ultrabroadband chirped mirror design obtained by frequency domain optimization. Even and odd layers stand for $TiO_2$ and $SiO_2$ layers, respectively.

In Fig. 4.2.2, the computed group delay vs. frequency function is shown after the final optimization process together with the measured values. Dispersion measurements were done for a pair of UBCM-s for higher accuracy and lower fluctuation in GDD. The measured GDD of the mirror pair is in the -35 .. -55 $fs^2$ range between 560 nm and 710 nm. The mirror pair presented was used for dispersion control in the experiment reported in Ref. [62] and resulted in 4.7 fs or tunable 7 fs pulses in the visible spectrum.

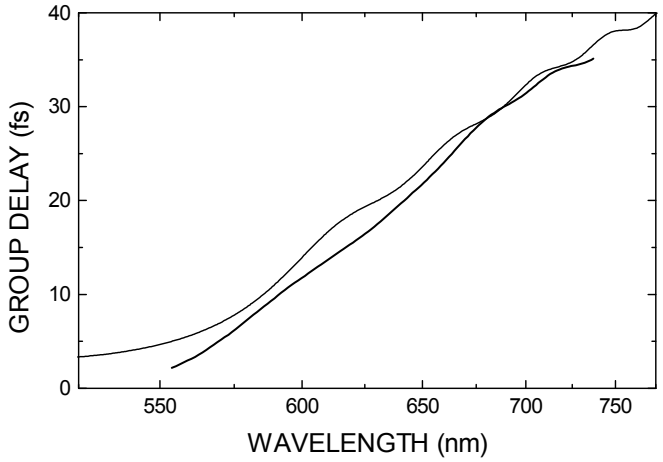


Fig. 4.2.2. Computed (dashed) and measured (continuous line) GDD of the ultrabroadband chirped mirror design after the final optimization and evaporation process. The design provides high reflectivity and a linear group delay versus frequency function over more than 145 THz.

## 4.3 Computer optimization

There is a practical problem in connection with the techniques described above: in practice, the dielectric layers are deposited on a substrate, e.g., on BK7 glass ($n_S \cong 1.51$) or fused silica ($n_S \cong 1.45$), whose refractive indices do not match the average value of the two coating materials used for evaporation. The situation is even worse on the top of the coating: the refractive index of air is 1.0. In the case of gradient index (e.g., chirped gradient index) structures, the problem can be efficiently solved by the use of quintic matching layers, which method is described e.g., in Ref. [63]. In the case of chirped mirror structures consisting of nearly quarterwave layers, however, it is difficult to find an analytical solution to the problem. Practically, it is an impedance matching problem that we usually face when we design AR coatings or dichroic mirrors that are transparent for the pump wavelengths. A straightforward way of solving the problem is to properly choose the optical thickness values of a limited number of top and bottom (impedance matching) layers of the design. In my practice, *numerical optimization procedures were used* in order to obtain suitable solutions.

Numerical procedures are widely used for optical coating design. For a review on these, I refer to the paper of Dobrowolsky and Kemp [64]. In my practice, most of the optimized coating designs are obtained by using the so called *simplex-method* [64]; however, for the *initial global search* slower but more efficient algorithms such as *generalized simulated annealing* [65, 66] or the g*enetic algorithm* (GA) [67] can be used. Nevertheless, the efficiency of each of the methods mentioned above strongly depends on the *proper choice of the target function and the performance (or merit) function*. Additionally, one has to *properly define the parameter space where the best solution of a specific application problem must be found* in accordance with the technology used for coating deposition. I call this parameter space *search space*. In general, it is a $2N$ or $2M$ dimensional space depending on whether the mirror structure is described by the individual layer parameters or in the spatial frequency domain introduced in the previous Chapter: $N$ is the number of layers in the system to be synthesized, $M$ stands for the number of the Taylor-series coefficients defined by Eqs. 4.2.1 and 4.2.2.

In the former case, one solution of the problem (a coating design) is described as a $2N$ dimensional vector $\mathbf{X} = \{(t_1,n_1), (t_2,n_2), \ldots , (t_N,n_N)\}$, where $t_i$ and $n_i$ represent the thickness and

the refractive index of the *i*-th layer of the system, respectively. To obtain a realistic solution, the refractive indices and the thickness must satisfy the following constraints: $n_L < n_i < n_H$, and $0 < t_i < t_{MAX}$ for each $i$ value, where $n_H$ and $n_L$ correspond to the lowest and highest refractive indices available. In the latter case, one solution of the problem (a coating design) is described as a $2M$ dimensional vector $\mathbf{X} = \{(c_o,d_0), (c_1,d_1), \ldots , (c_M,d_M)\}$, where $c_i$ and $d_i$ represent the Taylor-series coefficients defined by Eqs. 4.2.1 and 4.2.2. To obtain a realistic solution, the coefficients must fit the constraint on the layer thicknesses: $0 < t < t_{MAX}$ for each layer.

Without going into detail and referring to my corresponding patent in the United States of America [57], I define below two general *performance functions* for both the amplitude and phase properties, which are denoted as $MF_R$ and $MF_{GDD}$, respectively. In my practice, I have always had to find a compromise between the tolerances corresponding to the amplitude ($\delta R$) and the dispersive ($\delta GDD$) properties, whose overall value must be minimized by any of the optimization methods mentioned above. The performance functions are defined by the following equations:

$$MF_R(X) = \frac{1}{p}\sum_{j=1}^{p}\{[R(\lambda_j) - R_{OPT}(\lambda_j)]/\delta R_j\}^2 \qquad (4.3.1)$$

$$MF_{GDD}(X) = \frac{1}{p}\sum_{j=1}^{p}\{[GDD(\lambda_j) - GDD_{OPT}(\lambda_j)]/\delta GDD_j\}^2 \qquad (4.3.2)$$

where $R(\lambda_j)$ and $R_{opt}(\lambda_j)$ are the calculated and the desired reflection values, respectively, of the actual layer structure (fully described by vector $X$) at wavelength $\lambda_j$. Similarly, $GDD(\lambda_j)$ and $GDD_{opt}(\lambda_j)$ are the calculated and desired group-delay dispersion (GDD = $\partial^2\varphi/\partial\omega^2$) values at wavelength $\lambda_j$. Here $\varphi(\omega)$ denotes the phase change upon reflection from a dielectric mirror at frequency $\omega$. For oblique angles of incidences, $R(\lambda_j)$, $R_{opt}(\lambda_j)$, $GDD(\lambda_j)$ and $GDD_{opt}(\lambda_j)$ should correspond to the actual and desired reflectivities and the calculated and desired group-delay dispersion functions for *s*- or *p*-polarized light, respectively. *The novelty of my construction method is in the use of the merit function defined by Eq. (4.3.2); to the best of my knowledge, this had never been used before Refs. [21, 57] for optical coating designs.* Let me comment on why the GDD versus frequency (or wavelength function) is usually preferred to the phase vs. frequency ($\varphi(\omega)$) or group delay ($\tau = \partial\varphi/\partial\omega$) vs. frequency functions. In a femtosecond laser system, the operation of a femtosecond laser depends on the

intracavity GDD rather than the round-trip time in cavity, as discussed in Chapter 1.1. Upon reflection on a dielectric mirror a constant group delay changes the round-trip time by only a few femtoseconds, which is a very small value compared to the whole round-trip time of a (usually 1 to 4 m long) linear or ring cavity. Fixing the desired value of the group delay at a certain wavelength, we surely restrict the number of possible solutions, if they exist at all. However, the use of additional performance functions corresponding to higher-order derivatives of the $\varphi(\omega)$ function such as the third-order dispersion (TOD = $\partial^3\varphi/\partial\omega^3$), can be advantageous in some specific cases.

## 4.4 A numerical example: the first chirped mirror design tested in a laser oscillator

As an example, let us take one of my first designs [21, 57, 68], which was obtained by optimizing the layer thickness of a spatially chirped structure consisting of 42 alternate discrete layers of $TiO_2$ and $SiO_2$ with optical thickness around $\lambda/4$. During this initial work, I did not apply the methods presented in Chapters 4.1 and 4.2 directly. However, it was clear that a simple linear chirping of the Bragg wavelength does not result in *a linear group delay vs. frequency function*, since - among other problems - there are disturbing resonances in the computed group delay functions [19]. However, I was aware of the necessity of uniform coupling: besides the target function defined for the desired GDD function, during the first optimizations I defined a constant but not 100% reflectivity in Eq. 4.3.1! In other words, I left the problem of uniform coupling for the computer: I found this problem too difficult to solve analytically in a short time, and I was more interested in answering the question if a solution for this physical problem exists at all...

In this particular case, I worked with 42 D vectors only, since the refractive index values of the individual layers were not changed during the optimization process. The refractive index profile of the structure is shown in Fig. 4.4.1. It was obtained after several optimization processes with different target functions according to the dispersive properties of previous solutions. The corresponding optical layer thicknesses are depicted in the figure caption and in Ref. [57]. The design was developed for full dispersion control in a femtosecond pulse Ti:sapphire laser [57, 68]. Enhanced versions of the chirped mirror design shown in Fig. 4.4.1 were used in the experiment described, for example, in Ref. [69]. The mirror exhibited high reflectivity and nearly constant negative GDD of -41 ### 5 $fs^2$ over a

wavelength range from 720 nm to 890 nm. The computed GDD of the design is shown in Fig. 4.4.2. The structure still shows an increasing multilayer period toward the substrate, hence we call it a chirped mirror, even though the variation is far from what we can consider a regular spatial chirp.

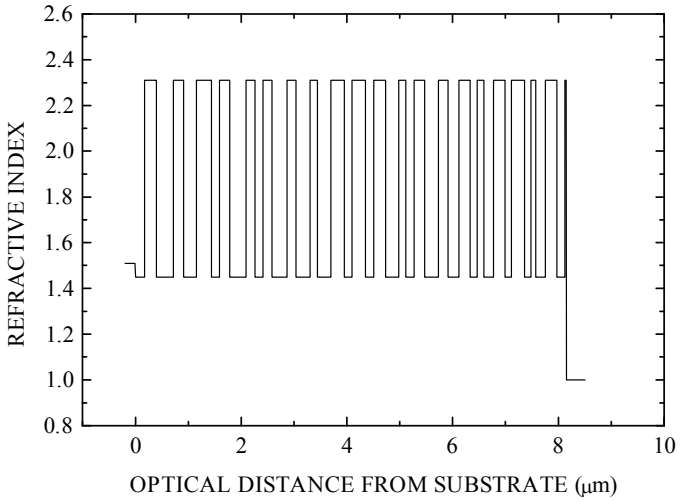


Fig. 4.4.1 The two value refractive index profile of a chirped dielectric laser mirror designed for full dispersion compensation in a mode-locked Ti:sapphire laser. Optical thickness coefficients of the design are [57]:

S | 0.87L 1.14H 1.58L 0.98H 1.18L 1.45H 0.75L 0.96H 1.57L 0.85H 0.73L 0.84H 1.45L 0.85H 1.31L 0.69H 1.30L 1.29H 0.69L 1.30H 0.81L 1.07H 1.25L 0.67H 0.81L 0.96H 1.35L 0.88H 1.03L 1.09H 0.62L 0.66H 0.87L 1.12H 0.62L 1.21H 0.63L 0.43H 0.93L1.07H 0.78L 0.16H | A.

S: substrate, $n_S$= 1.51; A: air, $n_A$ = 1.0; H and L: quarterwave layers of $TiO_2$ and $SiO_2$, respectively, at $\lambda$ = 790 nm, $n_H$ = 2.315, $n_L$ = 1.45

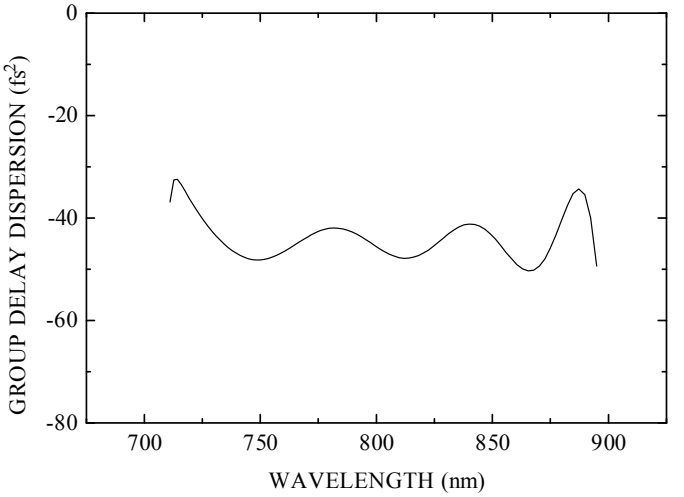


Fig. 4.4.2 Computed group delay dispersion of the chirped mirror design shown in Fig. 4.4.1

If the electric-field distribution inside this chirped mirror is computed as a function of the wavelength shown in Fig. 4.4.3a, it can be seen that the penetration depth (and thus the group delay) increases approximately linearly with the wavelength over the 720-890 nm range. For the electric field calculations, the results presented in Ref. [70] were used.

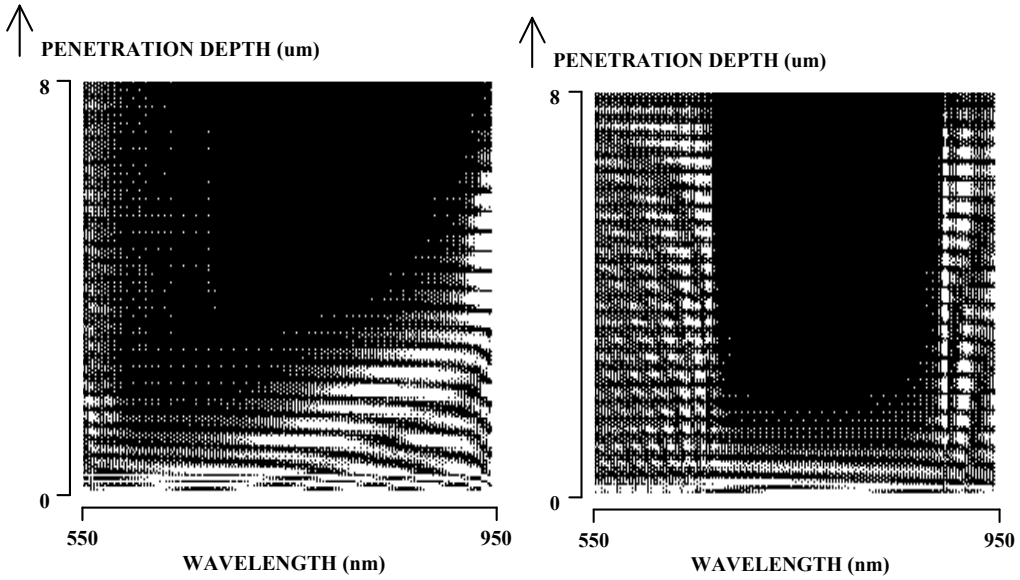


(a) (b)

Fig. 4.4.3a-b Computed electric-field distribution as a function of wavelength in (a) the chirped dielectric structure shown in Fig. 4.4.1 and in (b) a 44-layer low dispersion dielectric mirror consisting of alternating quarterwave layers of $TiO_2$ and $SiO_2$

The figure also gives a clear evidence of the high reflectivity of the mirror, as indicated by the disappearance of the optical field at the substrate-coating interface (penetration depth 8 μm). For comparative purposes, the electric-field distribution inside a traditional, low dispersion dielectric mirror consisting of 44 alternate quarterwave layers of $TiO_2$ and $SiO_2$ and centered at 770 nm is depicted in Fig. 4.4.3b. The penetration depth and thus the group delay is the smallest at the central wavelength of the quarterwave mirror and symmetrically increases with the detuning, as I explained in Chapter 2.2. It is clear that if one compares the electric-field distributions corresponding to the chirped mirror and the quarterwave mirror, chirped multilayer coatings are suitable for extending the bandwidth of standard low-dispersion quarterwave mirrors. However, I must note here that chirped dielectric laser mirrors exhibit an increasing group delay at the two ends of the high reflectivity range because of the same physical reason, and this is why their useful range is narrower than their high reflectivity range.

The achievable maximum negative GDD of chirped mirrors is limited by the maximum group delay difference that can be obtained between the extremes of the reflectivity range. This latter in turn related to the optical thickness of the coating. A simple approximate empirical expression for the maximum achievable group delay difference is [21]:

$$\Delta\tau_{\max} = \frac{2 \cdot (t_{chirped} - t_{qw})}{c} \qquad (4.4.1)$$

where $t_{chirped}$ is the optical thickness of the chirped mirror and $t_{qw}$ is that of a standard quarterwave high reflector (R > 99.5%) consisting of the same pair of alternating layer materials. In simple physical terms: the required high reflectivity of the dispersive mirror calls for a minimum optical thickness of $t_{qw}$ and only excess layers can introduce an appreciable frequency-dependent group delay around the center of the high reflectivity band. Assuming that the group delay varies approximately linearly with the frequency over the high reflectivity range, the corresponding upper estimate for the GDD is simply given by the ratio of ######$_{\max}$ to the mirror bandwidth ######. For the specific case of $TiO_2$-$SiO_2$ mirrors centered around 0.8 ###m, we have approximately $t_{qw}$ = 4 ###m (21 quarterwave layers) yielding approx. ######$_{\max}$ = 27 fs for our 8-###m-thick structures, in reasonable agreement with the results presented in Fig. 4.4.4.

With the number of layers fixed, ######$_{\max}$ scales linearly with the chosen central wavelength of the dispersive mirror. For a selected operating wavelength, ######$_{\max}$ and thus the magnitude of broadband negative GDD can be increased only by increasing the number of layers, this number being limited by scattering and absorption losses due to structural defects and impurities in the deposited layers, respectively [14].

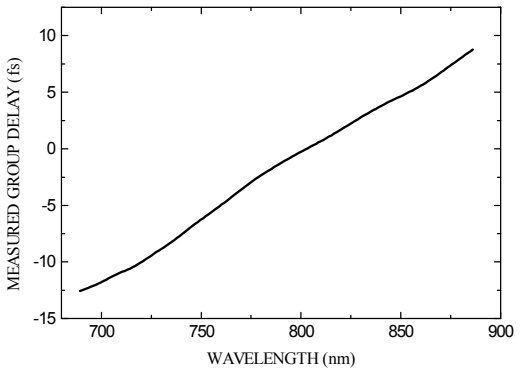


Fig. 4.4.4 Measured group delay versus wavelength function of the chirped dielectric mirror design shown in Fig. 4.4.1. The measurement was performed by the spectral phase interferometry method published in Ref. [40]

## 4.5 The effect of deposition errors

In this Chapter, I assume that I ended up with a design consisting of alternate discrete layers of high index (H) and low index (L) materials after the optimization process. Before the deposition of such a structure, the following questions arise: Can the design tolerate the inaccuracies in the layer thickness (and the refractive indices) appearing during the deposition process? If the answer is no, can we make a better design exhibiting lower sensitivity for deposition errors? Alternatively, can we improve the control of thickness/refractive index in our evaporation plant? In order to demonstrate the importance of these questions, I analyse the chirped mirror structure shown in Fig 4.4.1. I calculated the average deviation of GDD from its theoretical value when each layer thickness was varied by ±1% of the corresponding quarterwave layer: $\Delta t_i = \pm 0.0025\ \lambda_0 / n_i$ . In our example, the reference wavelength is $\lambda_0 = 775$ nm and the refractive indices of $TiO_2$ and $SiO_2$ are $n_H = 2.315$ and $n_L = 1.45$, respectively. Dispersion data were calculated for the wavelength range of 720 to 890 nm, the result of which is shown in Fig. 4.5.1.

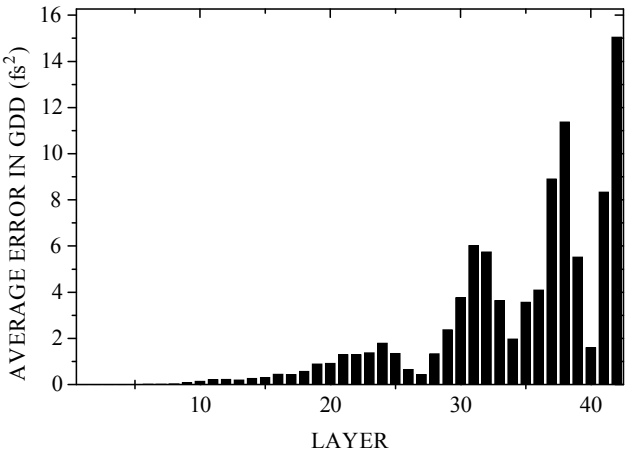


Fig. 4.5.1 The effect of deposition errors on the GDD vs. wavelength function of the chirped mirror design shown in Fig. 4.4.1

The striking feature of the plot is that dispersion of *this design is extremely sensitive to deposition errors*: for some layers the deviation from the prescibed dispersion value is, on average, as high as 15 $fs^2$, which is approximately 30% of the prescribed value. Note that the estimated variation of the layer thicknesses is a realistic value in our model; this estimated value can be applied for most evaporation plants. I do not need to mention that we were extremely fortunate with the dispersive properties of the chirped mirrors used for our first experiments, see Refs. [21, 68]. How can one improve the situation? First of all, by elaborating a better design that exhibitins a lower sensitivity to the deposition errors. Here I refer to the work of Greiner [71], who developed *robust optical thin film designs that are insensitive to the variation of layer parameters* by applying different search strategies. The design methods described in Ref. [71] can be adapted to our application problem as well. Second, the situation can be improved by applying enhanced thickness control during the evaporation. *The final solution to the problem, however, is based on the development of highly accurate methods for dispersion measurement on laser mirrors* [40, 41]. In the following, I briefly introduce our dispersion measurement apparatus and present representative GDD data corresponding to elements of a mirror-dispersion-controlled (MDC) Ti:S oscillator [57].

## 4.6 Dispersion measurement on laser mirrors

Generally, the apparatus I use is a Michelson interferometer [40] illuminated by a white-light source (tungsten halogen lamp). The setup is shown in Fig. 4.6.1. I place a low dispersion gold mirror in the "reference" arm and the chirped dielectric mirror to be measured in the "sample" arm. When one of the mirrors is tilted around a horizontal axis while the other mirror is vertical, horizontal interference fringes are generated by each spectral component of the white-light source at the exit plane of the interferometer. Transmission grating and an achromatic lens are used to create the spectrally dispersed image of a vertical section of the superimposed "white light" interference fringes on a CCD array; the section is created by a vertical slit. The interference patterns corresponding to different wavelengths are linearly dispersed in the horizontal direction, as shown in Fig. 4.6.2.

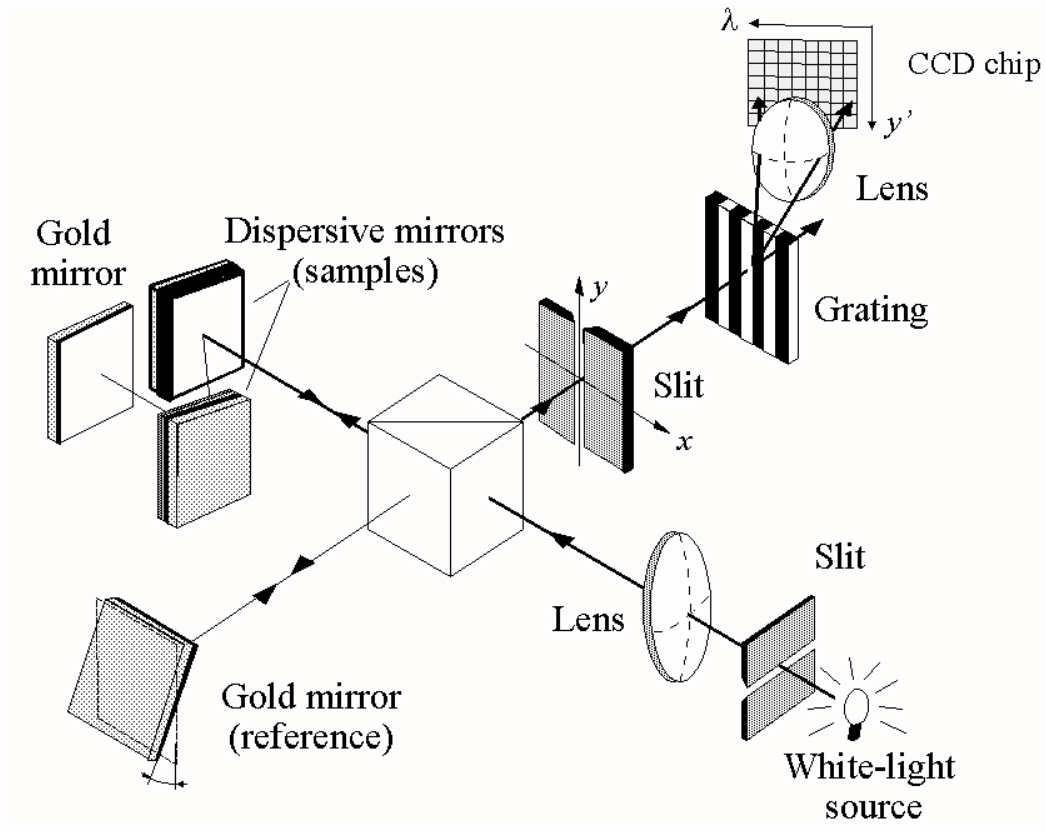


Fig. 4.6.1 Spectrally resolved white light interferometer for phase dispersion measurement on dielectric laser mirrors [40].

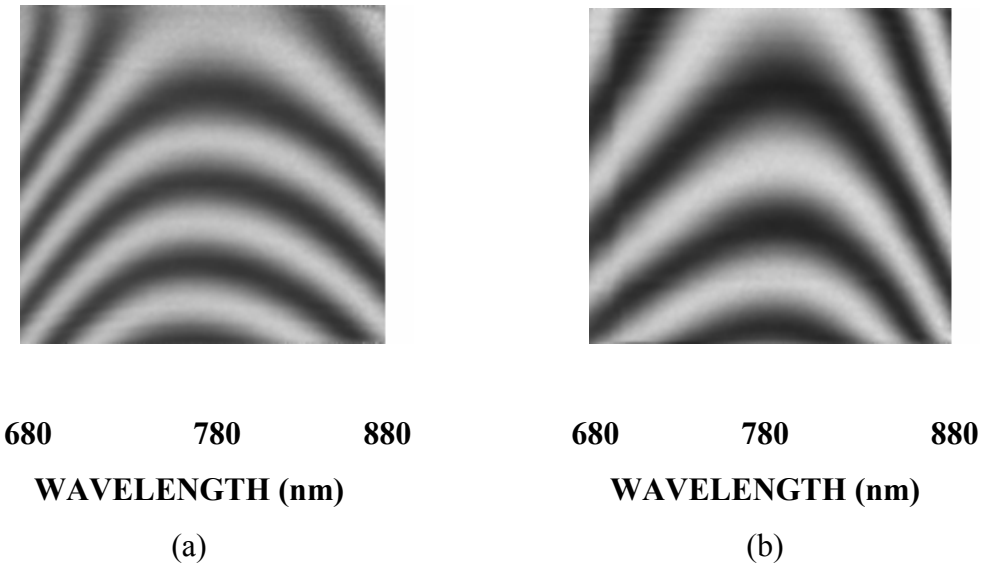


Fig. 4.6.2a-b Spectrally resolved white-light interference fringes recorded on the CCD chip (see Fig. 4.6.1), when pairs of chirped mirrors (a) with a pure negative quadratic phase and (b) with negative GDD and superimposed positive TOD are placed in one arm of a Michelson interferometer illuminated by a tungsten halogen lamp [40]

In the case of Fig. 4.6.2a, a pair of *chirped mirrors developed for full dispersion control in a mode-locked Ti:S oscillator* [21, 23, 57, 68, 69] were placed in the sample arm of the interferometer. To record the image shown in Fig. 4.6.2b, however, a pair of chirped mirrors developed for a *prism pair - chirped mirror compressor* [30, 40] *exhibiting negative GDD with a superimposed positive TOD* was used.

The period of the interference fringes in the vertical direction is proportional to the wavelength when using ideal flat mirrors for the measurement. If the mirror in the sample arm is to have no phase dispersion, the vertical pixel positions corresponding to the same phase difference, e.g., minima and maxima, would be a linear function of the wavelength [40]. Because of the second-order phase shift of one sample mirror (a) and the second-order phase shift with superimposed positive third-order dispersion of the other mirror (b) I was able to record the images shown in Fig. 4.6.2. By storing and computer-processing the spectrally resolved interference pattern detected on the CCD, we can easily obtain the group delay and GDD versus wavelength functions of the sample mirrors within a few minutes using a 100 MHz personal computer.

## 4.7 Chirped mirror set for a mirror-dispersion controlled Ti:sapphire laser oscillator

As an example, here I present the measured GDD versus wavelength functions of some chirped mirror pieces used to build a MDC Ti:S laser pumped by a Millennia (Spectra-Physics, Inc.) laser at the Advanced Photon Research Center of the Japan Atomic Energy Research Institute (Ibaraki, Japan) [72]. Figure 4.7.1 illustrates the schematic laser setup. The laser exhibits a standard linear cavity [68, 69] comprising a 2.1 mm long (optical path) Ti:S crystal ($\alpha$ = 6 $cm^{-1}$) whose dispersion is compensated by 7 reflections on chirped mirrors in one round-trip. M1 and M2 are standard quarterwave mirrors that are transparent for the pump wavelength. Measured GDD functions of the chirped mirror pieces are plotted in Fig. 4.7.2. We use 4 reflections on mirror M4 (dotted curve), 2 reflections on M5, and one reflection on M3. The overall GDD originating from these chirped mirrors is also plotted in Fig. 4.7.2 (continuous line). It can be seen that the overall GDD of the chirped mirrors is a nice, nearly constant function from 740 to 860 nm. It follows that it is possible to realize a nearly optimum GDD vs. wavelength function for most of the application problems mentioned above by measuring the GDD vs. wavelength functions of each chirped mirror piece after the deposition with high accuracy and by the proper selection of the mirrors.

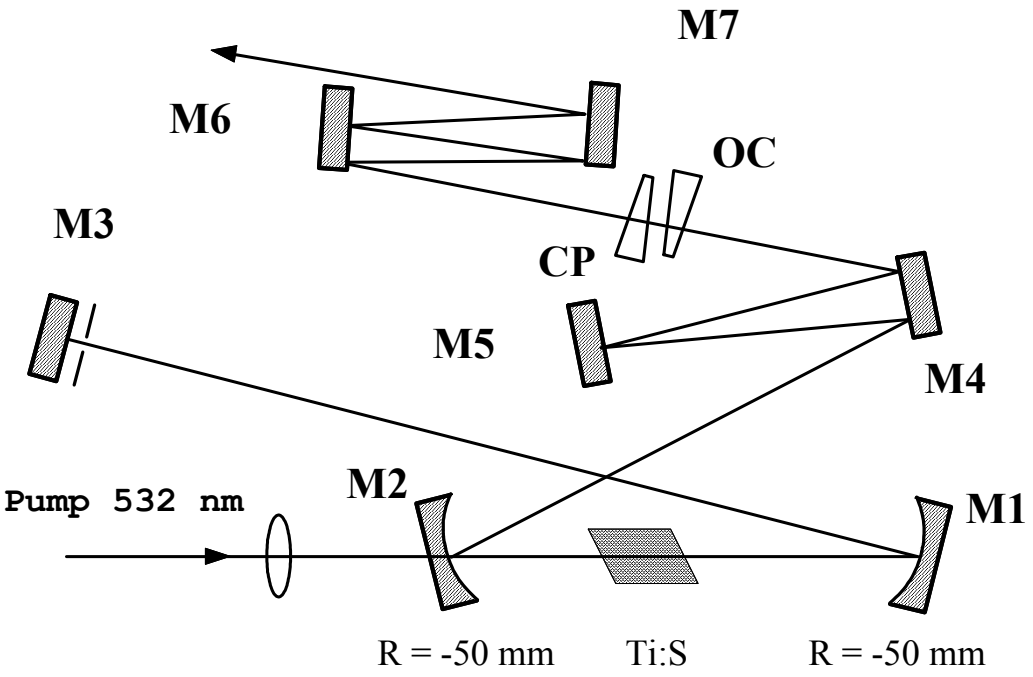


Fig. 4.7.1 Schematic laser setup of a mirror-dispersion-controlled KLM Ti:S laser [57, 68, 69, 72]. M1-M2: dichroic, curved folding mirrors; M3-M7: chirped dielectric laser mirrors; Ti:S: Ti:sapphire crystal; OC: T = 16% wedged output coupler; CP: wedged compensating plate.

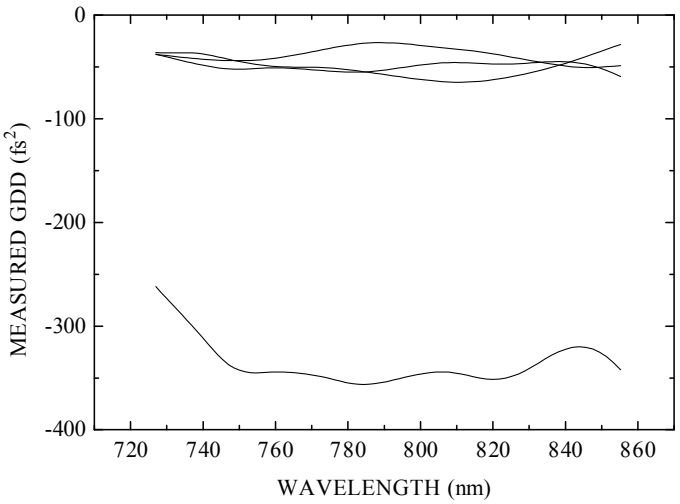


Fig. 4.7.2 Measured GDD vs. wavelength functions of the chirped mirror pieces used for building a sub-10-fs Ti:S oscillator shown [72]

# Chapter 5

# Multi-cavity thin-film Gires-Tournois interferometers: an alternative to realize "negative dispersion" mirrors

In this Chapter, an alternative approach for realizing dielectric laser mirrors with pure negative quadratic phase shift on reflection is introduced. I refer to them as *multi-cavity thin-film Gires-Tournois interferometers* (MCGTI): their dispersive properties originate from coupled resonances in multiple λ/2 cavities embedded in the layer structure in contrast to chirped mirrors. These novel devices exhibit extremely low reflection losses (R > 99.95%) when they are manufactured by our state of the art ion-beam sputtering technique and high-order dispersion-free group delay vs. frequency functions (e.g., -50+/-1 $fs^2$) over a bandwidth of 56 THz. Accordingly, they support clear, pedestal free, sub-15-fs pulses in mirror-dispersion-controlled solid state laser oscillators introduced in Chapter 4.7.

## 5.1 Parseval theorem of optical interference coatings

The increased bandwidth (≈150THz) of chirped mirrors relative to standard, quarterwave dielectric high reflectors (≈80THz) can be achieved only at the expense of reduced reflectivities (R ≤ 99.8%). This fact directly follows from the Parseval-theorem of optical interference coatings [22, 53]:

$$\int_{-\infty}^{\infty}\left(\frac{n'(x)}{n(x)}\right)^2 dx = \int_{-\infty}^{\infty} R(k)dk \qquad (5.1.1)$$

where $R(k) = |r(k)|^2$ is the intensity reflectivity at wavenumber $k$, ($k = \omega/c$), while $n'(x)/n(x)$ is the logarithmic derivative of the refractive index resulting in partial Fresnel reflections along the optical distance $x$. Obviously, given the technological constraint on the refractive index modulation and the overall optical thickness of a dielectric high reflector, the bandwidth of any high reflector can be increased only at the expense of reduced reflectivity.

## 5.2 Applications that require extremely low loss dispersive mirrors

A number of practical laser systems require minimum reflection losses and high-order dispersion-free group delay control over a frequency range of 50..80 THz, that still support (i) clear, pedestal free sub-15-fs pulses or, (ii) sub-100-fs pulses tunable over a 100..120 nm around 800 nm. Such applications might include (a) sub-15-fs pulse generation in compact, mirror-dispersion-controlled, diode pumped femtosecond pulse Cr:LiSAF and Cr:LiSGaF lasers [25, 26] or (b) low pump threshold, mirror-dispersion-controlled femtosecond pulse Cr:LiSAF [73] or Ti:sapphire [57] lasers.

Before Ref. [60] and [74] were published, two major types of dispersive mirrors had been tested in femtosecond pulse laser systems: (i) thin-film Gires-Tournois interferometers (GTI) [36, 37] and (ii) chirped dielectric mirrors (CM) discussed in detail in Chapter 4. As I mentioned in Chapter 2, there is a very important difference in the physical origin of their frequency dependent group delay, however: in GTI-s, the electric field is captured in Fabry-Perot like, resonant $\lambda/2$ cavities, while in CM-s the group delay is strongly connected with the frequency dependent penetration depth of the electric field. Thus (single cavity) GTI-s suffer from higher-order dispersion limiting the laser performance to 40-50 fs pulses [25], while CM-s currently allow pulse generation below 5 fs [32, 62].

## 5.3 Multi-cavity Gires-Tournois interferometer designed for the Coherent Vitesse XT tunable laser

During our recent studies [60, 74] we found that there is an alternative approach for obtaining *pure quadratic phase shift on reflection* from such dielectric mirrors: it can be realized with multi-cavity GTI-s (MCGTI-s) as well. The initial design was obtained by the needle optimization technique [75, 76] using a special, upgraded version of our "Optilayer" software. After a final refinement process we came to the solution shown in Fig. 5.3.1.

In conventional (single-cavity) thin film GTI-s, the layer structure consists of a $\lambda/4$ stack with a single $\lambda/2$ resonant cavity layer on the top of the quarterwave mirror [36, 37]. In MCGTI-s more than one (in this example three) separate, slightly detuned $\lambda/2$ cavities (layer 26, 30 and 34) with embedded $\lambda/4$ layers are responsible for the dispersive properties of the mirror.

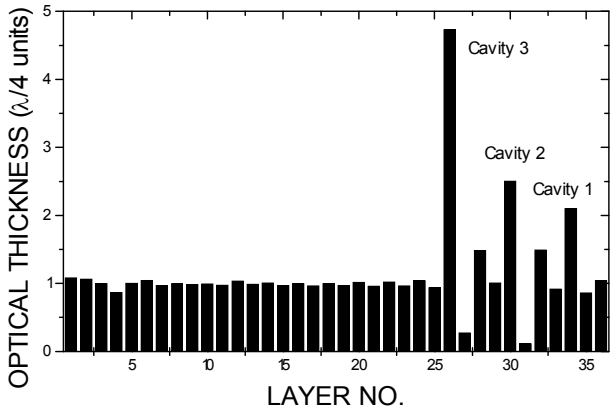


Fig. 5.3.1 Optical layer thickness coefficients of a multi-cavity thin-film Gires-Tournois interferometer. The design provides high-order dispersion-free negative GDD over a bandwidth of 56 THz with theoretical reflectivities higher than 99.97%. Even and odd layers stand for $SiO_2$ and $TiO_2$ layers, respectively

The computed GDD vs. wavelength function of the design is shown in Fig. 5.3.2. The central wavelength of the design was chosen to be $\lambda = 0.8$ μm in this specific case. The design provided a negative GDD of -50+/-1 $fs^2$ over a bandwidth of 56 THz. For comparative purposes, the computed GDD of a single cavity GTI is also plotted in the figure. The *quarterwave layer mirror stack* (layers 1 to 25) provided the extremely high reflectivity of the design that is shown in Fig. 5.3.3.

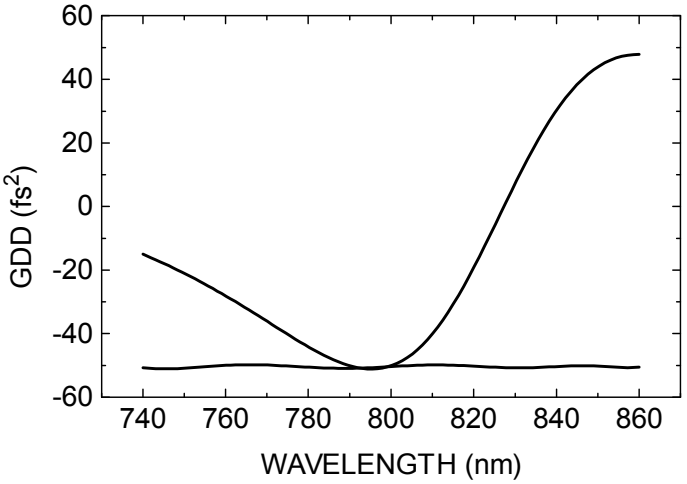


Fig. 5.3.2 Computed GDD of the multi-cavity GTI (continuos line) compared to that of a conventional single cavity GTI (dashed)

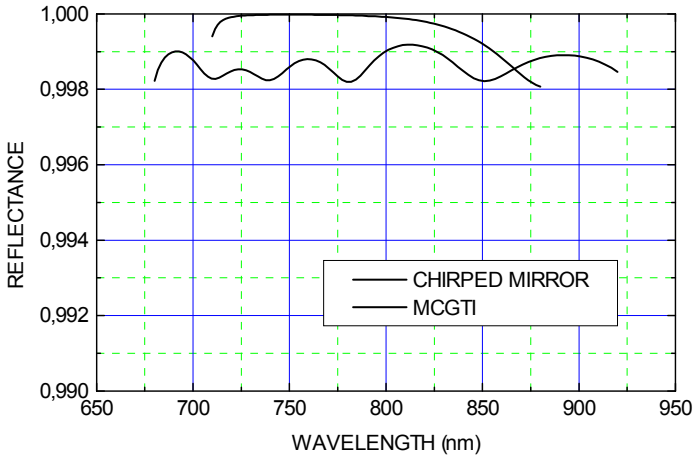


Fig. 5.3.3 Computed reflectance of the multi-cavity GTI (continuos line) compared to that of a standard chirped mirror design (dashed)

It is worth pointing out that the GDD function and the reflectivity shown in Fig. 5.3.2 and Fig. 5.3.3 (plotted with continuous lines) can be fabricated with the use of state-of-the-art coating deposition technologies, such as ion-beam sputtering [77]. Another important issue is that the layer structure can be easily adapted for any other wavelength regime from the ultra-violet to the near infrared simply by rescaling the layer thickness. Our recent laser experiments show that our multi-cavity GTI-s show negligible reflection losses even in the ultraviolet; the standing electric field is concentrated in the $SiO_2$ layers that have relatively low absorption and scattering losses.

## 5.4 Performance comparision of chirped mirrors and Multi-cavity Gires-Tournois interferometers

Before I present our experimental results, the following question should be addressed: can it be proved that dispersion of MCGTI-s originates from resonances rather than the frequency dependent penetration depth (like in case of negative dispersion mirrors referred as chirped mirrors)? Our answer is yes. In Fig. 5.4.1, computed group delay vs. wavelength function of a MCGTI with an increased GDD is shown. During the design, the overall optical thickness and number of layers forming the quarterwave stack was kept constant, only the optical thicknesses of the top layers were altered. From the calculation of the overall optical thickness of the top (phase correction) layers, the maximum group delay difference that could have been obtained over the high reflectivity range (see Eq. 4.4.1) was limited to 36 fs - if it is

connected with the frequency dependent penetration depth only. However, the computed difference is definitely higher: it reached values up to 45 fs.

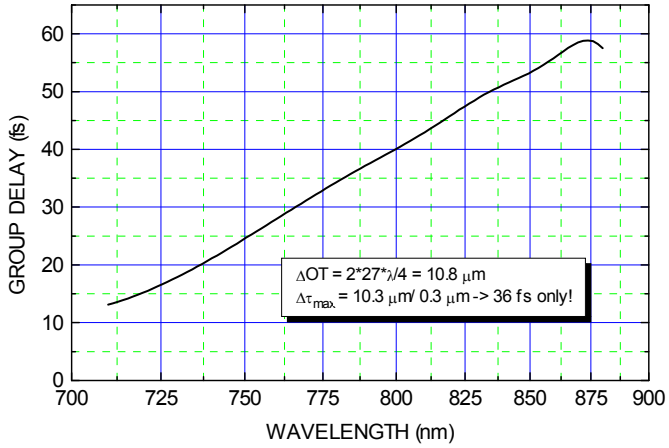


Fig. 5.4.1 Computed group delay vs. wavelength function of a multi-cavity GTI designed for higher values of GDD

I also studied the distribution of the standing wave electric field in the MCGTI design shown in Fig. 5.3.1, I found that the electric field is mostly localized in the (coupled) cavities shown in Fig. 5.3.1, while it has relatively low intensities in the impedance matching layers between them. I found that the electric field is captured by one or two of the cavities at each wavelength. By tuning the wavelength, the electric field is shifting gradually from one cavity to the next one. Finally, the change of the electric field in the layer structure results in a linear group delay vs. wavelength function according to the localization of the electric field. During the optimization process, the "strength" and length of the cavities are adjusted by the layer thicknesses.

As an example, measured GDD vs. wavelength function of a MCGTI designed for a mirror-dispersion-controlled, sub-100-fs, tunable Ti:S laser is plotted in Fig. 5.4.2 (the measured GDD function corresponds to the theoretical curve previously shown in Fig. 5.3.2).

Based on our experimental results, I am convinced that multi-cavity GTI mirrors will find their applications similarly to chirped laser mirrors owing to their simple structure (thus relatively low manufacturing costs), high reproducibility and extremely low reflection losses (R> 99.95%).

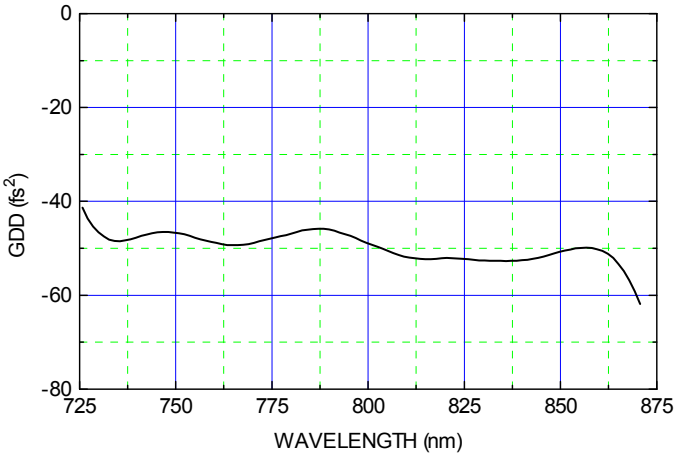


Fig. 5.4.2 Measured GDD of an ion-beam sputtered multi-cavity GTI designed for full dispersion control in a tunable sub-100-fs Ti:S laser oscillator

# Chapter 6

# Defining target functions for computer optimization

## 6.1 Reflection loss in dielectric high reflectors and its relation to the wavelength dependent group delay

In Chapter 5 I pointed out that there are several application problems where the requirement for minimum reflection loss on the mirrors is of primary importance, let me just mention diode pumped, mode-locked, mirror-dispersion-controlled fs solid-state lasers. I found that negative dispersion mirrors referred to as multi-cavity Gires-Tournois interferometers might have higher reflectivity than chirped mirrors and this can be explained by Parseval theorem introduced in Chapter 5.1. In dielectric high reflectors, the reflectivity can be expressed in the following form:

$$R(\lambda) = 1 - T(\lambda) - \Delta S(\lambda) - \Delta A(\lambda) \qquad (6.1.1)$$

where $\Delta T(\lambda)$, $\Delta S(\lambda)$, and $\Delta A(\lambda)$ stand for the wavelength dependent (!) transmission, scattering and absorption losses, respectively. So far I have dealt with ideal dielectric materials, i.e., materials without absorption and scattering. Unfortunately, this approximation is rarely valid even if we use state of the art coating deposition techniques such as ion-beam-sputtering [60, 77], and the situation is even worse in the case of standard electron beam evaporation technique [14].

In the previous chapter I wrote that through proper choice of the dispersive mirror coating design we can reduce the transmission loss $\Delta T(\lambda)$ at the expence of reduced bandwidth. However, the wavelength dependent absorption and scattering loss are more enhanced in dispersive dielectric high reflectors than in case of standard quarterwave dielectric high reflectors as it will be explained below.

Considering scattering loss $\Delta S(\lambda)$ I recall that the optical quality of substrates is described by the rms (root-mean-square) roughness ($\sigma$). According to Ref. [78] (and

assuming a wavelength independent reflection delay of $\tau = 1$ fs), the scattering loss ($\Delta S_\sigma$) of high reflectors corresponding to a rms surface roughness $\sigma$ can be described by the following formula at wavelength $\lambda$:

$$\Delta S_\sigma(\lambda) = \left(\frac{4\pi\sigma}{\lambda}\right)^2 \tag{6.1.2}$$

The results of Eq. 6.1.2 are the following: (i) the scattering losses decrease towards the longer wavelengths; (ii) a lower surface roughness (originating from the higher quality of the substrates or from the higher density of the deposited layers) reduces the scattering losses. In connection with (i), we recall that in chirped dielectric mirrors with anomalous dispersion the group delay increases towards the longer wavelengths. During my studies [14] I found that in dielectric high reflectors the wavelength dependent scattering and absorption losses are proportional to the corresponding reflection delay! This fact directly follows if we consider a finite bandwidth pulse with a central wavelength of $\lambda$. The wavelength dependent reflection delay $\tau(\lambda)$ corresponds to the optical distance of

$$L(\lambda) = c\,\tau(\lambda) \tag{6.1.3}$$

where $c$ stands for the speed of light in vacuum. Absorption (and scattering) losses depend on the propagation distance $L(\lambda)$:

$$\Delta A(\lambda) = 1 - \exp\left[-\alpha L(\lambda)\right] \tag{6.1.4}$$

where $\alpha$ stands for the absorption (scattering) coefficient of the optical material. The absorption coeffefficient can be calculated as:

$$\alpha(\lambda) = \frac{2\pi}{\lambda} k(\lambda) \tag{6.1.5}$$

where $k$ stands for the imaginary part of the complex refractive index $N(\lambda) = n(\lambda) - ik(\lambda)$. I note that we use the complex refractive in our calculations [12, 13] for computing the spectral reflectance and transmittance of the dielectric coating. In the case of small absorption (scattering) coefficients compared to the propagation distances calculated by Eq. 6.3 (which condition is fulfilled in our practical cases) and in case of wavelength independent absorption (scattering) coefficient, the wavelength dependent absorption (scattering) losses on dispersive dielectric mirrors can be approximated as:

$$\Delta A(\lambda) = const * \tau(\lambda) \tag{6.1.6}$$

The connection betwen the phase dispersion of dielectric mirrors and the absorption (scattering) losses is demonstrated in Figs. 6.1.1a-b, where the computed group delay versus wavelength function is compared to the corresponding absorption of the same mirror structure. Refractive index values are $n_S$ = 1.51 (BK7), $n_A$ = 1.0, $n_H$ = 2.31 and $n_L$ = 1.45. Extinction constants $k_H$ = 0.0001 and $k_L$=0.0001 of $TiO_2$ and $SiO_2$ respectively are used for the calculations.

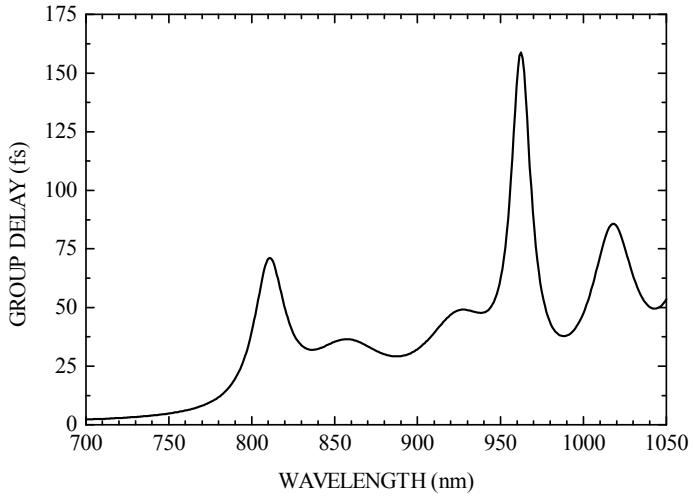


(a)

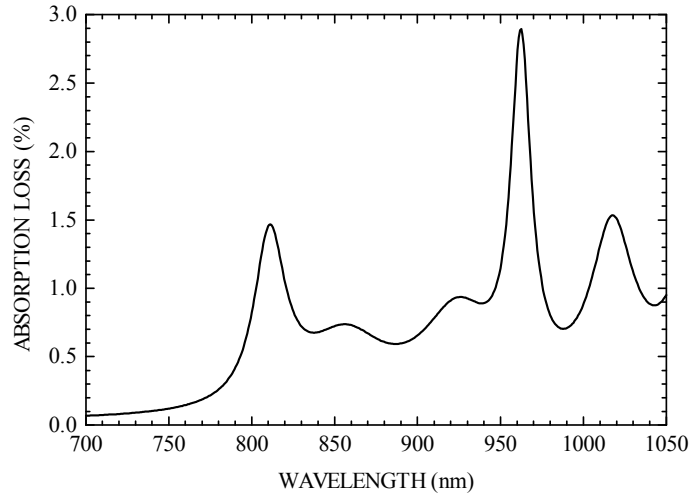


(b)

Fig. 6.1.1a-b Comparision of (a) group delay and (b) absorptance versus wavelength functions of the "classical" broadband dielectric mirror design of Substrate 0.6 $[H2LH]^9$ 0.5 $[H2LH]^9$ 0.42 $[H2LH]^9$ Air. H and L are quarterwave layers of $TiO_2$ and $SiO_2$ at the reference wavelength of 800 nm. At resonant wavelengths, the increased group delay results in increased absorption and scattering losses [14].

As a summary, I can say that reflection losses on chirped mirrors can be minimized by (i) reducing the absorption and surface roughness (σ) of the dispersive dielectric mirror and/or (ii) reducing the maximum value of the reflection delay. The former possibility was experimentally tested by depositing dielectric high reflectors with different coating materials and deposition technologies, the result of which is demonstrated in Fig. 6.1.2.

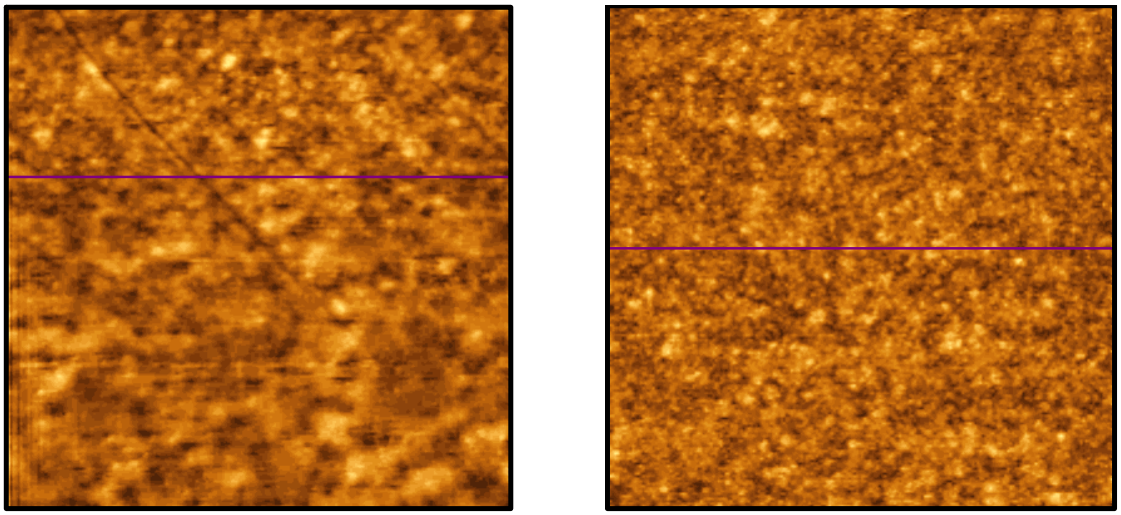

Fig. 6.1.2 Atomic Force Microscopy measurements on chirped laser mirrors using different coating materials and technologies for coating deposition. The lower grain size results in lower scattering losses of the mirrors.

By properly choosing the substrates, the coating materials and the technology for coating deposition, we were able to significantly decrease the surface roughness of our mirrors. Further technical details on the coating deposition technology are available in Refs. [14, 60, 77].

In case of dispersive dielectric mirrors such as chirped mirrors and multi-cavity Gires-Tournois interferometers, we can say that the maximum value of the group delay is traded off against the bandwidth of the mirror, as follows from the definition of the *GDD*:

$$GDD = \frac{d\tau}{d\omega} \cong \frac{\Delta\tau}{\Delta\omega} \qquad (6.1.7)$$

In other words, a certain amount of positive $GDD_{MEAS}$ in the cavity calls for a minimum negative GDD originating from dispersive dielectric mirrors for dispersion compensation. The reflection losses on the mirrors, however, can be reduced by reducing the overall group delay on reflection - which can be minimized at the expense of the reduced bandwidth ($\Delta\omega$)! This condition shows that overestimating the bandwidth specification for dispersive dielectric mirrors results in higher reflection losses and thus should be avoided!

## 6.2 Dispersion measurement on laser crystals

In order to design a compact laser setup comprising only chirped mirrors for intracavity dispersion compensation, precise information is required on the dispersion data not only of the dispersive mirrors but also of the laser active materials utilized. During my studies, however, I was unable to find dispersion data on some laser active materials, e.g., Cr:LiSGaF. On the other hand, the dispersion data I found in the literature did not fit my measured data in some other cases, e.g., in the case of a Cr:LiSAF crystal. Moreover, I observed strong dependence of the measured GDD on doping concentration and/or the supplier of the crystal.

In the following I summarize the method we developed [79] for accurate dispersion measurement on laser crystals, and present the measured dispersion data on colquiriite type solid-state laser active materials such as Cr:LiCAF, Cr:LiSAF and Cr:LiSGaF. Additionally, I present our dispersion data obtained for highly doped Ti:sapphire crystals as well. The dispersion curves were obtained by measuring the white-light interference fringes in the frequency domain, which is often referred to as the frequency-domain interferometer technique [80] or spectrally resolved white-light (SRWL) interferometry [81, 82]. We show that the same experimental apparatus is suitable for measuring the overall dispersion of laser cavities [83] comprising laser active media, prism pairs and dispersive dielectric mirrors.

Our experimental apparatus is basically the same as was used for group-delay measurement on dispersive dielectric mirrors [40], but we made some minor modifications. The optical elements to be characterized are placed in the "sample" arm of a Michelson interferometer. The interferometer is illuminated by a white-light source (tungsten halogen lamp). The white-light interference fringes appearing at the output of the interferometer are spectrally dispersed by a grating and imaged into a CCD camera by an achromatic lens. However, we had to slightly modify both the experimental setup and the evaluation process of the SRWL fringes when measuring refractive media because of the following physical problems: (i) At a certain wavelength, the spatial periodicity of the interference fringes is not constant, since the fringes are formed by two spherical waves with different curvatures. It is mentioned that the interferometer has to be aligned close to zero group delay difference in the two arms (as discussed later in details). Furthermore, the two mirrors of the Michelson

interferometer must be set parallel in order to avoid inaccuracies originating from the frequency dependent refraction in the "sample" arm. Consequently, the method described in Ref. [40] cannot be applied. (ii) Because of some of the cavity components are birefringent, two different interference patterns are formed corresponding to ordinary and extraordinary rays in the case of crystals and s- and p-polarized light for dispersive dielectric mirrors. In order to avoid overlapping of these two patterns, we placed a polarizer in front of the light source. (iii) An additional problem with laser active media is their fluorescence over the spectral range of our interest, that reduces the visibility of the SRWL interference fringes. One way to solve this particular problem is to use suitably chosen long wavelength pass filters. The birefringent laser active crystals were placed on a rotating table and were positioned as if they were built in laser cavities: the p-polarized light beam hits their surface at the Brewster angle and the propagation direction in the crystal is perpendicular to the optical axis (extraordinary rays, *E* parallel with the *c*-axis).

The intensity distribution of the SRWL interference pattern can be described by the following formula:

$$I(\omega) = I_S(\omega) + I_R(\omega) + 2\sqrt{I_S(\omega)I_R(\omega)}\cos(\varphi_{S,R}(\omega)) \qquad (6.2.1)$$

where $I_S$ and $I_R$ denote the intensities in the sample and reference arms, respectively, and $\varphi_{S,R}$ is the phase difference between the two arms of the interferometer at frequency ω. Detailed analyses on the forming of the SRWL fringes and determination of the phase difference $\varphi_{S,R}(\omega)$ are given in Refs. [81] and [82]. However, these works focus merely on determining the refractive indices of dye solutions [81] and optical glasses [82]. In connection with femtosecond laser systems, however, the higher derivatives of $\varphi_{S,R}(\omega)$ are important: the group delay ($\tau = \partial\varphi/\partial\omega$), the group-delay dispersion (GDD = $\partial^2\varphi/\partial\omega^2$) and third-order dispersion (TOD = $\partial^3\varphi/\partial\omega^3$) of the optical elements under study.

A typical normalized intensity distribution of a SRWL interference pattern is shown in Fig. 6.2.1, when a laser active crystal with an average dispersion of GDD ≅ 260 $fs^2$ is inserted in the interferometer.

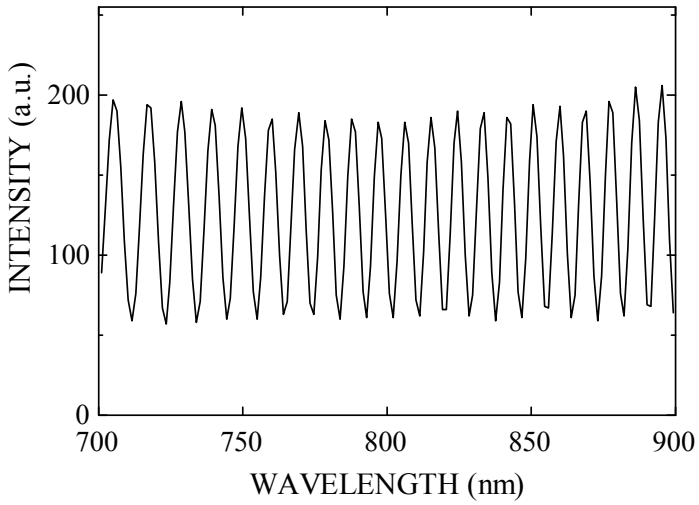


Fig. 6.2.1 Normalized intensity distribution of a spectrally resolved white-light interference pattern, when a laser active crystal exhibiting a GDD ≅ 240 $fs^2$ is placed in the sample arm of the Michelson interferometer

Note that the frequency dependent group-delay function can be determined by measuring the periodicity of the fringes in the frequency domain:

$$\tau \approx \frac{2\pi}{\Delta\omega} \tag{6.2.2}$$

where $\Delta\omega = \omega_2 - \omega_1$ and $2\pi = \Delta\varphi = \varphi(\omega_2) - \varphi(\omega_1)$, and $\omega_2$ and $\omega_1$ correspond to two neighbouring frequencies exhibiting a phase difference of $2\pi$. In practice, however, we used an enhanced computer algorithm for fast, high accuracy measurements.

Basically, there are two possible alignments for recording the SRWL fringes: setting the so called stationary phase point (SPP, $\partial\varphi\partial\omega = 0$) either to the low or to the high frequency side beyond the investigated frequency range [81]. Having no dispersive element in the interferometer, the periodicity of the fringes is constant in the frequency domain, and depends only on the path difference in air of the two arms. In general, it is worth working close to the SPP because the finite resolution of the spectrograph limits the maximum value of $\tau$ that can be measured by this method (see Eq. 6.2.2). It should be noted that this finite resolution is usually determined by the finite number of CCD elements. Another physical issue has to be considered, however: What is the sign of the GDD function, i.e. if the group delay increases or decreases with the frequency? The answer is easy if we determine the SPP positions for two different reference arm lengths, but not from a single shot measurement.

During my studies, I investigated the dispersive properties of Cr:LiSAF, Cr:LiCAF, Cr:LiSGAF and Ti:S crystals as laser active media used for ultrashort pulse generation. Since the refractive indices of these materials can be described by smooth functions, dispersion can be retrieved after expanding the measured phase retardation φ(ω) of the crystals around an arbitrarily chosen central frequency $\omega_0$ :

$$\varphi(\omega) = \varphi_0 + \varphi'(\omega - \omega_0) + \frac{1}{2}\varphi''(\omega - \omega_0)^2 + \frac{1}{6}\varphi'''(\omega - \omega_0)^3 \qquad (6.2.3)$$

where $\varphi_0=\varphi(\omega_0)$ and the derivatives φ', φ'' and φ''' are the Taylor expansion coefficients at $\omega_0$.

The Taylor expansion coefficients I obtained corresponding to the different laser active materials and doping concentrations are listed in Table 6.2.1. The reproducibility of my independent measurements was generally within a ±3% error bar, whose average values were taken for Table 6.2.1. To calculate the theoretical GDD values, we (A.P. Kovács) used the refractive index polynomials we found in the literature and a ray-tracing program. By comparing our measured data with the theoretical values, we were able to draw the following conclusions: (i) in the case of our Ti:S and Cr:LiCAF crystal the measured GDD values fit quite well with the data in Refs. [84, 85] and 86. However, for our Cr:LiSAF crystals, the results considerably differ from the data found in Ref. [3] (see Fig. 6.2.2).

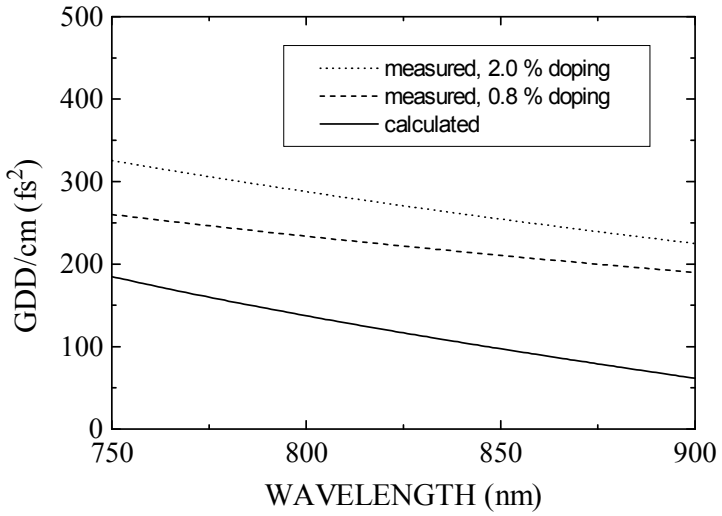


Fig. 6.2.2 GDD vs. wavelength functions plotted for 2x5 mm long LiSAF crystals with different Cr doping concentrations: (i) 0.8 % (Lightning Optical Corporation), (ii) 2.0 % (Strathclyde University, Glasgow). Dispersion of the crystals was measured at the Brewster angle for extraordinary rays. The calculated values correspond to the Sellmeier formula (see Ref. [3]).

Since we found that the dispersion of our Cr:LiSAF and Cr:LiSGaF crystals strongly depends on the doping concentration of these crystals, the discrepancy regarding our Cr: LiSAF crystals could originate from this fact, since no doping data were presented in Ref. [3].

| SAMPLE | $\omega_0$ ($fs^{-1}$) | $\lambda_0$ (nm) | $\varphi''$ ($fs^2$/cm) | $\varphi'''$ ($fs^3$/cm) |
|---|---|---|---|---|
| Cr:LiSAF (0.8%) | 2.23 | 845 | 213 | 168 |
| Cr:LiSAF(2.0%) | 2.23 | 845 | 256 | 240 |
| Cr:LiCAF(12%) | 2.40 | 786 | 253 | 240 |
| Cr:LiSGaF (0.8%) | 2.26 | 834 | 304 | 215 |
| Cr:LiSGaF (2.0%) | 2.26 | 834 | 308 | 322 |
| Ti:S ($\alpha$= 5 $cm^{-1}$) | 2.40 | 786 | 602 | 414 |

Table 6.2.1 Dispersion coefficients of a few solid-state laser active crystals for extraordinary rays. The GDD is calculated as: $GDD = \varphi'' + \varphi'''(\omega-\omega_0)$. The investigated spectral ranges are 760 to 900 nm for the Cr:LiSAF, Cr:LiSGaF and Cr:LiCAF crystals, and 700 to 900 nm for the Ti:S crystal. Crystal manufacturers: Lightning Optical Corporation (0.8% Cr doped LiSAF, 0.8% doped LiSGaF, 12% doped LiCAF), Strathclyde University, Glasgow (2.0 % Cr doped LiSAF and 2% Cr doped LiSGaF), and Crystal Systems (Ti:S).

It is worth noting that the same setup and evaluation method was successfully used for measuring the overall dispersion of laser cavities comprising prism pairs, dispersive dielectric mirrors and laser active crystals, thereby allowing us to optimize the intracavity dispersion of femtosecond pulse solid-state lasers. As an immediate result of our present measurements on laser active crystals suitable for direct diode pumping, sub-20-fs pulses have been generated from an extremely compact laser setup comprising Cr:LiSAF and Cr:LiSGAF crystals and chirped mirrors for intracavity dispersion control [26]. Additionally, by slight modification of our experimental apparatus, we can easily optimize extracavity pulse compressors consisting of prism pairs and dispersive mirrors [32].

## 6.3 Computing the target function for GDD optimization

As I mentioned in Chapter 1 the pulse duration of mode-locked solid-state lasers strongly depends on the intracavity overall negative GDD, which is related to their soliton-like pulse shaping mechanism. Hence the number of reflections on the chirped mirrors and their nominal GDD/reflection value have to be chosen in accordance with the actual dispersion of other intracavity elements such as the laser active medium (see Chapter 6.2). Accordingly, the target function defined by Eq. 4.3.2 must be derived as:

$$GDD_{OPT}(\lambda_j) = -\frac{GDD_{MEAS}(\lambda_j)+|\Delta GDD_{RES}|}{m} \tag{6.3.1}$$

where $m$ is the (integer) number of reflections on chirped mirrors in the cavity per round-trip, $GDD_{MEAS}(\lambda_j)$ is the measured overall (positive) GDD vs. wavelength function of other cavity elements, and $\Delta GDD_{RES}$ is the absolute value of the optimum overall (negative) GDD for mode-locked operation.

With precise information on the dispersion of Cr:LiSAF and Cr:LiSGaF crystals obtained by measuring their phase shift vs. wavelength functions in the frequency domain (see Chapter 6.2), we were able to construct compact mirror-dispersion-controlled Cr:LISAF and Cr:LiSGaF laser oscillators [26].

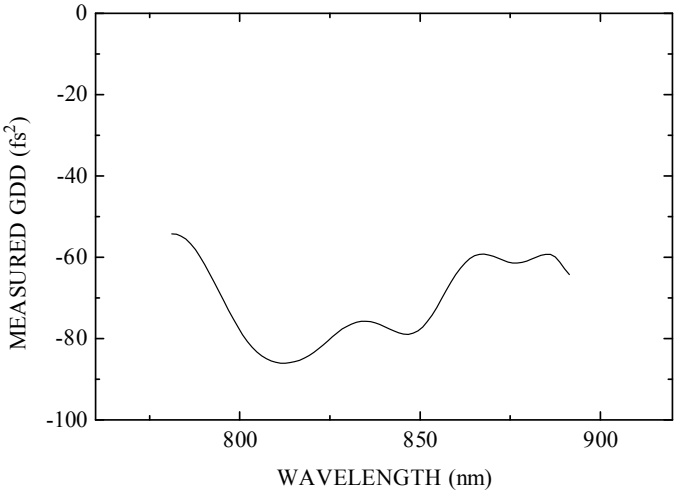


Fig. 6.3.1 Measured GDD vs. wavelength function of negative dispersion mirrors designed for sub-20-fs Cr:LiSAF and Cr:LiSGaF lasers [26]

For the experiment described in Ref. [26], chirped mirrors exhibiting an increaed GDD per reflection of ≅ -80 $fs^2$ from 800 to 900 nm were constructed. Measured GDD vs. wavelength function of the mirrors are shown in Fig. 6.3.1. Both of our Cr:LiSAF and Cr:LiSGaF lasers delivered sub-20-fs pulses from an extremely compact mirror-dispersion-controlled cavity being capable of direct diode pumping [26].

## 6.4 Ultra-broadband chirped mirrors for broadly tunable femtosecond Ti:S lasers

One of the main difficulties of using broadly tunable cw, ps and fs laser systems is the lack of ultra-broadband, low loss dielectric high reflectors for feedback in these systems. Fluorescence bands of broadband laser active materials such as Ti:S [1] are usually covered by several low dispersion quarterwave mirror sets that must be replaced when tuning these lasers out of the (relatively narrow) reflectance band, which complicates the practical application of these or similar laser systems such as OPO-s.

Recently, I succesfully solved the problem by developing ultra-broadband chirped mirrors (UBCM) for a broadly tunable cw and ultrafast Ti:S laser [27]. The main difference during its design compared to previous designs was a high transmittance was required at the pump wavelengths, i.e., $R_{opt}(\lambda_j) = 0$ in Eq. 4.3.1, and a higher tolerance was allowed in Eq. 4.3.2.

Figure 6.4.1 shows the calculated transmittance of one of my present state-of-the-art UBCMs. A high reflectivity (R > 99.6%) range from 660 to 1060 nm was obtained for normal incidence by computer optimization that covered most of the fluorescence band of the Ti:S. The mirrors were designed for high transmission (T > 90 %) at the pump wavelengths of 488 and 514 nm in order to test the UBCMs in a fs-Ti:S laser system (Coherent MIRA 900) pumped by a multiline 8.0 W $Ar^+$-laser (Coherent Innova 400).

This specific design is built up of alternating layers of $SiO_2$ and $TiO_2$ as low and high index materials, respectively, with optical thicknesses varying around a quarter of 800 nm, corresponding to our selected wavelength regime. Optical thickness co-efficients of the design are listed in the figure caption. The theoretical smooth variation of group delay vs. frequency of the UBCM's is plotted in Fig. 6.4.1 as well. We verified the dispersive properties of the chirped mirror coatings after the deposition process by using the white-light interferometric technique described in Ref. [40]. These mirrors were designed to have an average negative

GDD of -50 $fs^2$ and a positive TOD of +75 $fs^3$ around 800 nm to ensure nearly ideal dispersive conditions for mode-locked operation. The considerable extension of the high reflectivity range of the CMs was achieved at the expense of a slightly higher fluctuation in the negative GDD which, however, does not affect the formation of pulses longer than 50 fs.

Finally, it is worth pointint out that the design presented was succesfully implemented for commercial systems such as the Coherent MIRA 900 tunable fs-pulse Ti:sapphire laser or the Tsunami laser of Spectra-Physics.

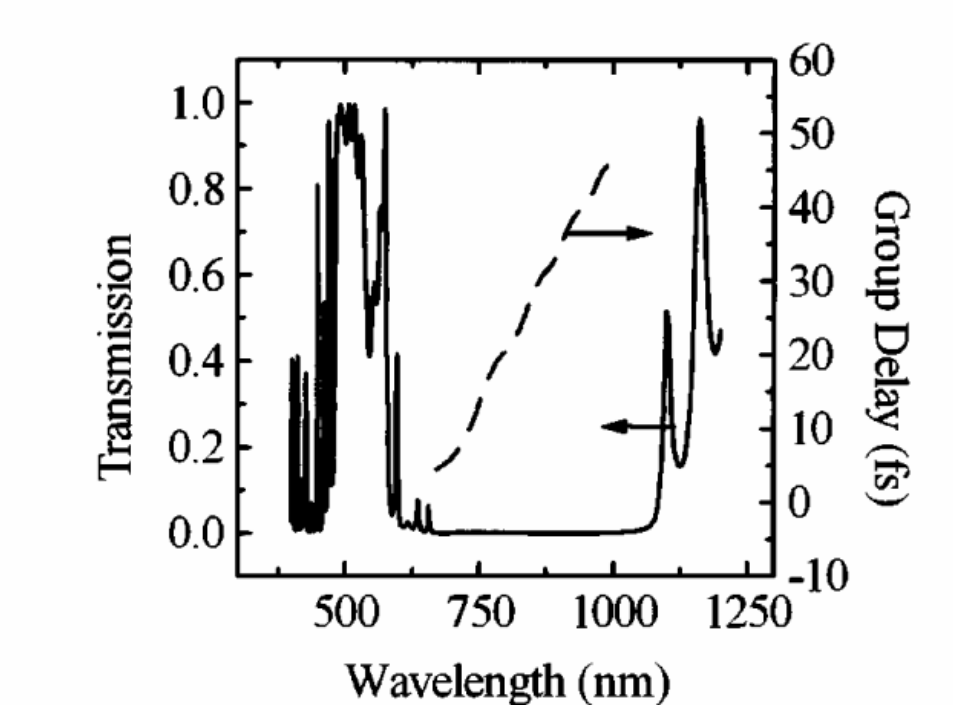


Fig. 6.4.1 Transmittance (solid line) and group delay (dashed line) of an ultra broadband CM vs. wavelength. Optical thickness coefficients of the design are:

Substrate | 1.31L 1.70H 1.43L 0.66H 1.55L 1.45H 1.04L 1.20H 1.14L 1.32H 1.47L 0.99H 0.97L 1.17H 1.46L 1.15H 1.18L 1.11H 1.09L 1.08H 1.11L 1.33H 1.19L 0.91H 1.11L 0.96H 1.05L 0.83H 0.93L 1.11H 1.01L 0.98H 0.85L 0.90H 0.79L 0.99H 0.80L 0.93H 0.96L 0.60H 0.69L 1.09H 0.97L 0.41H 0.59L 1.35H 0.90L 0.10H | Air.

S: substrate, $n_S$= 1.51; A: air, $n_A$ = 1.0; H and L: quarterwave layers of $TiO_2$ and $SiO_2$, respectively, at $\lambda$ = 790 nm, $n_H$ = 2.315, $n_L$ = 1.45.

**Conclusion, outlook**

My understanding of the phase behaviour of optical thin film devices brought revolutionary progress in the field of femtosecond pulse lasers and thin film optics. By the end of the 20th century, dozens of lasers utilizing chirped (or negative dispersion) mirror technology are used for ultrafast spectroscopy in laboratories all around the world. Let me just mention the Coherent Vitesse XT tunable fs pulse Ti:sapphire laser or the commercially available mirror-dispersion-controlled or prism pair/chirped mirror controlled 10-12 fs pulse Ti:sapphire oscillators from different vendors. Similarly, several vendors provide broadband thin-film optics for different application problems, such as the "Xwave Optics" set from Coherent Optics (Auburn) Group, CA, or the "Broadband Optics" set from Spectra-Physics. These optics are based on my "ultrabroadband chirped mirror" design first published in Optics Letters in 1997, and presented in Chapter 6.4 in this dissertation. In collaboration with MLD Technologies, CA, my R&D company named R&D Lézer-Optika Bt. also offers high quality, ion-beam-sputtered broadband and dispersive dielectric mirrors developed for different application problems. To list our recent customers would make this thesis a few pages longer, so I would like to mention just a few of them: Coherent Laser Group, Spectra Physics from USA, Prof. Kobayashi at Tokyo University in Japan and Rutherford Laboratory in England.

During the past few years, we (A. Kõházi-Kis and me at R&D Ultrafast Lasers Kft, Budapest) have developed different femtosecond pulse laser systems utilizing dispersive mirror technology, such as the high power 12 fs Ti:sapphire oscillators we installed at the Philipps Universitat Marburg, Germany and at the Terawatt Laser Laboratory of JATE University, Szeged, Hungary. In 1998, a new laboratory for ultrafast laser technology was founded at my Institution. It comprises a 10 W Ar-ion laser, a 100 fs tunable Ti:sapphire laser and a syncron pumped IR optical parametric oscillator. I do not need to mention that the two femtosecond pulse laser systems utilize chirped mirror technology for broadband feedback and dispersion control.

Currently, I am working on a research of ultrafast laser systems including fs laser and parametric oscillators, nonlinear frequency conversion and white-light continuum generation with photonic bandgap optical fibers. This research is supported by the OTKA foundation and the Bolyai Scholarship of the Hungarian Academy of Sciences. The results of my current research are the topic of new scientific papers - and a subsequent dissertation.

## References


[1] P.F. Moulton, J. Opt. Soc. Am. **B3**, 125 (1986).

[2] B.W. Woods, S.A. Payne, J.E. Marion, R.S. Hughes, L.E. Davis, J. Opt. Soc. Am. **B8**, 970 (1991).

[3] S.A. Payne, W.F. Krupke, L.K. Smith, W.L. Kway, L.D. DeLoach, J.B. Tassano, IEEE J. Quantum Electron. **28**, 1188 (1992).

[4] L.K. Smith, S.A. Payne, W.L. Kway, L.L. Chase, B.H.T. Chai, IEEE J. Quantum Electron. **28**, 2612 (1992).

[5] D. Kopf, J. Aus der Au, U. Keller, G.L. Bona, P. Röntgen, Opt. Lett. **20**, 1782 (1995).

[6] R. Knappe, K.J. Boller, R. Wallenstein, Opt. Lett. **20**, 1988 (1995).

[7] D.E. Spence, P.N. Kean, W. Sibbett, Opt. Lett. **16**, 42 (1991).

[8] Ch. Spielmann, P.F. Curley, T. Brabec, F. Krausz, IEEE J. Quantum Electron. **30**, 1100-1114 (1994).

[9] Z. Bor, B. Rácz, Opt. Comm., 54, 165 (1985).

[10] P.F. Curley, Ch. Spielmann, T. Brabec, F. Krausz, E. Wintner, A.J. Schmidt, Opt. Lett. **18**, 54-56 (1993).

[11] I.P. Christov, M.M. Murnane, H.C. Kapteyn, J. Zhou, C.P. Huang, Opt. Lett. **19**, 1465 (1994).

[12] F. Abeles, "Recherches sur la propagation des ondes electromagnetiques sinusoidales dans les milieus stratifies", Ann. Phys. **12** (5) 596-640, and 706-784 (1950).

[13] H.A. Macleod, "Basic theory", Chap. 2 in Thin Film Optical Filters, Adam Hilger Ltd., Bristol (1985).

[14] K. Ferencz, R. Szipõcs, Opt. Eng. **32**, 2525 (1993).

[15] G. DeBell, L. Mott, M. von Gunten: in Laser Optics for Intracavity and Extracavity Applications, Ph.M.Fauchet, K.H. Gunther, Eds., Proc. Soc. Photo-Opt. Instrum. Eng. 895, 254 (1988).

[16] A.F. Turner, P.W. Baumeister, Appl. Opt. **5**, 69 (1966).

[17] O.S. Heavens, H.M. Liddell, Appl. Opt. **5**, 373 (1966).

[18] J. Ebert, H. Pannhorst, H. Küster, H. Welling, Appl. Opt. **18**, 818 (1979).

[19] P. Laporta, V. Magni, Appl. Opt. **24**, 2014 (1985).

[20] A.M. Weiner, J.G. Fujimoto, E.P. Ippen, Opt.Lett. **10**, 71 (1985).

[21] R. Szipõcs, K. Ferencz, Ch. Spielmann, F. Krausz, Opt. Lett. **19,** 201-203 (1994).

[22] R. Szipõcs, A. Kõházi-Kis, Proc. SPIE **2253**, 140 (1994).

[23] A. Kasper, K.J. Witte, Opt. Lett. **21**, 360 (1996).

[24] L. Xu, Ch. Spielmann, F. Krausz, R. Szipõcs, Opt. Lett. **21**, 1259-1261 (1996).

[25] I.T. Sorokina, E. Sorokin, E. Wintner, A. Cassanho, H.P. Jenssen, R. Szipõcs, Opt. Lett. **21**, 1165-1167 (1996).

[26] I.T. Sorokina, E. Sorokin, E. Wintner, A. Cassanho, H.P. Jenssen, R. Szipõcs, Appl. Phys. **B65**, 245-253 (1997).

[27] E.J. Mayer, J. Möbius, A. Euteneuer, W.W. Rühle, R. Szipõcs, Opt. Lett. **22**, 528-530 (1997).

[28] J. Hebling, E. J. Mayer, J. Kuhl, R. Szipõcs, Opt. Lett. **20**, 919-921 (1995).

[29] D. Strickland, G. Mourou, Opt. Comm. **56**, 219 (1985).

[30] Ch. Spielmann, M. Lenzner, F. Krausz, R. Szipõcs, Opt. Comm. **120**, 321-324 (1995).

[31] R.L. Fork, C.H. Brito Cruz, P.C. Becker, C.V. Shank, Opt. Lett. **12**, 483 (1987).

[32] A. Baltuska, Z. Wei, M.S. Pshenichnikov, D.A. Wiersma, R. Szipõcs, Appl. Phys. B65, 175-188 (1997).

[33] Ch. Spielmann, R. Szipõcs, A. Stingl, F. Krausz, Phys. Rev. Letts. **73**, 2308 (1994).

[34] A.V. Tikhonravov, P.W. Baumeister, K.V. Popov , Appl. Opt. **36**, 4382 (1997).

[35] D.I. Babic, S.W. Corzine, IEEE J. Quantum Electron. **28**, 514 (1992).

[36] F. Gires, P. Tournois, C. R. Acad. Sci. **258**, 6112 (1964).

[37] J. Heppner, J. Kuhl, Appl. Phys. Lett. **47**, 453 (1985).

[38] Yu. T. Mazurenko, Appl. Phys. **B 50**, 101 (1990).

[39] A.M. Weiner, D.E. Leaird, D.H. Reitze,E.G. Paek, IEEE J. Quantum Electron. **28**, 2251 (1992).

[40] A.P. Kovács, K. Osvay, Z. Bor, R. Szipõcs, Opt. Lett. **20**, 788-790 (1995).

[41] K. Osvay, G. Kurdi, J. Hebling, A.P. Kovács, Z. Bor, R. Szipõcs, Opt. Lett. **20**, 2339-2341 (1995).

[42] M.B. Danailov, K. Diomande, P. Apai, R. Szipőcs, J. Mod. Opt. **45**, 5-9 (1999).

[43] P. Apai, S. Lakó, R. Szipõcs, M.B. Danailov, Laser Physics **10**, 444-448 (2000).

[44] L. Sossi, P. Kard, Eesti NSV Tead. Akad. Toim. Fuss. Mat. **17**, 41 (1968).

(An English translation of this paper is available from the Translation Services of the Canada Institute for Scientific and Technical Information, National Research Council, Ottawa, Ontario K1A OS2, Canada.)

[45] L. Sossi: A method for the synthesis of multilayer dielectric interference coatings. Eesti NSV Tead. Akad. Toim. Fuss. Mat. **23**, 229-237 (1974).

[46] L. Sossi: On the theory of the synthesis of multilayer dielectric interference coatings. Eesti NSV Tead. Akad. Toim. Fuss. Mat. **25**, 171-176 (1976).

[47] J.A. Dobrowolski, D. Lowe: Optical thin film synthesis program based on the use of Fourier transforms. Appl. Opt. **17**, 3039-3050 (1978).

[48] P.G. Verly, J.A. Dobrowolsk, Appl. Opt. **29**, 3672-3684 (1990).

[49] H. Fabricius, Appl. Opt. **31**, 5191-5196 (1992).

[50] R.R. Willey, Appl. Opt. **32**, 2963-2968 (1993).

[51] B.G. Bovard, Appl. Opt. **32**, 5427-5442 (1993).

[52] A.V. Tikhonravov, Appl. Opt. **32**, 5417-5426 (1993).

[53] J. Drussel, J. Grantham, P. Haaland, Opt. Lett. **18**, 1583-1585 (1993).

[54] W.H. Southwell, Appl. Opt. **24**, 457 (1985).

[55] H. Fabricius, Appl. Opt. **31**, 5216 (1992).

[56] W.H. Southwell, Appl. Opt. **28**, 5091 (1989).

[57] R. Szipõcs, F. Krausz, US Pat. No. 5,734,503 (1998).

[58] P. Tournois, P. Hartemann, Opt. Comm. **119**, 569 (1995).

[59] R. Szipõcs: "Frequency domain synthesis of ultrabroadband chirped dielectric mirrors for sub-5-fs optical pulses", Technical Digest of Ultrafast Optics 99 conference, Monte Verita, Ascona, Switzerland, July 11-16, 1999, 130-133 (1999).

[60] R. Szipõcs, A. Kõházi-Kis, S. Lakó, P. Apai, A.P. Kovács, G. DeBell, L. Mott, A.W. Louderback, A.V. Tikhonravov, M.K. Trubetskov, Appl. Phys. **B70**, S51-S57 (2000).

[61] F.X. Kartner, N. Matuschek, T. Schibli, U. Keller, H. Haus, C. Heine, R. Morf, V. Scheuer, M. Tilsch, T. Tschudi: Opt. Lett. **22**, 831 (1997).

[62] A. Shirakawa, I. Sakane, T. Kobayashi: Opt. Lett. **23**, 1292 (1998).

[63] W.H. Southwell, R.L. Hall, Appl. Opt. **28**, 2949 (1989).

[64] J.A. Dobrowolsky, R. A. Kemp, Appl. Opt. **29**, 2879 (1990).

[65] S. Kirkpatrick, C.D. Gelatt, M.P. Vecchi, Science **220**, 671 (1983).

[66] C.P. Chang, Y.H. Lee, S.Y. Wu, Opt. Lett. **15**, 595 (1990).

[67] S. Martin, J. Rivory, M. Schönauer, Appl. Opt. **34**, 2247 (1995).

[68] A. Stingl, Ch. Spielmann, F. Krausz, R. Szipõcs, Opt. Lett. **19**, 204-206 (1994).

[69] A. Stingl, M. Lenzner, Ch. Spielmann, F. Krausz, R. Szipõcs, Opt. Lett. **20**, 602 (1995).

[70] J. A. Apfel, Appl. Opt. **15**, 2339 (1976).

[71] H. Greiner, Proc. SPIE **2253**, 150 (1994).

[72] K. Yamakawa, M. Aoyama, T. Itoh, Ch. Spielmann, Jpn. J. Appl. Phys. **35**, L-989 (1996).

[73] G.J. Valentine, J.M. Hopkins, P. Loza-Alvarez, G.T. Kennedy, W. Sibbett, D. Burns, A. Valster, Opt. Lett. **22**, 1639 (1997).

[74] R. Szipõcs, G. DeBell, A.V. Tikhonravov, M.K. Trubetskov: "Multi-Cavity Thin-Film Gires-Tournois Interferometers For Broadband Dispersion Control in Femtosecond Lasers", Technical Digest of Ultrafast Optics 99 conference, Monte Verita, Ascona, Switzerland, July 11-16, 1999, 70-73 (1999).

[75] A.V. Tikhonravov, M.K. Trubetskov: in Optical Interference Coatings, F. Abeles, ed., Proc. Soc. Photo-Opt. Instrum. Eng. 2253, 10 (1994).

[76] A.V. Tikhonravov, M.K. Trubetskov, A.A. Tikhonravov: OSA 1998 Technical Digest Series 9, 293 (1998).

[77,15] G. DeBell, L. Mott, M. von Gunten: in Laser Optics for Intracavity and Extracavity Applications, Ph. M.Fauchet, K. H. Gunther, Eds., Proc. Soc. Photo-Opt. Instrum. Eng. 895, 254 (1988).

[78] H.E. Benett, J.M. Benett, in Physics of Thin Films, Academic Press, New York (1967).

[79] R. Szipõcs, A.P. Kovács, Z. Bor, "Dispersion Measurement on Crystals for ultrashort pulse generation using interference in the frequency domain", Conference on Lasers and Electro-Optics '97, Baltimore, paper CTuP32 (1997).

[80] K. Misawa, T. Kobayashi, Opt. Lett. **20**, 1550 (1995).

[81] C. Sainz, P. Jourdain, R. Escalona, J. Calatroni, Opt. Comm. **110**, 381 (1994).

[82] V.N. Kumar, D.N. Rao, J. Opt. Soc. Am. **B12**, 1559 (1995).

[83] W.H. Knox, Opt. Lett. **17**, 514 (1992).

[84] M. Beck, I.A. Walmsley, J.D. Kafka, IEEE J. Quantum Electron. **27**, 2074 (1991).

[85] R.W. Waynant, M.N. Ediger, eds., Electro-optics handbook, McGraw-Hill, New York, 11.20 (1994).

[86] B.W. Woods, S.A. Payne, J.E. Marion, R.S. Hughes, L.E. Davis, J. Opt. Soc. Am. **B8**, 970 (1991).

**Acknowledgement**

The author thanks A. Kõházi-Kis for the fruitful common work on the results presented in Chapters 3.1 and 3.3. The author also thanks K. Ferencz at the Research Institute for Solid State Physics and Optics and A.W. Louderback at MLD Technologies, Oregon, USA for manufacturing the mirrors used in the above mentioned experiments. G. DeBell and L. Mott (both of MLD Technologies, CA, USA) are also acknowledged for their collaboration on the work presented in Chapter 5.3. Helpful discussions with P. Apai, A. Baltuska, Z. Bor, M. Danailov, K. Ferencz, J. Hebling, A.P. Kovács, A. Kõházi-Kis, F. Krausz, E. Mayer, J. Möbius, K. Osvay, I. Sorokina, Ch. Spielmann, A. Stingl, V. Tikhonravov and E. Wintner are also gratefully appreciated. I especially thank F. Krausz for directing my attention to the problems of using conventional thin film optics in femtosecond pulse laser systems and helping me define the specification and test of the first chirped mirrors, Z. Bor for helping my work with relevant references and giving advice in a number of cases and A.P. Kovács for helping me in the work presented in Chapter 6.2 and performing the AFM measurements shown in Fig. 6.1.2. This research was supported by the OTKA Science Foundation of Hungary under grants CW-015285 and T-02056 and the Hungarian State Eötvös Fellowship.

**Summary**

In this dissertation I summarize the most important results I obtained during my studies on this topic up to now. I clarified the main physical effects responsible the frequency dependent phase change on reflection from multilayer dielectric mirrors and, as a consequence, introduced a novel technology for ultrashort pulse generation in 1993 that became known as *dispersive dielectric mirrors, negative dispersion mirrors, phase correction mirrors* or *chirped mirrors*.

After the general introduction, in Chapter 2, I introduce the two main physical effects responsible for phase dispersion of dielectric laser mirrors: the effect of the frequency dependent penetration depth and the effect of resonances.

In Chapter 3, I present a mathematical approach to explain the dispersive properties of gradient index (or rugate) dielectric mirrors based on Fourier analysis. I introduce the concept of chirped dielectric mirrors for broadband dispersion control, in which the Bragg wavelength is varied gradually along the optical distance measured from the substrate.

In Chapter 4, I discuss the design of discrete layer chirped mirrors. These special laser mirrors exhibite high reflectivity and negative GDD over broad frequency ranges. The design technique, deposition technology and quality control permit higher-order contributions to the mirror phase dispersion to be kept at low values or to be chosen such that high-order phase errors introduced by other system components (e.g., the gain medium, prism pairs) are cancelled. They can be utilized for broadband feedback, intra- and extracavity dispersion control in femtosecond pulse lasers. First I present a conversion routine developed for transforming gradient index chirped mirrors into discrete value step-index and, as a second step, into two-index equivalents. Then I introduce an alternative, more straightforward approach referred to as frequency domain synthesis of (two-index valued) chirped mirrors. Both approaches result in suitable initial designs for further optimization. Based on an initial design obtained by either of these means, we search for the best solution for a certain application problem, bearing in mind the constraints on the parameters set by the technology. Finally, I take a specific design goal: the first application problem I solved. I investigate the effect of deposition errors on this specific design, and show measured dispersion functions taken after the coating deposition process. The measured dispersion data correspond to a mirror set that was used to build a commercial sub-10-fs mirror-dispersion controlled Ti:sapphire laser.

In Chapter 5, an alternative approach for realizing dispersive dielectric laser mirrors with pure negative quadratic phase shift on reflection is introduced. I refer to them as multi-cavity thin-film Gires-Tournois interferometers: their dispersive properties originate from coupled resonances in multiple λ/2 cavities embedded in the layer structure in contrast to chirped mirrors. These devices exhibit extremely low reflection losses over a bandwidth of standard quarterwave mirrors.

In Chapter 6, I take different application problems, and show how to define the target functions for the computer optimization of these different designs. I also present some of the designs I obtained along with their measured dispersion functions.

The replacement of the conventional thin film optics with these novel optical thin film devices made it feasible to build Kerr-lens mode-locked, mirror-dispersion-controlled solid-state lasers delivering nearly bandwidth-limited 7.5 fs pulses from Ti:Sapphire lasers around 0.8 ###m, and sub-20-fs pulses from Cr:LiSAF and Cr:LiSGaF lasers around 840 nm. This technology has been commercialized for femtosecond pulse lasers as well; negative dispersion mirrors were developed for mirror-dispersion-controlled, tunable, sub-100-fs Ti:S lasers such as the Coherent Vitesse XT laser. Similary, I developed ultrabroadband chirped mirrors for broadband feedback and dispersion control in broadly tunable cw, ps and fs solid state lasers (such as the Coherent MIRA 900 laser). All of these applications are addressed in this dissertation.

Further applications of dispersive dielectric mirrors that have already been accomplished include, for example, their use for broadband feedback and dispersion control in broadly tunable fs pulse parametric oscillators, broadband third- and fourth-order dispersion control in pulse compression schemes used in CPA systems and in white light continuum compression experiments supporting pulses below 5 fs.

**Összefoglalás, a disszertáció tézisei**

Az alábbiakban fõbb vonalaiban ismertetem a dolgozat felépítését és tartalmát.

A disszertáció második fejezetben - az általános bevezetõ rész után -, ismertetem azt a két fõ fizikai jelenséget, ami meghatározza egy dielektrikum tükör fázisdiszperzióját: a frekvenciafüggõ behatolási mélység és a rétegrendszerben fellépõ rezonanciák jelenségét és szerepét.

A harmadik fejezetben a Fourier analízisbõl ismert matematikai formulák segítségével értelmezem a (folyamatosan változó törésmutató profillal rendelkezõ) dielektrikum tükrök diszperziós tulajdonságait. Itt vezetem be az ún. csörpölt dielektrikum tükrök fogalmát összefüggésben ezek szerkezetével és diszperziós tulajdonságaival: ezekben a tükrökben folyamatosan változtatom a réteg törésmutató profiljának Bragg-periódusát a felület normálisának irányában, aminek megfelelõen változik a fény különbözõ frekvencia-komponenseinek behatolási mélysége, így csoportkésleltetése is.

A negyedik fejezetben a diszkrét törésmutatójú rétegekbõl álló csörpölt dielektrikum tükrök tervezésével foglalkozom. Ezek a tükrök széles frekvenciatartományon rendelkeznek nagy reflexióval és negatív csoportkésleltetés diszperzióval. A tervezés technikája, a párologtatási technológia és minõségellenõrzés lehetõvé teszi, hogy ezen tükrök viszonylag kis magasrendû (harmad-, negyedrendû) diszperzióval rendelkezzenek, vagy pedig éppen olyannal, mely lehetõvé teszi a más rendszerkomponensektõl (pl. erõsítõ közegtõl, prizmapártól) származó magasrendû diszperziók kompenzálását. A csörpölt tükröket széles sávban használhatjuk femtoszekundumos lézerek fényimpulzusainak térbeli terelésére és/vagy diszperzió kompenzálására a lézerrezonátoron belül vagy kívül. Elõször egy olyan konverziós eljárást ismertetek, amelynek segítségével elõször a Fourier analízis eredményeként nyert gradiens törésmutatójú csörpölt tükrök diszkrét rétegû „ekvivalens”-ét állítom elõ, majd ennek két törésmutató értékkel leírható megfelelõjét. Ezt követõen bemutatok egy ennél egyszerûbb, gyorsabb és mindenképpen praktikusabb eljárást, amelyet a csörpölt tükrök „térfrekvencia tartománybeli szintézisének” neveztem el. Mindkét eljárás segítségével a (fizikailag megvalósítható) specifikációkhoz illeszkedõ rétegrendszereket nyerünk, melyek végleges szerkezetüket további optimalizációs eljárások után nyerik el. Befejezésül ebben a fejezetben ismertetem az elsõ alkalmazási problémára (Ti-zafír lézeroszcillátor rezonátortükrei) nyert elsõ megoldások egyikét, mely alapja volt az elsõ ilyen tárgyú publikációmnak. E konkrét példa kapcsán ismertetem a rétegnövesztési hibák hatását a tükrök diszperziós tulajdonságaira,

és bemutatom azt a mérési eljárást, melynek segítségével a legtöbb alkalmazás esetében megmértem az elkészített diszperzív tükrök diszperziós tulajdonságait. Konkrét példaként bemutatom egy csupán diszperzív tükrökkel diszperzió-kompenzált, szub-10-fs-os Ti-zafír lézer tükörkészletének mért diszperziós adatait.

Az ötödik fejezetben egy olyan, szintén új diszperzív tükörszerkezetet mutatok be, amely – hasonlóan a csörpölt tükörhöz – tisztán kvadratikus fázistolást hoz létre a frekvencia függvényében, azonban szerkezete és a mûködés fizikai alapja lényegesen eltér „csörpölt" tükrökétõl: diszperzív tulajdonságai a rétegszerkezet $\lambda/2$ optikai vastagságú „üregeiben" fellépõ csatolt rezonanciákon alapulnak, aminek következtében „többüreges, vékonyréteg Gires-Tournois interferométereknek" neveztem el õket. Ezek az speciális lézertükrök extrém kis reflexiós veszteséggel és állandó csoportkésleltetés diszperzióval rendelkeznek a csörpölt tükrökénél kisebb, de a negyedhullámú dielektrikum tükrök sávszélességét megközelítõ frekvencia-tartományokon.

A hatodik fejezetben különbözõ konkrét alkalmazási példák kapcsán bemutatom, hogy milyen szempontok alapján kell a tükrök számítógépes optimalizálása során az un. célfüggvényeket megválasztanunk. Itt bemutatok néhány tükörszerkezetet, amelyet e szempontok figyelembe vételével terveztem, illetve ismertetem ezen megoldások mért diszperziós függvényeit.

A fent felsorolt eredmények többek között lehetõvé tették, hogy a hagyományos optikai vékonyréteg szerkezeteket különbözõ típusú diszperzív dielektrikum tükrökre kicserélve prizmapárt nem tartalmazó, 7.5 fs-os impulzusokat elõállító Ti-zafír lézereket vagy 14 fs-os impulzusokat elõállító Cr:LiSAF és Cr:LiSGaF lézereket építsünk. Napjainkra ez az új technológia már megjelent a legújabb kommersz femtoszekundumos lézer rendszerekben is: ilyen negatív diszperzióval rendelkezõ lézertükröket alkalmaznak például a Coherent cég Vitesse XT nevû hangolható, femtoszekundumos Ti-zafír lézerében. Hasonlóan a fent ismertett alkalmazásokhoz, az általam kifejlesztett un. ultraszélessávú csörpölt tükrök is megtalálták helyüket a mindennapi életben: ilyen tükröket (pl. Xwave Optics, vagy BroadBand Optics néven) találhatunk a legújabb széles sávban hangolható cw, ps-os és fs-os lézerekben, mint például a Coherent MIRA 900-as lézerében vagy a Spectra-Physics Tsunami lézerében. A disszertációban mindezeket az alkalmazásokat részletesen ismertetem.

A diszperzív dielektrikum tükrök további, már megvalósított alkalmazásai között említhetjük még használatukat széles hullámhossz tartományban hangolható fs-os

parametrikus oszcillátorokban, csörpölt impulzusú lézererősítő rendszerekben, valamint 5 fs-nál rövidebb fényimpulzusok előállítását lehetővé tevő fehérfény kontinuum kompressziós kísérletekben.

*Új tudományos eredmények:*

1. Megmutattam, hogy a dielektrikum rétegekből álló lézertükrök frekvencia-függõ fázistolása (diszperziója) alapvetõen két fizikai jelenségre, a) az elektromágneses tér frekvenciafüggõ behatolási mélységére és b) a rétegrendszerben fellépõ Fabry-Perot interferométer szerû rezonanciákra vezethetõ vissza. A fizikai kép szempontjából a diszperzió értelmezésénél a frekvenciafüggõ fázistolás (kör)frekvencia szerinti elsõ deriváltja, a csoportkésleltetés és a fenti két jelenség között mutatható ki egyértelmû kapcsolat. Ezzel összefüggésben megmutattam, hogy a dielektrikum tükrökben fellépõ szórási és abszorpciós veszteségek – bizonyos megkötések mellett – arányosak a fent definiált csoportkésleltetéssel, összhangban a fizikai képpel.

2. Megmutattam, hogy az optikai vékonyrétegek szintézisénél széles körben alkalmazott Fourier-transzformációs módszer alkalmas adott diszperziós függvénnyel rendelkezõ dielektrikum tükrök szintézisére, amennyiben a $Q(k) = |r(k)|^2$ és $\phi(k) = \arg(r(k))$ behelyettesítéseket alkamazzuk, ahol $r(k)$ a dielektrikum tükör kívánt amplitudójú reflexiós függvénye. Ezen összefüggés alapján kimutattam, hogy meghatározott lineáris csoportkésleltetés-frekvencia függvény esetén az összefüggés segítségével nyert dielektrikum szerkezet *csörpölt szerkezetû*, vagyis a rétegrendszer törésmutató profiljának ($n(x)$) periódusa a hordozó felülettõl mért optikai távolság ($x$) függvényében az elõírt fázisfüggvény szerint változik. Megmutattam, hogy diszperzió-mentes szélessávú dielektrikum tükör gyakorlatilag nem tervezhetõ, mert a törésmutató profilban ez egy Dirac-delta függvényt igényelne.

3. Számítógépes optimalizásási eljárást dolgoztam ki, mely alkalmas elõírt (intenzitás) reflexiós és diszperziós függvénnyel rendelkezõ, diszkrét rétegekbõl álló dielektrikum tükrök tervezésére. Az eljárás segítségével elsõként terveztem olyan (csörpölt szerkezetû) dielektrikum tükröket, melyek több mint 80 THz-es tartományon rendelkeznek közel állandó negatív (anomális) csoportkésleltetés diszperzióval. Ezen tükrök segítségével elõször sikerült olyan prizmapárokat nem tartalmazó femtoszekundumos (Ti-zafír) lézeroszcillátort építeni, melynek impulzushossza a 10 fs nagyságrendjébe esett. Kimutattam, hogy az eljárás által nyert rétegrendszer lineáris csoportkésleltetés-frekvencia függvénye alapvetõen az elektromágneses tér frekvenciafüggõ behatolási mélységének a függvénye – összefüggésben a tükör csörpölt szerkezetével. Hasonló szerkezetû tükröket fejlesztettem ki – többek között – dióda pumpálásra alkalmas Cr:LISAF és Cr:LiSGaF lézerekhez, valamint szinkron gerjesztett KTP alapú optikai parametrikus oszcillátorokhoz.

4. Módszert dolgoztam ki diszkrét rétegekbõl álló csörpölt dielektrikum tükrök térfrekvencia tartományban történõ leírására, melynek segítségével ezen tükröket mint egy 6-8 dimenziós vektortér elemeit írtam le. A 4. pontban bemutatott számítógépes eljárást erre a vektortérre mint megoldási térre alkalmazva lehetõvé vált adott diszperziós függvényhez legjobban illeszkedõ (csörpölt) tükrökszerkezet megkeresése.

5. Összefüggésben a csörpölt szerkezetû dielektrikum tükrök azon elõnyös tulajdonságával, hogy reflexiós tartományuk lényegesen meghaladja az azonos dielektrikum rétegekbõl álló negyedhullámú tükrök sávszélességét, elsõként ultra-szélessávú dielektrikum tükröket terveztem széles sávban hangolható femtoszekundumos Ti-zafír lézerhez. Ezek a tükrök lehetõvé teszik a lézerek teljes erõsítési tartományukban (680-1060 nm) történõ hangolását mind folyamatos, mind ps-os vagy fs-os impulzus üzemmódban anélkül, hogy a lézerrezonátor tükreit a hangolás során cserélni kellene. A tükrök meghatározóan fontos tulajdonsága, hogy a) átlátszanak a lézer gerjesztési hullámhossz tartományán ($R<5\%$ @ 450-550 nm), b) nagy reflexióval rendelkeznek a lézer

hangolási tartományán (R>99,6% 680-1060 nm) és c) közel állandó, negatív diszperzióval rendelkeznek a lézer hangolási tartományán, mely elõsegíti a fs-os mûködést. Ezek a szélessávú csörpölt tükrök elõnyösen alkalmazhatóak egyéb femtoszekundumos lézeralkalmazások, mint például a fehérfény kontinuum kompresszió területén.

6. Kimutattam, hogy lehetséges tisztán (negatív) kvadratikus fázistolás-frekvencia függvénnyel rendelkezõ diszperzív dielektrikum tükrök tervezése, melyekben a diszperzió fizikai alapja – a csörpölt tükrökkel ellentétben – a rétegrendszer "üregeiben" felépülõ rezonáns, csatolt elektromágneses tér. Ezek a tükrök – amelyeket többüreges Gires-Tournois interferométereknek neveztem el – viszonylag keskenyebb, kb. 40-50 THz-es frekvenciatartományon rendelkeznek állandó csoportkésleltetés diszperzióval, ugyanakkor reflexiójuk jelentõsen meghaladhatja csörpölt szerkezetû társaikét, összefüggésben a Fourier-analízisbõl megismert, vékonyréteg rendszerekre is alkalmazható Parseval-tétellel.

**Publikációs lista**

*Az értekezés alapját képezõ publikációk:*


[1] K. Ferencz, R. Szipõcs: Recent development of laser optical coatings in Hungary, *Opt. Eng*. **32**, 2525-2538 (1993).

[2] R. Szipõcs, K. Ferencz, Ch. Spielmann, F. Krausz: Chirped multilayer coatings for broadband dispersion control in femtosecond lasers, *Opt. Lett*. **19**, 201-203 (1994).

[3] R. Szipõcs, A. Kõházi-Kis: Design of dielectric high reflectors for dispersion control in femtosecond lasers, in *Optical Interference Coatings*, Florin Abeles, Editor, Proc. SPIE **2253**, 140-149 (1994).

[4] E.J. Mayer, J. Möbius, A. Euteneuer, W. Rühle, R. Szipõcs: Ultrabroadband chirped mirrors for femtosecond lasers. Opt. Lett. **22**, 528-530 (1997).

[5] R. Szipõcs, A. Kõházi-Kis: Theory and design of chirped dielectric laser mirrors. Appl. Phys. **B65**, 115-135 (1997).

[6] R. Szipõcs, A. Kõházi-Kis, S. Lakó, P. Apai, A. P. Kovács, G. DeBell, L. Mott, A. W. Louderback, A.V. Tikhonravov, M.K. Trubetskov: Negative Dispersion Mirrors for Dispersion Control in Femtosecond Lasers: Chirped Dielectric Mirrors and Multi-cavity Gires-Tournois Interferometers. Appl. Phys. **B70**, S51-S57 (2000).


*Az értekezés eredményeit bemutató meghívott elõadások listája:*


[I1] R. Szipõcs, A. Stingl, Ch. Spielmann, F. Krausz: Chirped dielectric mirrors for dispersion control in femtosecond laser systems. *Generation, Amplification and Measurement of Ultrashort Laser Pulses*, Photonics West '95, San Jose, CA, invited talk (1995).

[I2] R. Szipõcs: Theory and experiment with chirped dielectric mirrors. European Quantum Electronics Conference '96, Hamburg, Germany, September 8-13, 1996, invited talk QThI4 (1996).

[I3] R. Szipõcs, A. Kõházi-Kis: Theory and design of chirped dielectric laser mirrors. *Ultrafast Optics 1997 Conference*, August 4-7, 1997, Monterey, CA, USA, invited talk TA-3 (1997).

[I4] R. Szipõcs: Theory and design of dispersive dielectric high reflectors for femtosecond pulse laser systems. OSA Topical Meeting on *Optical Interference Coatings,* Tucson, Arizona, June 7-12, 1998, invited talk No. 001 (1998).

*Az értekezés témaköréhez kapcsolódó egyéb saját publikációk:*

[R1] A. Stingl, Ch. Spielmann, F. Krausz, R. Szipõcs: Generation of 11-fs pulses from a Ti:sapphire laser without the use of prisms, *Opt. Lett.* **19**, 204-206 (1994).

[R2] A. Stingl, M. Lenzner, Ch. Spielmann, F. Krausz, R. Szipõcs: Sub-10-fs, mirror-dispersion-controlled Ti:sapphire laser, *Opt. Lett.* **20**, 602-604 (1995).

[R3] A.P. Kovács, K. Osvay, Z. Bor, R. Szipõcs: Group-delay measurement on laser mirrors by spectrally resolved white-light interferometry. *Opt. Lett.* **20**, 788-790 (1995).

[R4] J. Hebling, E.J. Mayer, J. Kuhl, R. Szipõcs: Chirped-mirror dispersion-compensated optical parametric oscillator. *Opt. Lett.* **20**, 919-921 (1995).

[R5] Ch. Spielmann, R. Szipõcs, A. Stingl, F. Krausz: Tunneling of optical pulses through photonic band gaps. *Phys. Rev. Lett.* **73**, 2308-2311 (1994).

[R6] Ch. Spielmann, M. Lenzner, A. Stingl, R. Szipõcs, F. Krausz, Femtosekundenlaser: Sind die Grenzen schon erreicht? Phys. Bl. **51**, 289-292 (1995).

[R7] Ch. Spielmann, M. Lenzner, F. Krausz, R. Szipõcs: Compact, high-throughput expansion-compression scheme for chirped pulse amplification in the 10 fs range. Opt. Commun. **120**, 321-324 (1995).

[R8] K. Osvay, G. Kurdi, J. Hebling, A.P. Kovács, Z. Bor, R. Szipõcs: Measuring group delay of laser mirrors with high accuracy. *Opt. Lett.* **20**, 2339 (1995).

[R9] L. Xu, Ch. Spielmann, F. Krausz, R. Szipõcs: Ultrabroad-band ring oscillator for sub-10fs pulse generation. *Opt. Lett.* **21**, 1259-1261 (1996)

[R10] I.T. Sorokina, E. Sorokin, E. Wintner, A. Cassanho, H.P. Jenssen, R.Szipõcs: Prismless passively mode-locked femtosecond Cr:LiSGaF laser. *Opt. Lett.* **21**, 1165-1167 (1996)

[R11] M. Nisoli, S. De Silvestri, O. Svelto, R. Szipõcs, K. Ferencz, Ch. Spielmann, S. Sartania, F. Krausz: Compression of high-energy laser pulses below 5 fs. Opt. Lett. **22**, 522-524 (1997).

[R12] I.T. Sorokina, E.Sorokin, E.Wintner, A.Cassanho, H.P. Jenssen, R. Szipõcs: 14-fs pulse generation in KLM prismless Cr:LiSGaF and Cr:LiSAF lasers: observation of pulse self-frequency shift. Opt. Lett. **22**, 1716-1718 (1997).

[R13] A. Baltuska, Z. Wei, M.S. Pshenichnikov, D. Wiersma, R. Szipõcs: All-solid-state cavity-dumped sub-5-fs laser. Appl. Phys. **B65**, 175-188 (1997).

[R14] I.T. Sorokina, E.Sorokin, E. Wintner, A. Cassanho, H.P. Jenssen, R. Szipõcs: Sub-20-fs pulse generation from mirror-dispersion-controlled Cr:LiSGaF and Cr:LiSAF lasers. Appl. Phys. **B65**, 245-253 (1997).

[R15] M.B. Danailov, K. Diomande, P. Apai, R. Szipõcs: Phase-conjugation of broad-band laser pulses in $BaTiO_3$. J. Mod. Optics **45**, 5-9 (1998).

[R16] P. Apai, S. Lakó, R. Szipõcs, M.B. Danailov: Broad-band photorefractive phase conjugation in a dispersive scheme. Laser Physics **10**, 444-448 (2000).

[R17] R. Szipõcs, A. Euteneuer, E. Finger, M. Hofmann, A. Kõházi-Kis: Multi-color, mode-locked Ti:sapphire laser with zero pulse jitter. Laser Physics **10**, 454-457 (2000).

[R18] R. Szipõcs, A. Kõházi-Kis, P. Apai, E. Finger, A. Euteneuer, M. Hofmann: Spectral filtering of femtosecond laser pulses by interfernce filters. Appl. Phys. **B70**, S63-S66 (2000).

*Könyvrészletek*

[R19] A.P. Kovács, R. Szipõcs, K. Osvay, Z. Bor: Group-delay measurement on laser mirrors by spectrally resolved white-light interferometry. *Ultrafast Phenomena IX*, Springer, Heidelberg, 145-146 (1994).

[R20] M.S. Pshenichnikov, A. Baltuska, R. Szipõcs, D.A. Wiersma: Sub-5-fs pulses: Generation, Characterisation, and Experiments. *Ultrafast Phenomena XI*, T. Elsaesser, J.G. Fujimoto, D.A. Wiersma, W. Zinth Eds., Springer, 3-7 (1998).